

**IMPROVING BIOCOMPATIBILITY AND CHRONIC PERFORMANCE OF NEURAL
PROBES USING SURFACE IMMOBILIZATION OF THE NEURAL ADHESION
MOLECULE L1**

by

Erdrin Azemi

B.S., University of Pittsburgh, 2004

Submitted to the Graduate Faculty of
Swanson School of Engineering in partial fulfillment
of the requirements for the degree of
Doctor of Philosophy

University of Pittsburgh

2010

UNIVERSITY OF PITTSBURGH
SWANSON SCHOOL OF ENGINEERING

This dissertation was presented

by

Erdrin Azemi

It was defended on

March 25, 2010

and approved by

Carl F. Lagenaur, Associate Professor, Department of Neurobiology

Douglas J. Weber, Assistant Professor, Departments of Physical Medicine and
Rehabilitation and Bioengineering

Kacey G. Marra, Assistant Professor, Departments of Surgery and Bioengineering

Simon C. Watkins, Professor, Departments of Cell Biology and Physiology and
Immunology

Dissertation Director: Xinyan Tracy Cui, Assistant Professor, Department of
Bioengineering

Copyright © by Erdrin Azemi

2010

IMPROVING BIOCOMPATIBILITY AND CHRONIC PERFORMANCE OF NEURAL PROBES USING SURFACE IMMOBILIZATION OF THE NEURAL ADHESION MOLECULE L1

Erdrin Azemi, Ph.D.

University of Pittsburgh, 2010

Neural interface technologies that link the nervous system and the outside world by either stimulating or recording from neural tissue, show great promise for patients suffering from various neurological injuries or disorders. However, the poor recording stability and longevity of neural interface devices (neural probes) is an imminent obstacle to their advance in widespread clinical applications. The dominant factor that affects chronic neural recordings has been reported to be the inflammatory tissue response including neuronal loss and gliosis at the electrode/tissue interface.

In this study, we proposed to modify the surface of neural probes with the neural adhesion molecule L1. The L1 molecule is known to specifically promote neurite outgrowth and neuronal survival. We hypothesized that surface immobilization of L1, may introduce a neuron friendly environment to maintain healthy neuronal density and promote neurite outgrowth around the recording electrodes. Consequently, this phenomenon could reduce gliosis formation. Silane chemistry and the heterobifunctional coupling agent, 4-Maleimidobutyric acid *N*-hydroxysuccinimide ester (GMBS), were used to covalently bind L1 onto the silicon surface. Polyethylene glycol (PEG)-NH₂ was co-immobilized to cap unreacted GMBS groups and prevent non-specific cell attachment. Primary murine neurons and astrocytes were cultured on L1 modified and control surfaces. The L1 surfaces showed promoted neuronal attachment and

neurite outgrowth but significantly reduced astrocyte attachment relative to controls. L1 vs. non modified control probes were implanted in the rat motor cortex for 1, 4, and 8 weeks. Extensive immunohistochemistry and quantitative image analysis were performed to assess the brain tissue response to implants. The results showed that the L1 modified probes had no loss of neurons around the implant interface and showed a significant increase of axonal density compared to the control at all time points. Additionally, significantly reduced glia cell activation and recruitment was observed at the vicinity of the L1 modified probes. As a final step, we have developed a method to evaluate the chronic recording performance of neural probes in the rat somatosensory cortex from whisker stimulation and cortical recordings.

Based on our results we conclude that the L1 biomolecule shows neuroprotective and neurogenerative properties while inhibiting gliosis. The L1 surface coating can be a promising strategy to improve the biocompatibility of all types of neural probes and their chronic performance in the brain.

TABLE OF CONTENTS

PREFACE.....	XXII
1.0 INTRODUCTION.....	1
1.1 MOTIVATION: THE NEED FOR CORTICAL NEURAL INTERFACE SYSTEMS	2
1.2 IMPLANT TISSUE RESPONSE AT THE ELECTRODE-TISSUE INTERFACE.....	6
1.2.1 Cells involved and the brain inflammatory response	6
1.2.2 Acute and chronic gliosis formation.....	7
1.2.3 Neuronal response at the implant/tissue interface.....	10
1.2.4 Hypothesis and approach	11
1.3 MODIFICATIONS OF NEURAL IMPLANTS	11
2.0 SURFACE IMMOBILIZATION OF NEURAL ADHESION MOLECULE L1 FOR IMPROVING THE BIOCOMPATIBILITY OF CHRONIC NEURAL PROBES: IN VITRO CHARACTERIZATION	14
2.1 ABSTRACT.....	14
2.2 INTRODUCTION	15
2.3 MATERIALS AND METHODS.....	18

2.3.1	Surface modification and characterization	18
2.3.1.1	Isolation and purification of the L1 protein	18
2.3.1.2	Covalent biomolecule immobilization	19
2.3.1.3	Surface characterization.....	21
2.3.2	Bioactivity and stability of immobilized L1.....	22
2.3.3	<i>In vitro</i> experiments	23
2.3.3.1	Primary neuron and astrocyte cell cultures	23
2.3.4	Immunocytochemistry	24
2.3.5	Data collection and analyses	24
2.3.6	Statistical analyses	25
2.4	RESULTS	25
2.4.1	L1 Protein Purification and Surface Characterization	25
2.4.2	L1 Bioactivity and Stability	28
2.4.3	<i>In vitro</i> cell culture tests.....	29
2.4.3.1	Neuronal attachment and neurite outgrowth.....	29
2.4.3.2	Astrocyte attachment.....	31
2.5	DISCUSSION.....	32
2.6	CONCLUSIONS.....	37
3.0	L1 SURFACE MODIFICATION OF SILICON BASED NEURAL PROBES MAINTAINS NEURONAL DENSITY AND MITIGATES GLIOSIS AT THE IMPLANT/TISSUE INTERFACE.....	38
3.1	ABSTRACT.....	38
3.2	INTRODUCTION	39

3.3	METHODS.....	43
3.3.1	Microelectrode L1 modification	43
3.3.2	Surgical procedures for neural implants	45
3.3.3	Brain tissue preparation for immunohistochemistry	47
3.3.4	Immunohistochemistry procedures.....	47
3.3.5	Quantitative brain tissue analyses.....	49
3.3.6	Statistical analyses	52
3.4	RESULTS.....	52
3.4.1	Implant/tissue immunoreactivity.....	52
	3.4.1.1 Neuron density and axonal immunoreactivity (NeuN and NF)	52
	3.4.1.2 Astroglia reaction (GFAP and Vimentin).....	58
	3.4.1.3 Microglia reaction (ED-1 and Iba1)	62
3.4.2	Qualitative observations.....	66
3.5	DISCUSSION.....	68
3.6	CONCLUSIONS	74
4.0	CHRONIC NEURAL RECORDING AND IMPEDANCE MEASUREMENT IN THE RAT BARREL CORTEX TO EVALUATE THE PERFORMANCE OF L1 COATED VS. UNMODIFIED NEURAL PROBES.....	76
4.1	INTRODUCTION	76
4.1.1	Probe modification and recording surgical procedure.....	80
4.1.2	Impedance spectroscopy and modeling	84
4.1.3	Neural recording experiments and analyses.....	85
4.1.4	Tissue analysis: Brain tissue preparation for immunohistochemistry..	88

4.1.5	Tissue analysis: Immunohistochemistry and quantitative analyses.....	89
4.2	RESULTS AND DISCUSSION	90
4.2.1	Impedance spectroscopy.....	90
4.2.2	Neural recording analysis.....	92
4.2.3	Tissue analyses	96
4.3	EXPERIMENTAL OPTIMIZATION.....	99
4.4	REMARKS AND FUTURE INSIGHTS	101
5.0	FUTURE EXPERIMENTS.....	103
	APPENDIX.....	105
	BIBLIOGRAPHY	110

LIST OF TABLES

Table 1. Water contact angle measurement for covalent immobilization of different molecules to silicon surface ($^{\circ}$). Data are expressed as mean \pm S.E.M.. Abbreviations (I-Immobilized, A-Adsorbed) (n=18).	26
Table 2. Quantitative DPI data on real-time changes in dimension (resolution $<0.1\text{\AA}$) and density (resolution <0.1 picogram/ mm^2). Immobilized L1, laminin, and PEG layers are expressed in terms of thickness and refractive index. Density and mass of the layers can be calculated from the refractive index.....	27
Table 3. Primary antibodies used during this study.....	48
Table 4. P-values calculated from t-test analysis of the values from the NeuN and NF data at different interval distances from the probe interface. Yellow cells show significant p-values < 0.05 calculated from t-test analysis comparing NM and L1 data at $100\ \mu\text{m}$ increments.	58

Table 5. P values calculated from t-test analysis of the values from the GFAP and Vimentin intensity data analysis at different interval distances from the probe interface. Yellow cells show significant p-values < 0.05 calculated from t-test analysis comparing NM and L1 data at 100 μ m increments..... 61

Table 6. P values calculated from t-test analysis of the values from the ED-1 and Iba1 intensity data analysis at different interval distances from the probe interface. Yellow cells show significant p-values < 0.05 calculated from t-test analysis comparing NM and L1 data at 100 μ m increments..... 66

LIST OF FIGURES

Figure 1. Different emerging neural interface technologies. (NeuroProbes).....	2
Figure 2. The two prevalent cortical devices. (A) The planar approach device also known as the Michigan probe (NeuroNexus Technologies). (B) The microwire device also known as the Utah array (BrainGate).....	4
Figure 3. Schematic of the acute and chronic tissue responses following neural probe implantation. The acute response (A) is characterized by vasculature damage, neuronal injury, plasma protein adsorptions, recruitment of activated microglia, and a broad region of reactive astrocyte around the implant. The chronic response (B) is characterized by a condensed sheath of cells primarily composed of activated microglia and reactive astrocytes around the insertion site. Degeneration of neuronal processes and addition neuronal loss may also be seen [60].	9
Figure 4. Schematic representation of the biomolecule immobilization process. L1 or laminin were covalently immobilized on MTS treated silicon substrates, using the	

heterobifunctional crosslinker GMBS. mPEG-NH₂ was used to cap the unreacted GMBS groups..... 20

Figure 5. Surface analysis of L1-PEG samples. (A) Alexa 488 antibody staining of L1 protein immobilized on a circular surface area. (B) Mouse neuronal cell growth on the area where L1-PEG is immobilized after one day in culture. Scale bar 50 μm. 28

Figure 6. Neuron attachment reported as average neurons/cm² ± s.e.m.(A) and average neurite outgrowth reported as average neurite length ± s.e.m. (B) of primary rat cortical cells on silicon surfaces with immobilized laminin-PEG, L1-PEG, and PEG (*p<0.05)..... 30

Figure 7. Representative images of primary rat cortical neurons plated on silicon surfaces with immobilized (A) laminin-PEG and (B) L1-PEG, after 3 days in culture. Cells were stained for β-tubulin III (green) and the nuclear stain DAPI (blue). Scale bar 100 μm. .. 31

Figure 8. (A) Astrocyte attachment on silicon surfaces with immobilized L1-PEG, laminin-PEG, PEG, and unmodified SiO₂ surface reported as average astrocytes/cm² ± s.e.m. (*p<0.05 against all conditions, and op<0.05 against laminin-PEG). (B) Representative image of primary rat cortical astrocytes plated on silicon surfaces with immobilized laminin-PEG after 2 days in culture. Cells were stained for GFAP (green) and the nuclear stain DAPI (blue). Scale bar 100 μm. 32

Figure 9. Brain Computer Interface schematic. Neural activity recorded from the brain is transmitted to a processor that operates an extraction algorithm on the recorded signal. The extracted control signal is fed to a robot controller to move the prosthetic arm, which generates feedback to close the control loop. Figure courtesy of Schwartz et al. [60]..... 40

Figure 10. Dimensions of the silicon based electrodes used during *in vivo* studies. Inset (A) schematic of the tethering technique used during probe implantation. Schematics were obtained from NeuroNexus Technologies (www.neuronexustech.com)..... 43

Figure 11. Schematic representation of L1 immobilization on the silicon surface of neural probes using MTS and GMBS covalent functionality..... 44

Figure 12. Representative image of probe location sites on the skull of a rat shown in black rectangles where the craniotomy was performed. Black circles represent location of skull screws used to anchor the probe assembly. (AP – Anteroposterior, ML – Mediolateral).46

Figure 13. ImageJ intensity analysis. (A) Horizontal representative image of a GFAP stained image. 20 μm step size oval bands are created from the implant interface location and average pixel intensity values from 1-255 are measured for each band and shown as a function of distance. Scale bar 100 μm . (B) Coronal schematic of the region used for normalizing the intensity values. 50

Figure 14. Neuron count analysis. (A) Representative image of double stained NeuN+ cells (green) and Hoechst+ (blue) nuclei. Boxes created to expand up to 600 μm away from the interface, while the probe's tract is placed in the middle of the boxes. Scale bar 100 μm . (B) Representative watershed algorithm computed from the green channel of the image A counting the NeuN+ cells at the 50 μm distance. (C) Raw NeuN+ cell count for image A as a function of distance from the interface. 51

Figure 15. Neuronal number and density adjacent to L1 modified implants are associated with a higher NeuN+ cell count than NM control implants. (A-C) Comparison of average NeuN+ cell counts between L1 and NM control probe at each different time point shown as the normalized average neuron number ($n=14\pm 2$). (A – week 1, B – week 4, C – week 8). (D-F) Comparison of average NeuN+ cell counts at different depths in the cortex 0-100 μm away from the interface for different time points (D – week 1, E – week 4, F – week 8). t-test comparisons between each group (NM vs L1) showed a significance difference $*p < 0.05$. No significant difference was seen between time points and depth within each group (NM or L1). 54

Figure 16. Representative images of NeuN+ cells (green). Probe tracts traced with an oval for better visualization. (A,C,E) Neuronal density around the L1 probe at week 1, 4, and 8 respectively. (B,D,F) Neuronal density around the NM probe at week 1, 4, and 8 respectively. Scale bar 100 μm 56

Figure 17. Mature axons adjacent to L1 modified implants are associated with a higher relative NF200 immunoreactivity than NM control implants. (A-C) Comparison of average NF intensity between L1 and NM control probe at each different time point shown as the normalized average intensity in arbitrary units (a.u.) ($n=14\pm 2$). (A – week 1, B – week 4, C – week 8). T-test comparison between the average intensity at 0-100 μm and the background intensity (420-520 μm) were made, significance was seen between these two measures ($*p<0.05$). (D-F) Comparison of average NF intensity at different depths in the cortex 0-100 μm away from the interface for different time points (D – week 1, E – week 4, F – week 8)..... 57

Figure 18. Representative images of NF 200 staining of 2 probe tracts shown per image. (A) L1 probe sites at week 4 time point. (B) NM control probe at week 4 time point. Both images, NF 200 (green) and Hoescht (blue). Scale bar 100 μm 58

Figure 19. Representative images of GFAP (A, B) and Vimentin (C, D) staining at the 8 week time point for L1 (A, C) and NM probe (B, D). GFAP and Vimentin (green), Hoescht (blue). Arrows in figure A indicate the position of 2 probe tracks. Scale bar 100 μm 59

Figure 20. Tissue reaction adjacent to L1 modified implants is associated with a lower relative GFAP immunoreactivity than NM control implants. (A-C) Comparison of average GFAP intensity between L1 and NM control probe at each different time point shown as the normalized average intensity in arbitrary units (a.u.) ($n=14\pm 2$). (A – week 1, B – week 4, C – week 8). (D-F) Comparison of average GFAP intensity at different depths in the

cortex 0-100 μm away from the interface for different time points (D – week 1, E – week 4, F – week 8)..... 60

Figure 21. Tissue reaction adjacent to L1 modified implants is associated with a lower relative Vimentin immunoreactivity than NM control implants. (A-C) Comparison of average Vimentin intensity between L1 and NM control probe at each different time point shown as the normalized average intensity in arbitrary units (a.u.) ($n=14\pm 2$). (A – week 1, B – week 4, C – week 8). (D-F) Comparison of average Vimentin intensity at different depths in the cortex 0-100 μm away from the interface for different time points (D – week 1, E – week 4, F – week 8)..... 62

Figure 22. Representative images of ED-1 (A, B) and Iba1 (C, D) at the 8 week time point for L1 (A, C) and NM probe (B, D). ED-1 and Iba 1 (green), Hoescht (blue). Scale bar 100 μm .
..... 63

Figure 23. Tissue reaction adjacent to L1 modified implants is associated with a lower relative ED-1 immunoreactivity than NM control implants. (A-C) Comparison of average ED-1 intensity between L1 and NM control probe at each different time point shown as the normalized average intensity in arbitrary units (a.u.) ($n=14\pm 2$). (A – week 1, B – week 4, C – week 8). (D-F) Comparison of average ED-1 intensity at different depths in the cortex 0-100 μm away from the interface for different time points (D – week 1, E – week 4, F – week 8)..... 64

Figure 24. Tissue reaction adjacent to L1 modified implants is associated with a lower relative Iba1 immunoreactivity than NM control implants. (A-C) Comparison of average Iba1 intensity between L1 and NM control probe at each different time point shown as the normalized average intensity in arbitrary units (a.u.) ($n=14\pm 2$). (A – week 1, B – week 4, C – week 8). (D-F) Comparison of average Iba1 intensity at different depths in the cortex 0-100 μm away from the interface for different time points (D – week 1, E – week 4, F – week 8)..... 65

Figure 25. Representative images of neurons (A, B) and microglia (C) on the surface of probes after removal from fixed brain tissue. (A) L1 probe after 1 week, (B) L1 probe after 4 weeks (A and B same scale bar 100 μm), and (C) NM control probe after 8 weeks. β -tubulin III – green, Iba 1 – green, Hoescht – blue. Scale bar 100 μm 67

Figure 26. Representative images of H&E histology at the 8 week time point for L1 (A) and NM probe (B). Scale bar 100 μm 67

Figure 27. Representative images of CS56 staining (red) at the 8 week time point for L1 (A) and NM probe (B). Scale bar 100 μm 68

Figure 28. Schematic of the rat’s whisker-to-barrel pathway. Rat whisker follicles are indicated by colored circles and at each level of the pathway an isomorphic arrangement of neuronal cell groups, reflecting the layout of the whiskers on the snout, can be found. These are called barrelettes in the primary trigeminal nucleus of the brainstem, barreloids

in the ventrobasal thalamic nucleus and most prominent barrels in the primary somatosensory (barrel) cortex..... 80

Figure 29. Dimensions of the silicon based electrodes used during recording *in vivo* studies. Inset (A): Components of the recording electrodes. Images were obtained from NeuroNexus Technologies (www.neuronexustech.com)..... 82

Figure 30. Image of implant in the barrel cortex of the rat brain (right). (a) skull screw used to ground the electrode (b) skull screw used as a counter during impedance measurements. Defined axis: ML (Mediolateral), AP (Anteroposterior – or Rostrocaudal [RC]). 83

Figure 31. Schematic of the whisker stimulation setup and the recording setup. Air jets were positioned perpendicular to whiskers and contralateral to the recording implant. Raw data from all 16 channels were recorded from different whisker stimulation trials..... 86

Figure 32. Impedance magnitude for L1 and NM probes at the (A) 1kHz frequency and (B) 10Hz frequency. For two of chronic probes, impedance recordings were terminated at day 42 because of apparatus (Gamry) failure. Data reported as mean \pm s.e.m. 91

Figure 33. Stimulus-evoked PSTHs and LFP traces. L1 modified probe (A) 12 days post implantation and (B) 27 days post implantation. NM control probe (C) 12 days post implantation and (D) 27 days post implantation. Sixteen channels recorded neural activity 1s prior and 1s past stimulus presentation. The red line represents the start of

stimulus application (air). Spike counts are averaged over the sixteen channels. LFP trace is averaged over the sixteen channels of the raw LFP data and the light gray line represents the standard error of mean. 93

Figure 34. Data analysis representation of recording quality over the 8 week study period for L1 and NM control probes. (B-E) Data reported as mean \pm s.e.m. 95

Figure 35. (A) Representative logarithmic power amplitude spectra showing the calculated fundamental frequency of the raw LFP signal for one channel. Bottom blue trace shows the raw LFP signal recorded over a 35 second period. 10 air stimulations were performed during this time, represented as an increase in amplitude (-0.02 – 0.02 mV y-axes). LFP data was passed through a Fourier analysis (Matlab software) to determine the logarithmic amplitude of the signal. The fundamental frequency was calculated from the peaks corresponding in the spectrum (y axis –Freq.) (B) Percent change of LFP power energy for L1 and NM control probes over time. The power energy level was calculated at the 10-20 Hz frequency band over 500 ms epoch before and after stimulus presentation. 96

Figure 36. Representative histology from the NM probe (A) GFAP staining for astrocytes shown in green and nuclei in blue. (B) ED-1 staining for activated microglia shown in green and nuclei in blue. (C) H&E staining. Scale bar 100 μ m. 97

Figure 37. Tissue analysis at the 8 week time point for different markers as a function of distance from the electrode interface. Comparison between the L1 and NM control probes. Data is shown as mean±s.e.m. 98

Figure 38. Data representing cell attachment and growth per surface area on untreated and modified Parylene-C wires. L1 treated wires showed a significant difference when compared to the untreated wires *p<0.05. β -tubulin III stains for neurons, ED1 stains for activated microglia, and GFAP stains for astrocytes..... 108

Figure 39. Representative images of β -tubulin III positive neurons grown on A) L1 modified Parylene C wire and B) laminin modified Parylene C wire. Scale bar 100 μ m. 109

PREFACE

This dissertation would not have been possible without the guidance, encouragement, and support of many individuals. First, I would like to express my gratitude to my advisor, Dr. Tracy Cui. She has provided me the freedom, the resources, and the guidance to become a confident researcher. I have learned many important lessons from her, which have made me a better scientist and will serve me in my future endeavors. I will always be grateful to her for instilling in me an academic mindset and advising me to be a daring researcher.

I would also like to extend my thanks to the members of my thesis committee. I have been the beneficiary of the many hours they have spent critiquing my work, and the diverse perspectives each one has brought to this research: Dr. Carl Lagenaur, for inspiring me with his work ethic and his eagerness to teach me cell culture and protein purification techniques; Dr. Doug Weber for co-advising me throughout the last three years, and providing tremendous help and insight with neurophysiological recording techniques while letting me use his laboratory facilities; Dr. Kacey Marra for guiding me during my graduate studies and for always being there when I needed assistance; Dr. Simon Watkins and the members of the Center for Biological Imaging for allowing me to access all their available resources and for providing the opportunity to work late nights.

There are many others who have given valuable feedback throughout my graduate career and although I cannot thank all of them here, I will mention a few. Dr. William Stauffer, for being a friend and a co-worker, and for teaching me the basics of my research. Dr. Glenn Gobbel for his guidance during a collaboration using adult neural stem cells. To all the undergraduate students that I have mentored, for helping with experiments and data analysis and teaching me how to be a successful mentor. The NTE Lab members for all of your encouragement and constructive criticism along the way.

I would particularly like to thank the Department of Bioengineering at the University of Pittsburgh and Dr. Harvey Borovetz for creating such an amazing program and providing me the opportunities and resources to apply my research ideas. The Center for the Neural Basis of Cognition for offering me the prospect to apply and get a two year NSF grant.

To all my friends, thank you for being there during good times and busy times. In particular my good friend, Oana Udrea, thank you for your support and encouragement each and every way you could.

My parents, Dashi and Remi, and my brother Dritan, who have always been there and have encouraged me in whatever I set my mind to do. I could never thank my parents enough for the sacrifices they made by moving to the United States to support my future. I am so proud of my brother, his achievements and his beautiful family, Shannon, Mira and Luc. I love you all and I hope I will always make you proud in whatever I do. Finally, to my wonderful boyfriend, Dr. Sinan Filiz, thank you for being my best friend, and for giving me love, hope, and laughs every day.

1.0 INTRODUCTION

The idea of using neural signals to control external prosthetics first surfaced 3 decades ago. Since then an abundance of research has been devoted to understanding the neuronal circuitry of the relevant brain structures, developing computer hardware and software algorithms to translate neuronal potentials into prosthetic control, and engineering biocompatible recording electrode arrays. However, the clinical translation of these arrays has been greatly impeded due to several fundamental and unresolved research questions. Neural signal degradation during chronic implantation of these electrodes in the brain tissue remains the main challenge, raising questions such as: Is the signal degradation the result of insertion trauma, micromotion, mechanical mismatch, or consequences of a gliosis formation that arises simply from a chronic foreign body response? Other questions involve the fate of neurons adjacent to the recording electrodes. Are these neurons killed during insertion injury, do they die through the inhibitory cues expressed by the cells that mediate gliosis, or are they shifted by gliosis activated cells? What are the best methods to minimize or treat implant injury, and what roles do electrode size, shape, surface chemistry, mechanical impedance, and insulating material play? Research is being conducted worldwide to answer these questions and others that arise during the way. Only when these questions are answered can this technology successfully be applied to widespread use in humans.

1.1 MOTIVATION: THE NEED FOR CORTICAL NEURAL INTERFACE SYSTEMS

Research to develop technology that links the nervous system and the outside world by either stimulating or recording from neural tissue has been examined for decades. This area of research, which is referred to as; brain-machine interfaces, brain-computer interfaces, neural prostheses, or neural interface systems, offers to assist people suffering from sensory, motor, or other neurological disabilities [1-3]. In addition, the emerging technology could provide fundamental scientific knowledge about the human nervous system and its function.

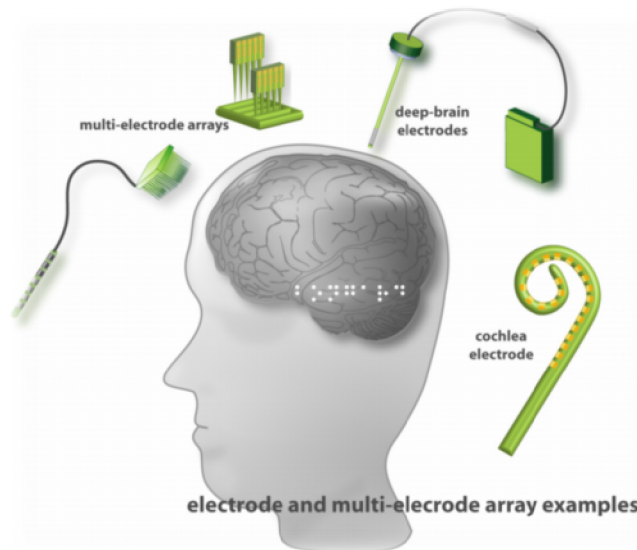


Figure 1. Different emerging neural interface technologies. (NeuroProbes)

To date the most successful neural interfaces available to humans in widespread clinical applications are the electrical stimulation devices. These devices include the cochlear implants, which help to restore audition in the hearing impaired [4], and the deep brain stimulator (DBS), which relieve symptoms of Parkinson’s disease and dystonia when available drug therapies fail [5] (Figure 1).

Neural interfaces that record electrical potentials from the brain can predict cognitive intentions in the form of motor outputs such as movement of a computer cursor, a robot, or an artificial limb [2]. These systems are at an early stage in clinical trials [6-11] and are designed as assistive technologies to help patients suffering from spinal cord injury trauma, strokes that interrupt descending motor pathways, degenerative disorders such as amyotrophic lateral sclerosis (ALS), cerebral palsy, muscular dystrophy and/or limb amputation [3, 8-15]. The clinical need for these prostheses increases as the world population's average age increases. These prostheses also have the potential use in interfacing with rising environmental and technological changes in society.

Developed over 40 years ago, the first neural recording electrodes were reported to be microwires [16]. These microwires were composed of fine stainless steel or tungsten wires (diameter of 20-50 μm) and insulated with Teflon or polyimide. Since then, significant research has been done in manufacturing and perfecting the technology and composition of these electrodes. To date, the most well-known recording electrodes in the neural research and clinical fields are the planar silicon substrate based microprobe devices developed at the University of Michigan, now owned by NeuroNexus Technologies [17], and the microwire array developed at the University of Utah, now owned by BrainGate [18] (Figure 2). The NeuroNexus silicon probes are fabricated using methods applied in the semiconductor industry. Boron etch-stop micromachining is used as an initial processing step of the silicon wafer to precisely delineate the shape of the probe which can have defined features within $\pm 1 \mu\text{m}$. Several steps are used to deposit silicon dioxide and silicon nitride for insulation, followed by photolithography to pattern the interconnects and the recording sites (typically iridium). Standard shank thickness is 15 μm but the boron doping process offers the ability to manufacture a wide variety of 2D, and most

recently 3D designs that can vary in the number of electrode sites and shank configurations (Figure 2A). During chronic implantations, these probes are implanted manually in the brain using forceps through the incised dura layer. The probe's percutaneous connectors are secured to the skull and in contrast to the microwires, a flexible ribbon cable allows for these probes to

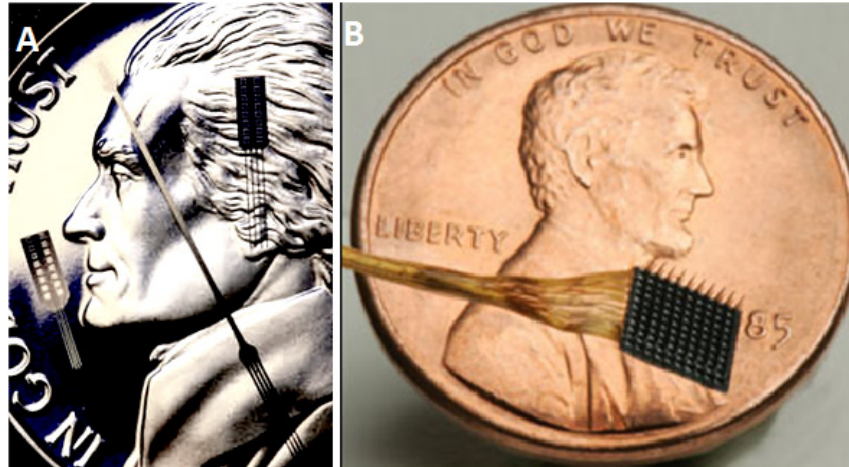


Figure 2. The two prevalent cortical devices. (A) The planar approach device also known as the Michigan probe (NeuroNexus Technologies). (B) The microwire device also known as the Utah array (BrainGate).

float with the brain as it pulses. The BrainGate arrays are micro-machined using a solid block of silicon and an acid-etching technique that results in a 3D array typically composed of 10 x 10 arrangement of needles protruding from a 4 x 4 mm surface (Figure 2B). These silicon needles (1 – 1.5 mm in length) are converted into electrodes by the application of a four part multi-layer metal deposition of Pt, Ti, W then Pt of total thickness 10,000 Angstroms onto the first 50 – 100 μm of each tip to allow for recording. These arrays can be implanted into the cortex through the dura layer using a high-speed controller tool. These arrays are machined to adjust to cortical movement during chronic implantation. To date, BrainGate neural implants have been FDA approved for clinical trials, while the NeuroNexus probes remain as research prototypes. The

clinical trials in the arena of motor prosthetics using BrainGate implants are conducted by Donohue et al. [7, 8, 10]. Human implantation during these cases has been strictly investigational. Thus far, several tetraplegic patients have undergone trial implantations and have successfully controlled a robotic arm, computer cursor, and even a wheelchair through their brain signals [7, 8, 10].

Several other prototypes of microelectrode arrays exist for research applications and are made of significantly different material compositions, geometries, manufacturing processes, degrees of invasiveness, and degrees of biocompatibility [12, 19-22]. However, the majority of all of the above mentioned neural probes are reported to fail within weeks to months after implantation [23-27]. Research investigators aim to characterize and optimize individual aspects of probe designs that are believed to contribute to their failure, such as substrate composition, geometry, surface features, and insertion techniques [28-30]. While others seek to develop electrodes with alternative surface configurations and applied polymer or drug-eluting coatings [31-33]. However, although the engineering aspect of the neural interface technology has been advancing, to date, no microelectrode configuration has successfully evaded the foreign body response. This obstacle is one of the major impeding factors to the advancement of cortical neural interfaces in widespread clinical applications.

1.2 IMPLANT TISSUE RESPONSE AT THE ELECTRODE-TISSUE INTERFACE

When an artificial material is inserted in the host body creating a wound, the body is programmed to respond with a series of molecular and cellular events to repair the resulting damage. Host reactions following implantation of biomaterials in the body include initial tissue injury, blood material interactions, provisional matrix formation, acute inflammation, chronic inflammation, granulation tissue development, foreign body reaction, and fibrosis/fibrous capsule development [34]. The observed inflammatory response in the brain follows similar events. However, due to the novelty of brain implant systems, our understanding of cortical inflammatory response and the function of the molecule/cell interactions involved is at an early stage. Several assumptions and hypotheses made by researchers who are studying the effects of biomaterial implants in the brain tissue are discussed below.

1.2.1 Cells involved and the brain inflammatory response

Astrocytes are highly differentiated cells that are distributed in the central nervous system (CNS) in a contiguous fashion and make numerous essential contributions to normal function in the healthy CNS, including regulation of blood flow, providing energy metabolites to neurons, participation in synaptic function and plasticity, and maintenance of the extracellular balance of ions, fluid balance and transmitters [29]. In addition, astrocytes are known to respond to all forms of CNS insults such as infection, trauma, ischemia, and neurodegenerative disease. This process is commonly referred to as reactive astrogliosis. Epidermal growth factor (EGF), fibroblast growth factor (FGF), endothelin 1, and adenosine triphosphate (ATP) are some of the

several molecular triggers that lead to proliferation of reactive astrocytes *in vivo* [35]. Our understanding about the functions and effects of reactive astrogliosis and its impact on neural function is at an early stage.

In addition to astrocytes, microglia represent the second major population of glial protective cells within the CNS. Microglia are derived from the monocyte lineage and are ubiquitously distributed throughout the brain and spinal cord. One of their main functions is to monitor and sustain neuronal health. These cells are known to be very sensitive to any minor disturbances in CNS homeostasis, and they readily become activated (changing in both phenotype and function) during most neuropathologic conditions, including peripheral nerve injury, trauma and stroke, inflammatory disease, and neurotoxicant-induced neuronal injury [36]. Another function taken on by microglia when activated is to cluster around a foreign body and degrade it enzymatically. When a foreign body cannot be degraded, the phenomenon is called “frustrated phagocytosis”. During frustrated phagocytosis pro-necrotic substances are released into the immediate vicinity of the foreign body, which eventually contribute to cell death [36]. Hypotheses are made that this phenomenon might also occur during probe implantation in the brain.

1.2.2 Acute and chronic gliosis formation

The response to neural implants in the CNS is a complex response involving interactions between at least 4 cell types: microglia/macrophages (brain and blood-borne), astrocytes, meningeal fibroblasts, and neurons (Figure 3). Mechanical trauma caused by a stab wound insertion of a neural implant can sever blood vessels, neuronal cell processes, glia cells,

extracellular matrix, and collagen fibrils. Blood vessel rupture releases erythrocytes, clotting factors, and other inflammatory factors which aid in macrophage recruitment and eventual cell/tissue rebuilding [37]. Following this implant injury a series of other molecular cascades are followed by activation and recruitment of glia cells. More specifically tissue response to neural implants has been categorized into two stages: the acute inflammatory response and the chronic inflammatory response (Figure 3). The acute response (Figure 3A) is triggered by device insertion and begins to subside after a week. During the acute response, the activated microglia are recruited immediately around the implant site and can be visualized by immunohistochemical staining as early as 1 day post-implantation [38]. Pro-inflammatory cytokines released by activated microglia recruit and activate astrocytes, which respond with increased expression of glial fibrillary protein (GFAP) and a change in morphology [39]. It has been shown that this acute response is temporary, as removal of an implant immediately after insertion leaves little evidence of a cellular reaction in the tissue a month after recovery [40-42]. On the other hand, the chronic response (Figure 3B) to cortical implants, remains for as long a period as has been studied (up to six months) in rats and non-human primates [38, 43-48]. The chronic inflammation response is characterized by the presence of activated microglia, macrophages, and reactive astrocytes, which are a part of gliosis encapsulation of the implanted electrodes. The progression of events of gliosis formation around implanted cortical recording electrodes has been documented in several studies [29, 30, 37, 38, 49-59]. Although tissue reaction varies from species to species and type/size of implant, it has been shown at 1 to 2 weeks, GFAP staining reveals a reactive astrocyte region around the implants with a radius of 500 μm . This reactive region shrinks over time, and the layer of cells immediately adjacent to the implant becomes more dense and organized. At 2 and 4 weeks, activated astrocytes around the implant have

extended their processes toward the implant. At 6 weeks, the mesh of astrocytic processes has become so strong and dense that in some cases the removal of the implant did not result in the collapse of cellular processes into the implant void [58]. It is important to note that in most of the histological studies the electrodes were not connected to an external electrical connector attached to the skull, also called tethering of the probe. Such untethered electrodes may underestimate the actual reactivity caused by electrically active implants that may transmit forces caused by the connection to the implanted electrode.

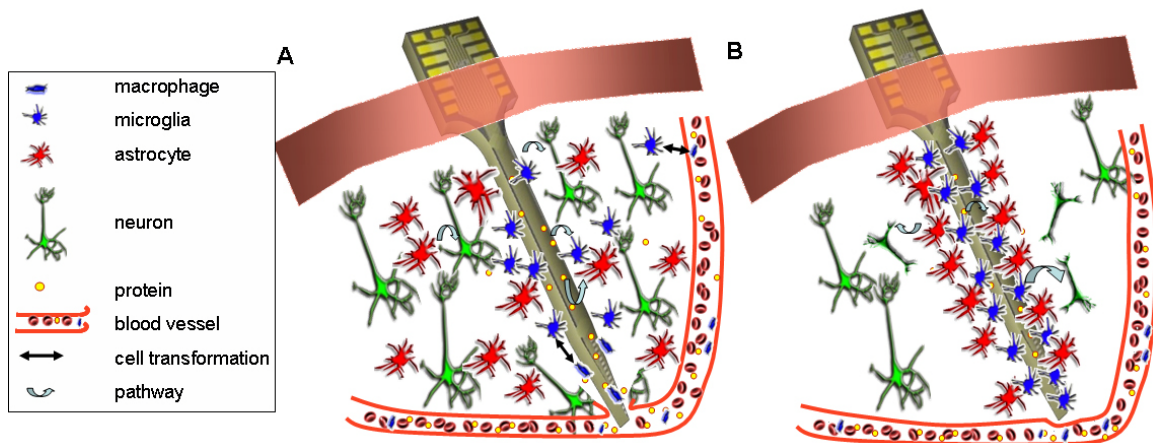


Figure 3. Schematic of the acute and chronic tissue responses following neural probe implantation. The acute response (A) is characterized by vasculature damage, neuronal injury, plasma protein adsorptions, recruitment of activated microglia, and a broad region of reactive astrocyte around the implant. The chronic response (B) is characterized by a condensed sheath of cells primarily composed of activated microglia and reactive astrocytes around the insertion site. Degeneration of neuronal processes and additional neuronal loss may also be seen [60].

1.2.3 Neuronal response at the implant/tissue interface

The density of neurons and axonal proximal to the electrode has been reported to vary from implant to implant, and even between electrodes implanted at different sites in the same animal [30, 37, 54-56, 58]. This can be due to the shape of the implant, implant placement in the brain tissue, electrode position, species differences, and gliosis formation and its implications to neuronal fate.

Several studies have reported the decrease of neuronal density around implants and have called this phenomenon a “kill zone” [30, 37, 54, 55]. The “kill zone” is defined as the region of significantly lower or nonexistent neuronal density found within approximately 50 to more than 100 μm away from the electrode. Even very small increases in the separation between the electrode and local neuronal and axon population can insulate the electrode completely, as electrodes must be within a 100 μm distance to get a significant signal. While gliosis formation effectively seals off the implant, it is also known to block neurite growth and axonal regeneration both chemically and physically [51, 61]. It has been shown that one class of molecules, chondroitin sulfate proteoglycans (CSPGs), are up-regulated by reactive astrocytes and are one of the main inhibitory molecules in glial scar and encapsulation [35].

Several other possible causes have been suggested to describe the neuronal response, such as neuronal death due to insertion trauma or chronic inflammation [37], inevitable migration and micromotion of the implant that increase the distance between the electrode and adjacent neurons [55], implant material not being attractive to neuronal attachment and growth [60], development of chronic gliosis [29, 58, 62, 63] which may suppress neuronal activity or form a sheath that isolates neurons from recording electrodes, and finally localized

neurodegeneration caused by the inflammatory persistence of the cellular encapsulation around these implants [51].

1.2.4 Hypothesis and approach

The following hypothetical assumptions are made when it comes to the failure mechanisms and degradation of neural signals: 1) Gliosis encapsulation insulates the electrode surface by reducing electrochemical impedance and impedes diffusion and perhaps current flow which in turn decrease signal to noise ratio of the recorded data, 2) Gliosis formation around the implant increases the distance of electrode surface from recording neurons by pushing away neuronal bodies, and 3) Neuronal cell death or axonal damage secondary to implantation trauma and associated with the inflammatory response reduces or eliminates electrophysiological activity. We believe that these problems could be solved by presenting the brain with a “biologically inspired electrode”. This could lead to solving the long-term goal of enhancing and sustaining neuronal connectivity with the electrode sites.

1.3 MODIFICATIONS OF NEURAL IMPLANTS

Researchers are continuously altering the material compositions and geometries of cortical arrays with hopes of discovering a combination that will allow for chronic and stable recordings. Despite numerous efforts, it might be 5-10 years until a microelectrode array design suspends the host immune response effectively and remains fully functional. The basics of the addressed problem are to ideally regulate the tissue/interface environment so that neurites are attracted to

the vicinity of the recording surface before encapsulation takes place. Gliosis suppression is another goal.

A number of ongoing surface modification studies are attempting to address the probe/tissue interface issue using different approaches. Several techniques have been attempted in order to mitigate the response of cortical tissue to implanted microelectrodes. Some studies focus on modifying probe insertion techniques, which have been shown to effect on initial implant injury response. Rennaker et al. suggest that improvement of insertion techniques, such as slow versus fast insertion, have an effect on signal to noise ratio of recordings [64]. While Kralik et al. shows improved recordings using drivable microelectrode arrays. Kralik et al. attempted to avoid the encapsulation and loss of neural signals by slowly inserting the electrode deeper into the brain tissue at different time points [65]. Several other studies are working on modifying material properties and design of the probes. These studies report that more compliant materials will reduce inflammation [28, 42], and that providing a probe with holes along the shaft will reduce gliosis and allow for neurite stability [28]. Moxon et al. reports etching the surface of electrodes by creating nano-scale surface features, increases neuronal cell adhesion, and thus increases longevity of recordings [33].

The surface properties of neural implants have been studied and modified using micro/nano surface science. The general hypothesis of these studies is that increasing electrode surface area properties will enhance recording stability. Conductive polymers have been applied to silicon-substrate microelectrodes probes to decrease site impedance [32, 66, 67]. Laminin coatings have been also applied on the surface to reduce gliosis [68]. More recently, nanotubes formed from conductive polymers have been applied to electrode sites, both reducing site impedance and providing a platform for controlled drug release [69, 70]. Systemic and local

release of anti-inflammatory molecules and drugs is a sought after approach by several researchers. Anti-inflammatory drugs such as dexamethasone have been used locally and systemically used to try to reduce activation of astrocytes and microglia at the implantation site [71-75]. Dexamethasone is a drug in the class of steroid hormones that serves as anti-inflammatory and anti-immunosuppressant. In addition, Purcell et al. show that systemic release of the drug Flavopiridol reduces the impedance due to gliosis but has no effect on recording stability [31]. Flavopiridol is an experimental drug used for inducing apoptosis in cancerous cells.

Several investigators have also proposed neural stem cells approaches to improve the biocompatibility of these electrode arrays [76-78]. Our group has shown that neural progenitor cells (NPCs) can differentiate and strongly adhere to laminin-immobilized surfaces, providing a stable matrix for these cells to be implanted in brain tissue on the neural probe's surface. In addition, NPCs were found to improve the astrocytic reaction around the implant site [78].

Although many of these methods are promising and have the same goal, none have emerged as a definitive solution to the problem of reactive tissue response. The importance of improving tissue inflammation is determinant to the recording stability of these implants for chronic applications. The main challenge remains in the lack of the ultimate solution due to the manufacturing techniques and the material composition of these probes. In this thesis, we describe one solution that could provide a better integration of the probe with the brain tissue and thus better chronic recording stability.

2.0 SURFACE IMMOBILIZATION OF NEURAL ADHESION MOLECULE L1 FOR IMPROVING THE BIOCOMPATIBILITY OF CHRONIC NEURAL PROBES: IN VITRO CHARACTERIZATION

2.1 ABSTRACT

Silicon-based implantable neural electrode arrays are known to experience failure during long-term recording, partially due to undesirable host tissue responses. Surface modification and immobilization of biomolecules may provide a means to improve their biocompatibility and integration within the host brain tissue. Here we report the immobilization of L1 and laminin biomolecules on the silicon surface and compare their effects on neuronal and astrocyte cultures *in vitro*. Laminin, an extracellular matrix (ECM) protein that interacts with a variety of cell types, is known to be an excellent substrate for neuronal attachment and growth. L1 is a neuronal adhesion molecule that specifically promotes neurite outgrowth and neuronal survival. Silane chemistry and the heterobifunctional coupling agent, 4-Maleimidobutyric acid *N*-hydroxysuccinimide ester (GMBS), were used to covalently bind these biomolecules onto the silicon surface. Surface immobilization of biomolecules was verified by goniometry, dual polarization interferometry (DPI), and immunostaining techniques. Silicon dioxide coated wafers were used to mimic the surface of silicon-based implantable neural probes. After covalently binding the biomolecules, polyethylene glycol (PEG)-NH₂ was used to cap the unreacted GMBS

groups. Primary murine neurons and astrocytes were used to evaluate the interaction of the modified surfaces. Both L1 and laminin modified surfaces promoted neuronal attachment, while the L1 surface demonstrated significantly higher levels of neurite outgrowth ($p < 0.05$). In addition, the laminin surface promoted astrocyte attachment, while the L1 surface showed significantly reduced levels of astrocyte attachment relative to controls ($p < 0.05$). These results demonstrate the unique properties of L1 as a potent promoter of neurite outgrowth and a possible inhibitor of astrocytes. This further illustrates L1's vast potential to improve the biocompatibility and chronic recording performance of neural probes.

2.2 INTRODUCTION

Silicon-based neural probes that permit recording and stimulation of specific sites in the brain experience failure during long-term recording, partly due to biocompatibility issues [2, 37, 60, 79]. Their inability to chronically interface with the neurons in the brain is an imminent obstacle to their use in clinical applications, such as treatment of full or partial paralysis, which requires these implants to maintain a stable performance for the lifetime of the recipient.

Implanted electrodes record brain activity by detecting extracellular field potentials of neurons in reference to a ground. The closer the electrode is to a neuron, the better the signal strength and the quality of the recordings. To obtain reliable signals, the distance from microelectrode to neuron should be within 50-100 μm range [54, 59, 80].

Immunohistological examinations have shown a significantly lowered neuronal density around the implant at different time points [37, 58, 59]. Several possible causes have been

suggested. First, current implants are anchored to the skull on one end, and remain floating in the brain tissue on the end where the recording sites are located. Migration and micromotion of the implant occur, which may increase the distance between the electrodes and the neighboring neurons, as well as cause chronic inflammation [55]. Second, current implant material is not attractive to neuronal attachment and growth [29]; therefore neuronal processes may tend to migrate away from the implant. Furthermore, neuronal death or degeneration may occur simply through insertion of the probe or through factors that are released during chronic inflammatory responses [37, 51].

Chronic gliosis results in glial sheath formation, which encapsulates the probe and isolates it from the surrounding brain tissue (Figure 3). Gliosis is believed to be mediated by macrophages, activated microglia, and reactive astrocytes. The reactive astrocytes are characterized by enhanced migration, proliferation, hypertrophy, upregulation of GFAP, and increased matrix production. The glial sheath, including a mesh of astrocytic processes, is formed after 2 weeks (Figure 3A), becoming compact and dense over a period of 6 weeks [2, 29, 37, 49, 55, 58-60, 79, 81] (Figure 3B). Gliosis is hypothesized to cause significant impairment of implant functionality by increasing the electrode impedance, decreasing local neuron density, and reducing axonal regeneration around the implant [37, 49, 54, 59].

Several studies have addressed different methods of improving the performance of the chronic neuron-implant interface by modifying these implants using novel biomaterial and cellular designs. Some approaches use surface immobilized cues to improve the attachment and growth of neurons, including electrochemical deposition of conducting polymers and neuron promoting biomolecules on the electrodes [67, 82, 83], covalent immobilization of bioactive laminin-derived peptides on dextran-coated [84] and amino silane-modified silicon substrates

[85], electrostatic layer-by-layer deposition of laminin [86], microcontact printing of poly-L-lysine [87], and electrospinning of silk-like polymer containing the laminin fragment IKVAV [88]. Soluble cues such as nerve growth factor and dexamethasone have also been incorporated for controlled-release to promote neuronal ingrowth or reduce glial inflammation [71, 74, 89], in addition to studies using drug reducing agents to decrease this inflammation [31]. Others have proposed modification techniques using adult neural stem/progenitor cells on the surface of the probe for better integration of implant and tissue [76-78].

Many of the research efforts described above immobilize laminin or sequences of laminin onto the surface of neural probes for improved biocompatibility [82-86, 88]. Laminin is an extracellular matrix protein (ECM) and basement membrane component that has been shown to promote attachment of various cell types including neurons, astroglia, and fibroblasts [88, 90-92]. This fact highlights the shortcoming of using non-neuron specific laminin on the surface of neural probes where an enhanced glial response is undesirable [37, 60]. The ideal surface modification for a neural probe would promote only neuronal attachment and neurite ingrowth, while minimizing glial attachment and proliferation. L1 is a neural cell adhesion molecule, which is expressed in developing and differentiated neurons of the central nervous system (CNS) and Schwann cells of the peripheral nervous system (PNS) [93-95]. L1 mediates neuron-neuron adhesion via homophilic binding and has been shown to promote neurite outgrowth and neuronal attachment *in vitro* [96-99]. Unlike ECM proteins, L1 comes from the immunoglobulin family and is known to show tightly regulated patterns of expression during development of the nervous system, as well as selectivity in cellular binding partners [95, 100]. When surface-bound, human recombinant L1 supports significantly higher levels of neuron attachment and neurite outgrowth relative to the ECM protein fibronectin and poly-D-lysine, while inhibiting the attachment of

astrocytes, meningeal cells, and fibroblasts [99]. For these reasons, L1 was chosen as a candidate molecule to modify the silicon surface of neural probes to specifically promote neuronal attachment and inhibit glial cells. The long-term objective of this research is the improvement of neuron-electrode compatibility *in vivo* for further enhancement of long-term recording capabilities.

In this work, L1 is purified from murine brain tissue. To compare the efficacy of L1 and laminin as substrates for neuronal or astrocytic cell attachment and growth, these proteins were covalently immobilized on silicon dioxide wafers along with polyethylene glycol (PEG). Surface analysis, including water contact angle measurements, dual polarization interferometry (DPI) [101], and immunochemistry, were performed to characterize the modified silicon surfaces. Quantitative assessment of neuron and astrocyte attachment, and neurite outgrowth on the different silicon surfaces was performed with primary cultures and by using immunohistochemistry and fluorescent imaging techniques.

2.3 MATERIALS AND METHODS

2.3.1 Surface modification and characterization

2.3.1.1 Isolation and purification of the L1 protein

The cell adhesion molecule L1 was purified by immunoaffinity chromatography as described by Lagenaur et al.[96]. The L1 protein was affinity purified from detergent-containing extracts of crude membrane fractions of murine brains using 5H7 coupled monoclonal antibody packed columns. The membranes were solubilized in 1% 3((3Cholamidopropyl)dimethyl-

ammonio)-propanesulfonic acid (CHAPS) (Anatrace), centrifuged at 40,000 g for 30 min, and the supernatant was applied two times down the column. The antigen was eluted with 0.1 M diethylamine (Sigma-Aldrich) at pH 11.5 and immediately neutralized with 1M Tris(hydroxymethyl)-aminomethane hydrochloride (Sigma-Aldrich) at pH 6. The diethylamine and Tris still present in the collected L1 solution was removed by dialyzing against phosphate buffer saline (PBS) (Sigma-Aldrich) one day prior to use. All of the above procedures were performed at 4°C.

L1 protein concentration was measured by the FluoroProfile (Sigma-Aldrich) epicocconone-based reagent kit [102]. The fluorescence was measured by a fluorimeter (SpectraMax M5, Molecular Devices) using different concentrations of bovine serum albumin (BSA) (Sigma-Aldrich) as standard.

2.3.1.2 Covalent biomolecule immobilization

Silicon wafers (p type <100> oriented) coated with 2500 Å wet thermal oxide (International Wafer Services Inc., CA) were used to mimic the non-conductive silicon dioxide surface of the probes. Wafers, 7.62 cm in diameter, were cut into approximately 1x1 cm samples with a diamond pen. The heterobifunctional crosslinker method described by Bhatia et al. [103], was modified to covalently immobilize proteins on the silicon substrates. The silicon samples were cleaned and hydroxylated with HNO₃ (8.0 Normal) (Sigma-Aldrich) for 30 minutes, followed by immersion for 5 minutes each in alcohol and chloroform (Sigma-Aldrich). The cleaned samples were immersed in a 2% solution of (3-mercaptopropyl) trimethoxysilane (MTS) in dry toluene (Sigma-Aldrich) for 2 hours in a glove bag under N₂ inert gas. The thiolated samples were then rinsed in dry toluene, followed by immersion in absolute alcohol, and

treatment for 1 hour with 4-maleimidobutyric acid *N*-hydroxysuccinimide ester (GMBS) (Sigma-Aldrich) dissolved in a minimum amount of *N,N*-dimethylformamide (DMF) (Fisher Scientific) and diluted in absolute alcohol to a final concentration of 2 mM. The samples were then washed three times and immersed in absolute alcohol for 15 min in preparation for transfer to a sterile hood. Three different concentrations of L1 (25µg/ml, 50µg/ml, or 100 µg/ml) or 40 µg/ml laminin (Sigma-Aldrich) were applied for 1 hour at 4°C on the GMBS surfaces where the protein solutions formed a circular droplet. The biomolecule-immobilized samples were rinsed with PBS, and treated with 100 µM mPEG-NH₂ (Nektar) solution for 30 min to cap any active NHS ester groups of the GMBS still present on the surface. The control PEG samples were treated with only 100 µM mPEG-NH₂ solution for 30 minutes right after the crosslinker step. A schematic representation of the immobilization is given in Figure 4.

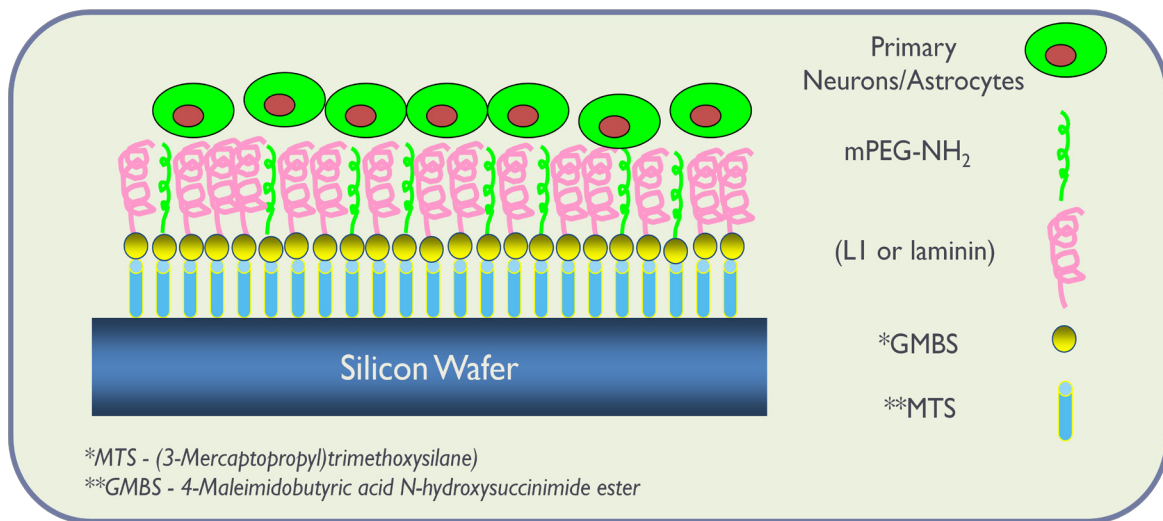


Figure 4. Schematic representation of the biomolecule immobilization process. L1 or laminin were covalently immobilized on MTS treated silicon substrates, using the heterobifunctional crosslinker GMBS. mPEG-NH₂ was used to cap the unreacted GMBS groups.

2.3.1.3 Surface characterization

To verify the steps of surface chemical reactions, wettability of the surfaces after each step of treatment was characterized by water contact angle measurements. The measurements were performed with a VCA-Optima contact angle system (AST Products Inc.). Approximately 0.5 μL deionized water (18.2 $\text{M}\Omega\cdot\text{cm}$) drops were placed on the surfaces using a micro-syringe. Contact angle values were calculated from the captured image files using the software provided (VCA Optima XE) by the manufacturer. Three measurements per condition were analyzed and were taken promptly after completion of each modification step followed by drying under N_2 .

The thickness, mass, and density of the multilayer structure present after each step of biomolecule immobilization were performed using the dual polarization interferometry (DPI) analytical biophysical technique. This technology allows for measuring of structural changes in real time and at subatomic resolution of reacting biomolecule layers at the solid-liquid interface [101]. *AnaLight*® Bio200 interferometer (Farfield Scientific Inc, USA) was used during experiments. The instrument measures two polarization responses traversing through a multilayer waveguide chip. Changes in the resulting optical interference pattern, caused by perturbation and interaction of immobilized species within the evanescent field created above the waveguide surface, are measured over time. Movement of the interference fringe pattern or phase shifts are converted into thickness and refractive index directly using Maxwell's equations. Immobilized density (surface layer concentration) and mass (amount of immobilized biomolecule) can also be derived from these values. L1 or laminin was coated onto the surface of channels of a MTS waveguide chip treated with the GMBS crosslinker. PBS (pH 7.4) served as running buffer at 30 $\mu\text{l}/\text{min}$. L1 and laminin were each loaded and injected in the same buffer and mPEG-NH₂ was loaded during the last step to keep the procedure consistent throughout all

experiments. Data was collected and analyzed using *AnaLight*® DAQ and Explorer proprietary software.

In addition, immunostaining against L1 was performed to qualitatively verify the successful immobilization of this biomolecule. The L1 protein was immobilized on the crosslinker modified samples in a known circular area. The L1 immobilized samples were incubated for 45 minutes in 10% goat serum (GS) (Sigma-Aldrich) in PBS and stained with 5H7 L1 monoclonal primary antibody at 4°C overnight, followed by 2 µg/ml Alexa 488 (Invitrogen) secondary antibody in 10% GS for 1 hour. Digital images of the stained samples were taken using a fluorescence microscope.

2.3.2 Bioactivity and stability of immobilized L1

The bioactivity of different concentrations of immobilized L1 (25, 50, and 100 µg/ml) was quantitatively verified by primary mouse neuronal cell cultures (details in the next section). Nitrocellulose coated glass samples with different adsorbed L1 concentrations were used as positive controls. Bioactivity was indicated by neuronal growth, attachment, and visible neurite outgrowth one day after mouse cerebellum cell cultures.

The stability of 100 µg/ml L1 was evaluated by incubation of the modified samples in DMEM media without added growth factors, for 0, 3, and 7 days at 37°C in 5% CO₂. The L1 present on the surface at the different time points was quantified by measuring the gray level intensity of the L1 immunostained images.

2.3.3 *In vitro* experiments

2.3.3.1 Primary neuron and astrocyte cell cultures

E18 Sprague Dawley rat cortices were purchased from BrainBits, LLC. Neuronal cell culture was performed following the methods by Brewer et al. [104]. The rat cortices were triturated with a 1 ml pipette and removed from Hibernate Media™ (Brain Bits, IL) by centrifugation at 800 x g for 1 minute. The cells were re-suspended in Neurobasal (Fisher)/B27 (Gibco)/0.5 mM glutamine/25 μM glutamate (Sigma-Aldrich) culture medium. Cell counts were performed using trypan blue and cells were plated at a density of 1.5×10^5 cells/cm². These rat cortical neurons were grown in culture for three days at 37°C in 5% CO₂. During preliminary bioactivity verification experiments, fresh mouse cerebellum neuronal cell cultures were cultured at a cell density of 1.5×10^5 cells/cm² in serum based media containing 10% horse serum (HS) (Hyclone) and Dulbecco's Modified Eagle's Medium (DMEM) (Gibco). These mouse cerebellum neurons were grown for one day at 37°C in 5% CO₂. Astrocyte enriched cultures were prepared by tryptic digestion of a rat cortex or mouse cerebellum. The resulting suspension was plated on uncoated tissue culture plates and grown in DMEM with 10% fetal calf serum (FCS) (Hyclone). These glial cells were passaged once a week, up to 4 weeks. For experiments, glia were treated with 0.25% trypsin (Sigma-Aldrich), and plated at 1.5×10^5 cells/cm² in 10% FCS/DMEM. Astrocytes were grown in culture for two days at 37°C in 5% CO₂.

Surface modified silicon samples were placed in 24 well cell culture plates (Corning Costar). 20 μL drops of high density cell suspensions were plated on the silicon samples and incubated for one hour. The corresponding media for neuron or astrocyte culture was flooded into the chamber following this period. Ten samples per condition were used during these

experiments and the protocol was repeated three times to observe reproducibility. Nitrocellulose coated glass coverslips with adsorbed L1 served as positive controls for cell growth throughout *in vitro* experiments.

2.3.4 Immunocytochemistry

Prior to immunochemical labeling the cells were fixed in 4% paraformaldehyde for 10 min. Monoclonal antibodies against neuronal class III β -tubulin (Covance) and the astrocyte-specific marker glial fibrillary acidic protein (GFAP) (Dako) were used. The samples with attached cells were incubated for 45 minutes in 4% GS and PBS to block nonspecific binding. Then the samples were incubated for 1 hour at room temperature in anti- β -tubulin III (2 μ g/ml) in 4% GS or anti-GFAP (0.4 μ g/ml) in 4% GS. Following three washes in PBS, the samples were incubated for 1 hour in Alexa 488 goat anti-mouse secondary (2 μ g/ml) in 4% GS. Cells were counterstained using the nuclear dye Hoechst 33258 (Sigma-Aldrich) (2 μ g/ml) in PBS.

2.3.5 Data collection and analyses

Digital images of the stained cells were taken using a fluorescence microscope. Cell counts and neurite measurements on the β -tubulin III and GFAP stained images were obtained using the software MetaMorph™ (Molecular Devices, PA). Neuron attachment was determined by counting the number of neurons that showed co-localization of β -tubulin III and Hoescht nuclear stain and had at least one neurite longer than cell body dimensions. Astrocyte attachment was determined for cells that showed co-localization of GFAP and Hoescht nuclear stain. Cell

attachment was analyzed for 10 (20x magnification) viewing fields per sample for a minimum of 10 random samples per experimental condition.

Neurite outgrowth was measured as the total path length of the longest neurite that extended from each cell body. Neurite length data is presented as an average length per cell number in 10 (20x magnification) viewing fields per condition.

2.3.6 Statistical analyses

Statistical analysis were performed using the analytical software SPSS[®] (SPSS Inc., IL). For experiments that involved the comparison of two conditions the standard Student's t-test ($\alpha=0.05$) was performed. For comparisons involving multiple conditions, ANOVA followed by Bonferroni's post-hoc analysis was used ($\alpha=0.05$).

2.4 RESULTS

2.4.1 L1 Protein Purification and Surface Characterization

The L1 protein was purified from young murine brains. The concentrations of the L1 protein solutions were quantified after each purification using the FluoroProfile protein assay. The concentration of L1 was found to be approximately 100 ± 15 $\mu\text{g/ml}$ per batch.

Silane chemistry and the heterobifunctional crosslinker GMBS were combined to immobilize L1 and laminin on the silicon dioxide surfaces. Water contact angle measurements for each reaction step and the summary of the data are shown in Table 1. After cleaning with

HNO₃, the silicon surface exhibited a low initial contact angle of 27.3±1.4°. HNO₃ treatment created a clean hydrophilic silicon surface upon each subsequent functionalization of the other biomolecules could be carried out. After 2 hrs in MTS the silicon surface exhibited a significantly higher contact angle (66.2±1.3°) than cleaned silicon (p<0.05). The significant increase of hydrophobicity of the MTS layer indicates the successful attachment of this molecule (Table 1). The subsequent surface after immersion for 1 hr in the GMBS crosslinking solution displayed a decreased contact angle of 58.5± 1.6°. The decrease of hydrophobicity after GMBS treatment indicated the successful covalent binding of the crosslinker to the MTS linked surface. Both protein-PEG treatments increased the GMBS surface's hydrophobicity, with laminin-PEG and L1-PEG surface contact angles being 75.1±1.8° and 69.8±1.7°, respectively. This is expected since these proteins are relatively hydrophobic as indicated by the significantly higher contact angles for the adsorbed samples (85.0±1.6 ° and 70.1±1.5 °, respectively). PEG-NH₂ adsorbed on clean silicon exhibited a low contact angle (24.7±1.5°) differing significantly from mPEG-NH₂ immobilized on the GMBS treated surface, 59.1±1.3°. This difference may indicate an insufficient coverage of this molecule on the surface, in which case exposed GMBS surface, is affecting the readings.

Table 1. Water contact angle measurement for covalent immobilization of different molecules to silicon surface (°). Data are expressed as mean±S.E.M.. Abbreviations (I-Immobilized, A-Adsorbed) (n=18).

SiO ₂ (U)	MTS	GMBS	Laminin-PEG	L1-PEG	PEG(I)	PEG(A)	laminin(A)	L1(A)
27.3 ± 1.4	66.2 ± 1.3	58.5 ± 1.6	75.1 ± 1.8	69.8 ± 1.7	59.1 ± 1.3	24.7 ± 1.5	85.0 ± 1.6	70.1 ± 1.5

The surface immobilization of L1-PEG, laminin-PEG, and PEG were characterized using dual polarization interferometry. DPI provides direct information on thickness and refractive

index of the surface layers. The thickness of the immobilized layer, measured in Angstroms, provides an absolute quantification of surface bound molecules along one axis. Density and mass values, when considered together with thickness, can give an accurate indication of the orientation of biomolecules at the solid-liquid interface. When compared to known crystal structures, this can provide important information pertaining to the accessibility of active sites within the protein structure or even the degree to which the protein structure deforms and denatures on the solid substrate. Step by step characterization of the binding events are shown in Table 2. The immobilized L1, laminin, and PEG biomolecules had a mass amount of 2.67, 2.97, and 0.24 ng/mm², respectively. The surface density of the L1-PEG, laminin-PEG, and PEG layers was found to be 0.54, 0.28 and 0.64 g/cm³, respectively (Table 2).

Table 2. Quantitative DPI data on real-time changes in dimension (resolution <0.1Å) and density (resolution <0.1 picogram/mm²). Immobilized L1, laminin, and PEG layers are expressed in terms of thickness and refractive index. Density and mass of the layers can be calculated from the refractive index.

	Refractive Index	Thickness nm	Mass ng/mm ²	Density g/cm ³
GMBS	1.46	1.03	0.70	0.67
L1	1.43	6.37	3.37	0.53
L1-PEG	1.43	6.26	3.37	0.54
GMBS	1.44	0.87	0.50	0.58
laminin	1.38	12.66	3.41	0.27
laminin-PEG	1.39	12.25	3.47	0.28
GMBS	1.44	0.89	0.55	0.62
mPEG-NH ₂	1.45	1.24	0.79	0.64

Specific antibody staining for the L1 protein confirmed the presence of immobilized L1 on the GMBS modified surface. 5 μl of L1 was applied forming a bubble onto the surface (Figure 5A). The intensity was higher at the edge of the L1 drop due to surface tension effects.

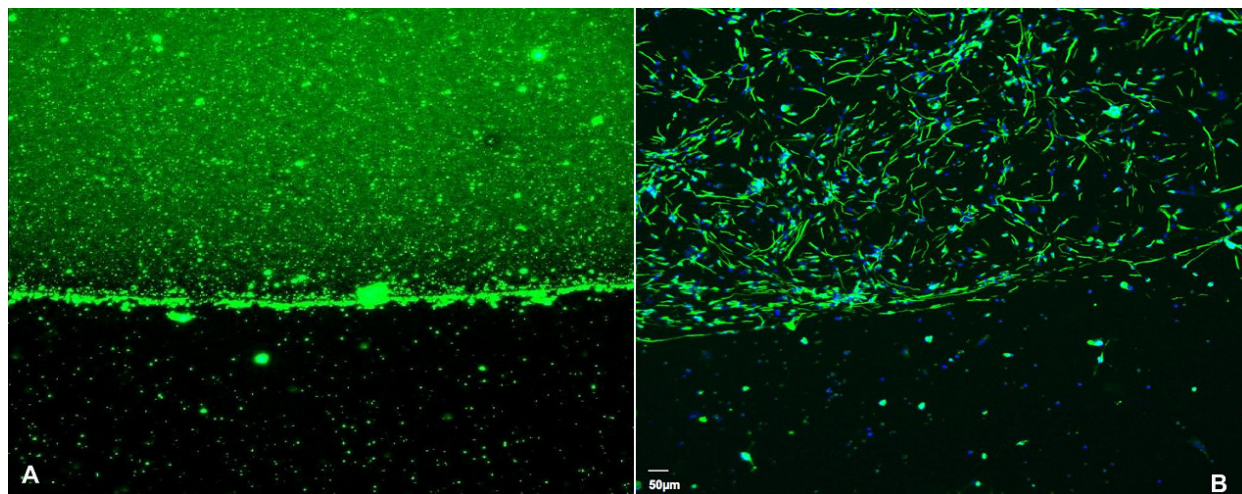


Figure 5. Surface analysis of L1-PEG samples. (A) Alexa 488 antibody staining of L1 protein immobilized on a circular surface area. (B) Mouse neuronal cell growth on the area where L1-PEG is immobilized after one day in culture. Scale bar 50 μm .

2.4.2 L1 Bioactivity and Stability

Mouse cerebellar cells were plated on surfaces treated with different concentrations of L1 and the β tubulin III positive cells were counted after 1 day of growth (Figure 5B). The neuron attachment increased with the increase of L1 concentration used for immobilization, indicating that L1's bioactivity is dose-dependent. Specifically, at the lower L1 concentration of 25 $\mu\text{g}/\text{ml}$ neuron attachment was 108 ± 17 cells/ cm^2 , and at 100 $\mu\text{g}/\text{ml}$ of L1 neuron attachment was 404 ± 36 cells/ cm^2 (mean \pm s.e.m.). Qualitatively, we observe that the surfaces treated with higher

concentration of L1 show longer neurite extension. This concentration effect can also be observed in figure 5B, in which neurites are the longest around the edge of the L1 drop where L1 is most concentrated.

The L1 concentration (100 $\mu\text{g/ml}$) that promoted adequate neuron attachment and neurite outgrowth was chosen to be used for the rest of the *in vitro* experiments for quantitative analysis.

The stability of the L1 coating was evaluated by incubation of L1 immobilized samples in DMEM media at different time points. The gray level intensity of the immunostained L1 spot after 3 days did not show any significant change respective to day 0. However, after 7 days the intensity of the L1 stained spot significantly decreased by 25% respective to day 0.

2.4.3 *In vitro* cell culture tests

2.4.3.1 Neuronal attachment and neurite outgrowth

As mentioned before, L1 is a cell adhesion molecule that promotes neurite extension and neuronal survival, while laminin is a multifunctional ECM protein that associates with several cell types. Here, we investigated the effects on neuronal growth and neurite extension on different surface modifications using primary rat cortical neurons cultured in a defined media containing Neurobasal, B27, glutamine, and glutamate. Primary neuron attachment and neurite outgrowth data are shown in Figure 6.

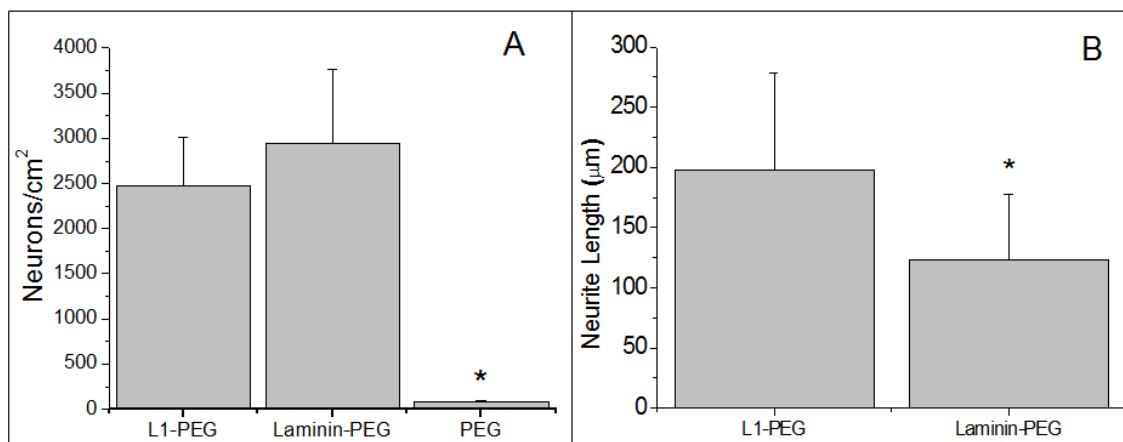


Figure 6. Neuron attachment reported as average neurons/cm² ± s.e.m.(A) and average neurite outgrowth reported as average neurite length ± s.e.m. (B) of primary rat cortical cells on silicon surfaces with immobilized laminin-PEG, L1-PEG, and PEG (*p<0.05).

Neuron attachment was seen only on the surfaces with immobilized laminin-PEG, L1-PEG, and PEG. The clean silicon surface, MTS, and GMBS immobilized surfaces, used as controls, did not support neuron attachment. The density of neurons was significantly lower on the PEG surfaces (p<0.01). There was no significant difference on neuronal density between the L1 and laminin immobilized surfaces (Figure 6A). However, neurite outgrowth, shown in figure 6B, demonstrated that the average length of neurites on L1-PEG immobilized surfaces was significantly higher than on laminin-PEG immobilized surfaces (p<0.05). The length of neurites on PEG surfaces was not quantified due to the very sparse neuron attachment. Representative fluorescent images of these data are shown in figure 7.

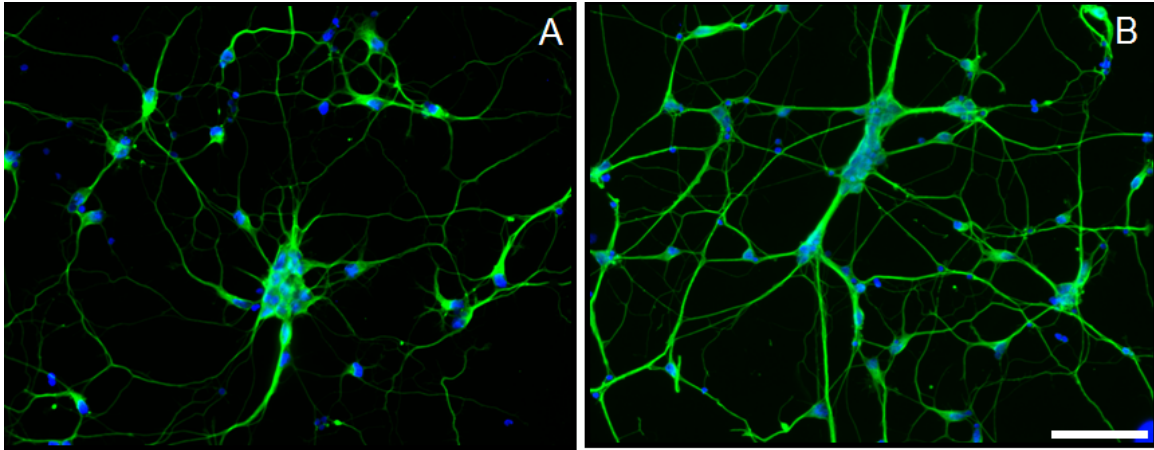


Figure 7. Representative images of primary rat cortical neurons plated on silicon surfaces with immobilized (A) laminin-PEG and (B) L1-PEG, after 3 days in culture. Cells were stained for β -tubulin III (green) and the nuclear stain DAPI (blue). Scale bar 100 μm .

2.4.3.2 Astrocyte attachment

Astrocytic cells play a major role in the brain/tissue response to implants. Therefore, it is imperative to characterize the attachment and growth on candidate surfaces. The attachment of primary astrocytes to silicon surfaces immobilized with either laminin-PEG, L1-PEG, PEG or no modification are compared in figure 8A. Unmodified silicon surfaces showed attachment and growth of astrocytes. A significant two-fold increase in the number of attached astrocytes was observed on the laminin-PEG immobilized surfaces compared to control. Statistical analysis showed no difference between PEG surfaces and unmodified control. On the other hand, the number of astrocytes on the surface with L1-PEG immobilized was significantly lower than any other surfaces ($p < 0.05$).

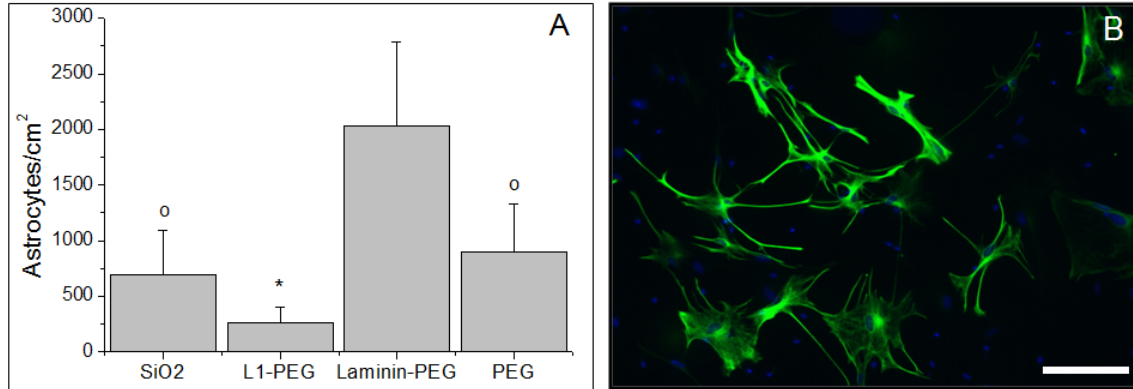


Figure 8. (A) Astrocyte attachment on silicon surfaces with immobilized L1-PEG, laminin-PEG, PEG, and unmodified SiO₂ surface reported as average astrocytes/cm² ± s.e.m. (*p<0.05 against all conditions, and op<0.05 against laminin-PEG). (B) Representative image of primary rat cortical astrocytes plated on silicon surfaces with immobilized laminin-PEG after 2 days in culture. Cells were stained for GFAP (green) and the nuclear stain DAPI (blue). Scale bar 100 μm.

2.5 DISCUSSION

Silicon neural probes that can record single-unit activity from the cortex of animals or human patients for research purposes or clinical applications have been under development for the past 30 years [2, 60]. The most challenging problem is how to maintain a healthy neuron-electrode interface for long-term applications. The goal of our study is to address biocompatibility issues between the probe and the brain tissue, which are thought to contribute to the chronic failure of these devices.

In order to record single-unit activity in the brain, recording electrodes must be in intimate contact with the signaling neurons of the host. Previous work has made significant progress improving the electrical and biocompatible properties of the recording electrodes on silicon based neural probes [66, 67, 74, 82, 83]. However, the recording electrodes account for

only a small percentage of the total surface area of this device, which is made of silicon. The underlying motivation for the research described here is that the silicon surface will be the most important factor in mediating the macroscopic biological responses due to its relatively large area.

An ideal surface modification for a neural probe will maintain the density of neurons in close proximity while at the same time retarding reactive gliosis. Previous research has shown that L1 promotes survival and growth of neurons and neurite extension [93, 96, 97]. Furthermore, evidence has demonstrated that L1 enhances neuronal differentiation of neural precursors and inhibits astrocytic differentiation via heterophilic interactions [98]. The feasibility of using these properties to the advantage of silicon probes is investigated here through cell culture studies where silicon wafers are used as a substrate in place of traditional cell culture substrates like tissue-culture polystyrene, glass, or nitrocellulose. A common approach to improving biocompatibility is deposition of laminin on the surface of silicon probes [86]. In this study laminin is used as the standard to which L1 functionality is compared. The first requirement for recording is neurons in close proximity to the probe, and laminin is an excellent substrate for neural adhesion. Our results indicate that L1 is just as effective at promoting neuron attachment to silicon surfaces as is laminin. Furthermore, it was observed that neurons which do in fact attach to the L1 surfaces extend significantly longer neurites compared to neurons attached to laminin. The implications of this for the long-term stability of recordings is still unclear, although from this observation we hypothesize that the neurons are “healthier” and more likely to remain in intimate contact with the probe over a long period of time.

The method of depositing a biomolecule on a surface can have significant implications to its specific functionality, as well as towards how the host and the probe interact in general. A

myriad of approaches exist for deposition of molecules that range from simple absorption to patterned micro-contact printing. Silicon dioxide surfaces can be conveniently functionalized to allow covalent attachment of molecules on the surface. Biomolecules are attached to the silicon substrate through two “linking” molecules. The first linking molecule (MTS) utilizes silane chemistry to form an S-O-S connection to the silicon surface. It then presents a sulfhydryl group for the second layer to interact with. The second linking molecule (GMBS) is termed a heterobifunctional crosslinker because of its activated *N*-hydroxysuccinimide (NHS) esters and maleimide functional groups, and their ability to react with amine and sulfhydryl groups, respectively. Using the GMBS heterobifunctional crosslinker offers an advantage over homobifunctional crosslinkers such as glutaraldehyde, which may self-cross link and result in poorly defined layer structures and poor reproducibility (seen in our preliminary trials). Based on the DPI data, the surfaces modified using the above chemistry present a well-defined monolayer of protein. L1 appears to be a globular-like structure when covalently immobilized on the GMBS treated surface. This can be observed by the thickness data (6.37 nm) and the density data (0.53 g/cm^3) suggesting that when this protein is on the surface it is closely packed. In addition, when PEG is added on the L1 surface, the mass and density doesn't significantly change, suggesting that the L1 protein is tightly packed and almost fully reacted with all NHS ester groups. In contrast, laminin portrays an elongated structure based on its high thickness (12.66nm) and its low density (0.27 g/cm^3). The significant change in mass between laminin and laminin-PEG layer suggests that there is space between immobilized laminin, which allow for reaction of PEG with the free NHS ester groups. The observed laminin spacings are probably due to steric hindrance effects between the chains of this protein. When PEG is immobilized on the GMBS surface alone the thickness and mass changes are low, suggesting that this molecule due

to its long chain is folding on the surface and forming a thin and packed layer. The folding of the PEG molecule on the surface might not allow for functional immobilization of this molecule. This improper immobilization is also suggested by the hydrophobicity of this surface implying the exposure of the underlying surface.

In vitro models can be a gross oversimplification of the *in vivo* situation. The goal of this study was simply to explore the potential for L1 to mediate close contact with neurons. For this reason, it was decided that the neuron culture should be performed in a serum-free media. While the absence of serum proteins makes this model even more remote from the *in vivo* situation, it does allow for better isolation of the functionality of the surface. In undefined media, serum proteins will adsorb to the surface and mediate cell attachment. The goal was to prepare a surface, which mediated promotion of neuron attachment, and the model was appropriate. Conversely, the goal of the astrocyte studies was to examine whether the surface could limit their attachment and growth. For this purpose, a serum based culture model was more appropriate since the defined Neurobasal media does not favor the growth of astrocytes and would cloud the effects due to the surface alone. It has been shown previously that L1 surface selectively promoted neuronal growth in the mixed culture of neurons, astrocytes and fibroblasts [99]. The crucial portion of our results is that even in the presence of serum proteins; astrocytes do not attach and grow well on L1 surface. It is interesting to hypothesize about the mechanism behind this.

Astrocytes attached on cleaned silicon surfaces without any pretreatment in serum containing media. They presumably do so by binding to the cell adhesive serum proteins adsorbed on the artificial surface. The PEG treated surfaces are supposed to minimize protein adsorption thereby minimizing cell attachment [105]. However, as pointed out before, our

covalently bound PEG surface is mildly hydrophobic which mitigates the ability of PEG to prevent protein fouling and further cell attachment. In the case of the laminin-PEG surface, higher concentration of binding sites on laminin than the adsorbed serum protein lead to higher astrocyte binding and growth. The surface characterization suggests that most of the GMBS binding sites were occupied by L1 and little PEG is actually present. In this case then the decreased astrocyte attachment should be a result of the surface bound L1. The direct effect could come from L1's bioactivity. As mentioned, L1 has been found to inhibit the astrocytic differentiation of neural precursors and proliferation of astrocytes [98]. The exact mechanism has not been discovered, but we speculate that the same signaling pathway might have inhibited the attachment and growth of astrocytes in our experiment. Since astrocytes need to bind to the cell-adhesive serum proteins to attach to the artificial surface, the reduced astrocyte counts could also originate from the reduction of non-specific serum protein adsorption of the L1 bound surface. Pre-adsorbed albumin surface is well known to be anti-fouling [106]. The immobilized L1 may present a surface chemistry similar to albumin that leads to less protein adsorption. Future protein adsorption studies may shed more light on this issue.

A further consideration is the implementation of these methods to long term recording situations. The stability tests show that the L1 coating is not stable over 7 days at 37°C in media. This suggests that the immobilized L1 itself would not be responsible for the long term survival and interaction of neurons with the recording probe. We hypothesize however that the stability of this coating is sufficient for the initial attachment of neurons and neurite outgrowth. In other words, it seems as though the L1 coating is sufficient to provide the neurons a "foothold" in the critical region where recording is possible. Combined with L1's observed effect on astrocyte

attachment, this possibly could alter the initial conditions of the implant milieu enough that the long term dynamics are also altered.

These results are promising for the objective of this study. They suggest that if L1 is immobilized on the probe's silicon surface, it can support neurons and promote neurite extension toward the surface of the probe. In addition, since astrocyte growth is not promoted, the astrocytic reaction around the implanted probe may be reduced.

2.6 CONCLUSIONS

L1 protein can be successfully immobilized on the silicon surface in a fashion, which retains its functionality. In a defined culture system, L1 enabled high-density neuronal attachment and promoted significantly longer neurite outgrowth compared to surfaces with immobilized laminin. Furthermore, while the laminin surface promoted the growth of astrocytes, the L1 surface greatly reduced astrocyte attachment compared to both laminin and control samples. In conjunction with previous work focused on promoting improved electrical properties and enhanced neuron attachment at the electrode sites, this work opens a path to a comprehensive surface modification approach for existing technologies to enable a stable, long-term neural interface for neuroscience research and clinical applications.

3.0 L1 SURFACE MODIFICATION OF SILICON BASED NEURAL PROBES MAINTAINS NEURONAL DENSITY AND MITIGATES GLIOSIS AT THE IMPLANT/TISSUE INTERFACE

3.1 ABSTRACT

Chronically implanted neural electrode arrays have the potential to assist patients suffering from various neurological traumas or neurological disorders. While these electrodes perform well in acute recordings, they often fail to function reliably during clinically relevant chronic settings, due to loss of neurons and gliosis encapsulation. Surface modification of these implants may provide a means to improve their biocompatibility and integration within the host brain tissue. We propose a method to improve the brain-implant interface by modifying the probe's surface with the neural adhesion molecule L1. L1 may introduce a biological neuron friendly environment to maintain healthy neuronal density around the recording electrodes, and consequently reduce gliosis formation. In this study, we assess the tissue response of L1 modified vs. non modified (NM) control silicon based neural probes implanted in the rat cortex at acute and chronic time points. The potential impact of L1 on neuronal health and survival and glial cell activations are evaluated with extensive immunohistochemistry and quantitative image analysis.

The results of our study show that glial inflammation persists in the surroundings of the NM control probes at all tested time points in rat cortex. In addition, significant decreases of neuronal and axonal densities were seen in the vicinity of the NM control probe. On the other hand, the immediate area (100 μm) around the L1 modified probe showed no loss of neuronal bodies and a significantly increase of axonal density relative to the NM control probe. Significantly less microglia and astrocyte activations were observed in the surroundings of the L1 modified probe than the NM control probe. These improvements in tissue response induced by the L1 coating are likely to lead to improved functionality of the implanted neural electrodes during chronic settings.

3.2 INTRODUCTION

Microfabricated neural electrode arrays can be implanted in the brain to stimulate or record populations of neurons with single neuron resolution. These devices have advanced several fields of neuroscience research. One such field is the study of brain-machine interfaces, where recorded neuronal signals from the brain are used to control an external device such as a computer cursor or a robotic arm [2, 11, 25, 27, 60, 107] (Figure 9). These studies have paved the way for cortical neural prostheses, which could potentially benefit patients with full or partial paralysis. Proof-of-concept devices have been tested in humans [7-10]. However, these devices have not demonstrated consistent and reliable recordings of neural signals for durations beyond several months. The unstable performance of these neural probes during long-term studies has hindered the translation of this technology in clinical applications.

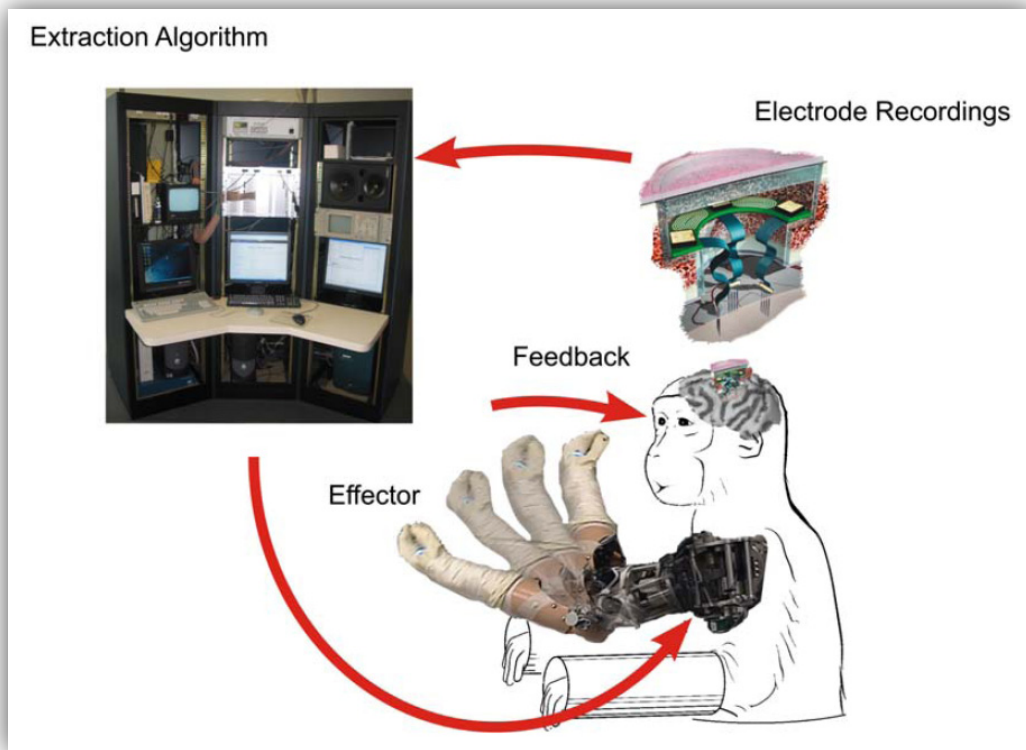


Figure 9. Brain Computer Interface schematic. Neural activity recorded from the brain is transmitted to a processor that operates an extraction algorithm on the recorded signal. The extracted control signal is fed to a robot controller to move the prosthetic arm, which generates feedback to close the control loop. Figure courtesy of Schwartz et al. [60].

Chronic neural recordings via microfabricated neural probes deteriorate over time, regardless of the electrode type or the animal model employed [24, 37, 54, 60]. The lifetime of electrode recordings has been reported to last between a few weeks up to a few months. One reason for recording failure is thought to be the loss of neurons surrounding the electrode area over time. Immunohistological examinations have shown a significantly lowered neuronal density around the implant, progressing over time from as early as one-week post implantation [37, 54, 60]. As neural recordings require proximity between the electrode and the neuron (up to 100 μm), loss of neurons near the implant will lead to loss of recordable signals [54]. Another

cause of reduced electrode performance over time is chronic gliosis, which results in a dense cellular sheath that encapsulates the neural probe and isolates it from the surrounding brain tissue [37, 54, 55, 60]. Gliosis is believed to be mediated by macrophages, activated microglia, and reactive astrocytes [37, 58]. At the beginning of brain injury as soon as the probe is implanted in the brain, microglia cells are activated and start to produce a variety of proinflammatory and neurotoxic factors. Microglia act in concert with macrophages that have penetrated the blood–brain barrier to phagocytose degenerating axons and myelin at the site of injury. Astrocytes, which become activated within hours after injury, are the second type of brain cells in the inflammatory response [37, 55]. Over a chronic time point activated astrocytes wall off the implant and the lesion created by it. Although the activation of the glial cells and their response to injury may prevent further tissue damage, they are known to also inhibit neuron axonal re-growth [108].

Research methods to alter the implant surface are being developed to achieve a chronically stable electrode-tissue interface. Some of these approaches include biomaterial designs that inhibit surface protein adsorption [109, 110], improve neuronal attachment and growth to the surface [86, 109, 111], or allow for the controlled release of anti-inflammatory molecules to reduce inflammatory gliosis [74, 75]. Although most of the above-mentioned approaches have shown promise, it is still considered a challenge to achieve long-term stable connections between the probe and the brain tissue at the cellular and/or biomolecular level.

We propose a more effective method to mediate the implant-tissue mismatch and to improve biocompatibility by introducing a neuron adhesion molecule on the probe's surface. The neural cell adhesion molecule L1 is a glycoprotein of the immunoglobulin superfamily expressed in most neurons in the central nervous system (CNS). During CNS development, L1 is targeted to

the surface of developing axons and growth cones and mediates outgrowth, adhesion, fasciculation, and guidance of axons as well as neuronal migration and survival [93, 98, 99]. L1 has also been suggested in CNS regeneration in adult vertebrates. After spinal cord injury in zebrafish, the expression of L1.1, a homolog of the mammalian L1, is increased in successfully regenerating descending axons but not in ascending projections that fail to regenerate [112]. Several studies show the effect of L1 on enhancing the recovery of rats from spinal cord injury. The above mentioned results were achieved when the: 1) L1 expression in neurons and glia was induced by viral transduction [113], 2) L1 overexpressing embryonic stem cells were transplanted [114], and 3) axonal growth-inhibiting environment was enriched in exogenous L1 [115]. These findings indicate that L1 is a molecule promoting CNS regeneration or preventing neuronal death.

In this study, we hypothesize that L1 immobilized on the surface of neural probes will maintain neuronal health around the implant and induce axonal regeneration or projections toward the electrodes right after implantation. By maintaining neuronal density, the inflammatory cell adhesion and activation after injury may be reduced. Our previous *in vitro* work has shown that the presence of L1 on the surface inhibited the glial cell attachment and growth. Similar mechanisms that happen *in vitro* might also occur *in vivo* and these mechanisms could potentially reduce the inflammatory gliosis at the probe-tissue interface.

3.3 METHODS

3.3.1 Microelectrode L1 modification

Four shank chronic silicon probes available from NeuroNexus Technologies were chosen to be used during this study. The design and fabrication of these probes has been previously described from Drake et al. [116]. Three end points after electrode implantation were investigated: 1 week, 4 weeks, and 8 weeks. Rats were implanted with non functional electrodes with thickness of 15 μm , length of 4mm, shank width of 60-100 μm , and tip spacing of 200 μm (Figure 10).

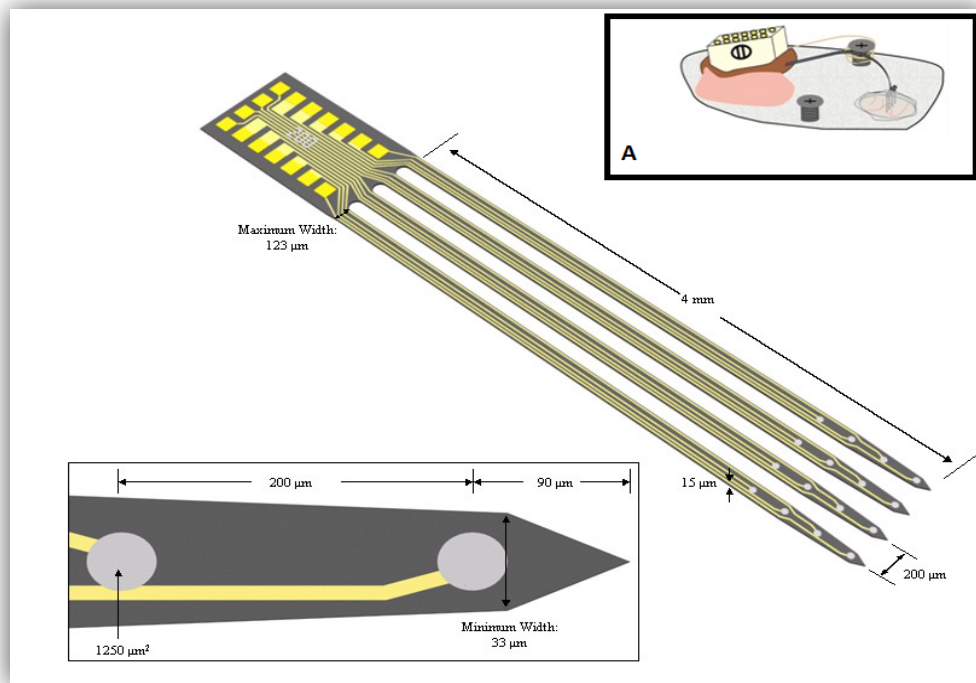


Figure 10. Dimensions of the silicon based electrodes used during *in vivo* studies. Inset (A) schematic of the tethering technique used during probe implantation. Schematics were obtained from NeuroNexus Technologies (www.neuronexustech.com).

L1 immobilization was performed on the surface of probes using silane chemistry. This approach allows surface patterning and immobilization of proteins or peptides on silicon substrates with the help of the hetero-bifunctional cross-linking reagent, 4-maleimidobutyric acid N-hydroxysuccinimide ester (GMBS) [103]. Poly(ethylene glycol)-NH₂ (PEG-NH₂) was added after laminin immobilization, to block the remaining reactive GMBS groups and to inhibit non-specific protein adsorption to the surface [109] (for more see section 2.3.1.2).

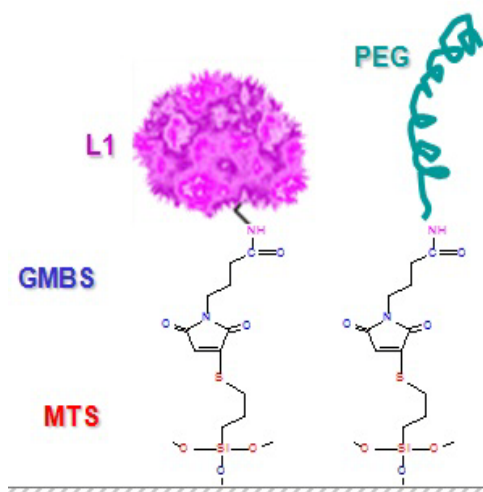


Figure 11. Schematic representation of L1 immobilization on the silicon surface of neural probes using MTS and GMBS covalent functionality.

The surface modification was performed using the experimental procedures similar to those previously reported [103, 109]. Briefly, after cleaning and hydroxylation with HNO₃, the probes were carefully immersed in a 2% solution of (3-mercaptopropyl) trimethoxysilane (MTS) and treated for 1 hour with 2 mM of GMBS. L1 (100 µg/ml) was applied for 1 hour at 4°C on the GMBS treated probe's surface. The L1 immobilized probes were rinsed with PBS (pH 7.4), and

treated with 100 μ M mPEG-NH₂ solution for 30 min to cap the rest of the active NHS ester groups of the GMBS (Figure 11). The probes were implanted immediately after this process.

3.3.2 Surgical procedures for neural implants

Twelve adult male Sprague-Dawley rats (250 ± 20 g) were used throughout this study; with four animals used per time point (1/4/8 weeks). The animals were housed in the facilities of the University Of Pittsburgh Department Of Laboratory Animal Resources and given free access to food and water. All experimental protocols were approved by the university Institutional Animal Care and Use Committee. The implanting techniques were followed as previously described by Vetter et al. [24]. The probes were implanted in the motor area of the cerebral cortex of the animal. General anesthesia was achieved for 5 min with a mixture of 5% isoflurane and 1 L/min O₂ prior to surgery and maintained throughout the surgical procedure at 1-3% isoflurane. The state of anesthesia was closely monitored for changes in reduction of respiratory rate, heart rate, and absence of the pedal reflex. The animal was placed into a stereotactic frame and its head was shaved over the incision area. The animal's skin was disinfected with isopropyl alcohol and betadine and a sterile environment was maintained throughout the surgical procedure. Ophthalmic ointment was applied to the eyes to prevent drying from exposure to anesthesia. A midline incision was made along the scalp, the skin retracted, and the periosteum was cleared to expose the bregma and midline. A 2-3 mm craniotomy was hand-drilled above the motor cortex (coordinates from bregma: AP: -0.5, ML: \pm 2.5-3.5). This provided for a more controlled craniotomy than the iatrogenic damage that can be exposed from electric drills. Two probes were implanted on each hemisphere of every rat (L1 and NM control probe) (Figure 12). Several

stainless steel bone screws were placed in the skull to retain the dental acrylic head-cap. The non-functional probes were mounted on the dental acrylic around the craniotomy the same way they would be mounted during surgical recording procedures (Figure 10A). After probe mounting, the dura layer was incised using a fine dura pick (Fine Science Tools). The bond-pad region of the microelectrode was grasped with Teflon-coated microforceps and the penetrating shanks were inserted manually through the pia mater into the motor cortex. To minimize bleeding and tissue reaction, surface blood vessels were avoided during insertion. The craniotomy was filled with a biocompatible silicone elastomer (Kwik-Sil, World Precision Instruments, Inc.) followed by dental acrylic. The overlying skin was sutured around the dental acrylic head-cap and the animal was allowed to recover under close observation in the surgical room. To minimize variability associated with the surgery, all implants were performed by the same surgeon.

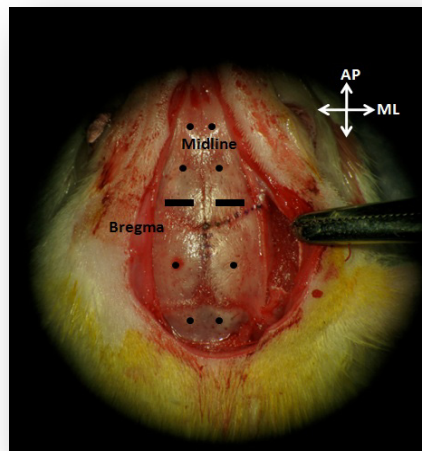


Figure 12. Representative image of probe location sites on the skull of a rat shown in black rectangles where the craniotomy was performed. Black circles represent location of skull screws used to anchor the probe assembly. (AP – Anteroposterior, ML – Mediolateral).

3.3.3 Brain tissue preparation for immunohistochemistry

After 1 week, 4 weeks, or 8 weeks, each animal was anesthetized with 50 mg/ml ketamine, 5 mg/ml xylazine, and 1 mg/ml acepromazine (Henry Schein) administered via the intraperitoneal (IP) cavity with a dosage of 0.1 ml/100 g body weight. The animals were transcardially perfused with 4°C PBS prewash followed by 4% paraformaldehyde in PBS. The brains were removed and postfixed overnight (4°C). Following the retrieval of the electrodes for further histology, the rat brains were placed into 30% sucrose (4°C) sucrose solution until they sunk to the bottom. The brains were then cryoprotected with Optimal Cutting Temperature (O.C.T.) compound (Tissue-Tek). Horizontal frozen tissue sections were cut to a final depth of ~4 mm from the surface of the cortex for all brains while skipping a section. Serial sections (20µm) were mounted directly to a SuperFrost Plus (Fisher) glass slides for better frozen tissue adhesion during immune staining. We utilized hematoxylin and eosin (H&E) stain to visualize general tissue morphology, while immunohistochemistry was used to visualize specific cellular markers. Chondroitin Sulfate antibody (CS56) was also used to visualize the up regulation of CSPGs in activated astrocytes around the implant site.

3.3.4 Immunohistochemistry procedures

To study the brain tissue response, sections taken from all brains were stained simultaneously for each antibody of interest at one time to minimize variability during data analysis. Six consecutive serial sections were used to stain for six different cell markers at four different depths in the brain. One serial section at each depth was stained using H&E and one using CS56.

The stains were chosen to visualize the presence of neuronal nuclei (NeuN), astrocytes (GFAP), activated microglia/macrophages (ED-1), mature axons (NF-200), microglia (Iba1), and astrocytes/fibroblasts/endothelial cells (Vimentin) (Table 3).

Table 3. Primary antibodies used during this study

Primary Antibodies	Host	Isotype	Clonality	Vendor	Dilution	Specificity
NeuN	mouse	IgG1	monoclonal	Millipore	2 µg/ml (1:500)	neuronal nuclei
GFAP	rabbit	IgG	polyclonal	Dako	0.2 µg/ml (1:500)	mature astrocytes
CD68 (ED-1)	mouse	IgG1	monoclonal	Serotec	0.2 µg/ml (1:500)	activated microglia/macrophages
Iba1	rabbit	IgG2b	monoclonal	AbCam	1 µg/ml (1:250)	microglia/macrophages
NF200	mouse	IgG1	monoclonal	Millipore	0.2 µg/ml (1:500)	mature axons
Vimentin	mouse	IgG1	monoclonal	Millipore	2 µg/ml (1:500)	immature and reactive astrocytes, microglia, endothelial cells, and fibroblasts

Horizontal tissue sections were cut to a final depth of ~3 mm from the surface of the cortex for all brain. The six sections ranged from ~200 µm to ~3000 µm below the surface of the cortex and were spaced at four different intervals.

Tissue sections were hydrated in buffer (PBS), blocked with 10% normal goat serum in PBS for 45min followed with PBS containing 0.5% Triton X-100 (Sigma). The tissue sections were then incubated overnight at 4°C, with the primary antibodies prepared in blocking solution with concentrations shown in Table 3. The next day sections were rinsed with PBS and incubated for 1 hour in either goat anti-rabbit IgG (H + L) Alexa 488 or goat anti-mouse IgG1 Alexa 488 (Invitrogen) secondary antibodies diluted at a ratio of 1:200 in blocking solution. All sections were counterstained with Hoechst (Invitrogen) nuclear dye to observe all cell nuclei and cover-slipped with Fluoromount-G (Southern Biotechnology Associates) to preserve fluorescence over time. Buffer was used in place of primary antibodies for control tissue samples.

The extracted probes were also stained to visualize the cells still present on them. The probes were stained following the above mentioned protocol using Iba1 and β -tubulin III antibody (specific for neurons), followed by counterstaining with Hoechst (see Section 2.3.4).

3.3.5 Quantitative brain tissue analyses

Confocal fluorescent and optical Differential Interference Contrast (DIC) images were acquired using a Nikon A1 confocal microscope with 10x or 20x objectives. Images for each specific antibody were taken in a single session to control for variability during image analysis. The exposure time was consistent within each marker and was set below saturation of the digital camera. During laser scanning confocal imaging each pixel was acquired with the same laser power and detector gain (sensitivity) setting for each antibody stained tissue. For analysis purposes a 10x objective was used with the electrode sites centered in the camera field. Four sections at different depths in the brain (approximately Depth 1 = 300 μ m, Depth 2 = 700 μ m, Depth 3 = 1100 μ m, and Depth 4 = 1500 μ m) below the rat cortex surface were imaged per each stain to observe the tissue response at different depths along the shaft of the implanted probe.

Average pixel fluorescent intensity as a function of distance from the electrode-tissue interface was calculated using ImageJ (National Institute of Health), a public domain Java-based image processing program developed at the NIH. A macro was written to perform the desired analysis with this program. Briefly, (GFAP/ED-1/Iba1/NF/Vimentin) images were cut where one out of four tracks interfaces fit within a window of \sim 1200 μ m in height and \sim 400 μ m in width. The DIC (bright field) image was first selected to draw a closed circular curve around the electrode-tissue interface location. The circular closed curve was verified with the matching

nuclei stained images. The closed curve served as the template at which thereafter 20 μm segmented regions were calculated for their average gray scale pixel intensity (1-255 a.u.). The average intensity was calculated up to a distance of 520 μm from each side of the interface location (Figure 13). To correct for background differences, the intensity was normalized to the mean profile (found to be at the distance of 420 μm - 520 μm) of each image and averaged across the results for each time point condition and depth. This distance was chosen based on its consistency within each cellular stain to reach background intensity.

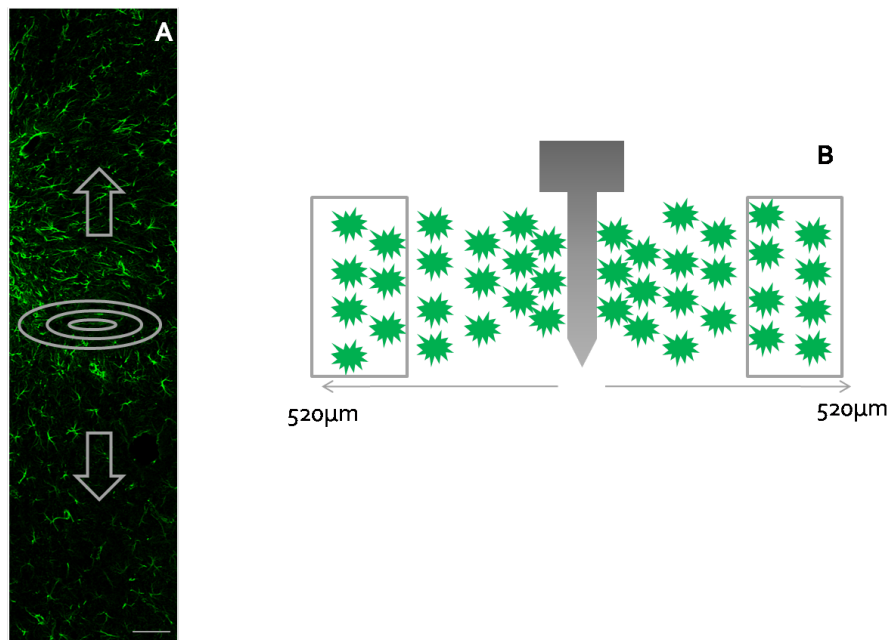


Figure 13. ImageJ intensity analysis. (A) Horizontal representative image of a GFAP stained image. 20 μm step size oval bands are created from the implant interface location and average pixel intensity values from 1-255 are measured for each band and shown as a function of distance. Scale bar 100 μm . (B) Coronal schematic of the region used for normalizing the intensity values.

NeuN stained images were quantified by estimating the number of neurons as a function of distance from the electrode interface. ImageJ using a watershed installed macros was used

during this analysis. NeuN stains for neuronal cell bodies and Hoechst stains for all cell nuclei. Both images of NeuN and Hoechst were processed for cellular shape counts. The images were segmented using a marker-based watershed algorithm and counting cells at 50 μm increments away from the interface up to 600 μm away from each side of the probe's interface (Figure 14). The results were normalized to the neuron count from 500-600 μm away from the interface and averaged across results from each time point condition and depth.

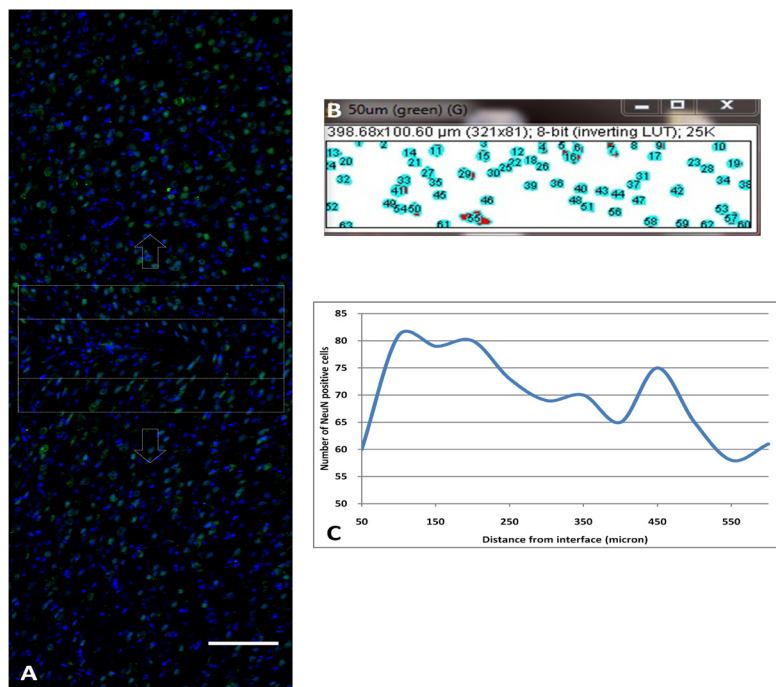


Figure 14. Neuron count analysis. (A) Representative image of double stained NeuN+ cells (green) and Hoechst+ (blue) nuclei. Boxes created to expand up to 600 μm away from the interface, while the probe's tract is placed in the middle of the boxes. Scale bar 100 μm . (B) Representative watershed algorithm computed from the green channel of the image A counting the NeuN+ cells at the 50 μm distance. (C) Raw NeuN+ cell count for image A as a function of distance from the interface.

3.3.6 Statistical analyses

Statistical analyses were performed using the SPSS statistics software (SPSS, Inc.). For experiments that involved the comparison of two conditions, the standard Student's t-test ($\alpha=0.05$) was performed. T-test analysis were used to compute p-values comparing NM and L1 data at different distance increments such as 0-100 μm from the interface and up to 400-500 μm away from the implant/tissue interface. Differences were considered significant for $p < 0.05$.

For comparisons involving multiple conditions, one-way standard analysis of variance (ANOVA) was used. NM or L1 probe data was compared this way through the 3 different time points and also through different depths. When a significant difference was found between groups Tukey's Honest Significant Difference (HSD) post-hoc test was utilized to identify pairwise differences. Differences were considered significant for $p < 0.05$.

3.4 RESULTS

3.4.1 Implant/tissue immunoreactivity

3.4.1.1 Neuron density and axonal immunoreactivity (NeuN and NF)

Neuronal cell loss around the electrode sites is thought to be one of the reasons neural implants fail to reliably perform at chronic time points [37, 51, 54, 60]. L1 is known to specifically promote neurite outgrowth and neuronal survival *in vitro* [96, 109]. The impact of electrode implantation on the surrounding neuronal population was assessed by immunostaining for NeuN, a nuclear antigen found only in neuronal cells, and NF-200, which stains for mature

axons. The normalized cell counts of viable neurons around the implant's interface at different time points are plotted in figure 15A-C as a function of distance (mean \pm s.e.m.). For the NM control probe neuronal decrease was evident within the 100-200 μ m zone around the implant at all time points. The L1 modified probe maintained a normal density of neuronal cell bodies around the electrode interface, with a slight increase at the week 1 time point. Significant differences using t-test analysis were found between L1 and NM control NeuN+ cell counts at all time points from 0-200 μ m away distance from the interface (Table 4).

The distance for the neuron/electrode communication is known to be approximately within 50-100 μ m [37, 54]. Normalized cell counts within the 100 μ m zone around the probe along different depths of the implants for the L1 and NM conditions are plotted in figure 16D-F. Pair student's t-tests were performed comparing the different depths and significant difference was seen between L1 and NM control at the all data besides: week 4 at depth 1 condition. For the NM probe a lower than background neuronal cell count was observed at all time points, with no statistically significant difference found between time points. For the L1 modified probe there was an initial slight increase in cell count at week 1, and then at later times the neuronal density seemed to reach the background level (normal tissue far from the implant) and remain unchanged. Neuronal cell count was also maintained at different depths along the L1 modified probe. Fluorescent image representations of the NeuN+ cells are shown in Figure 16.

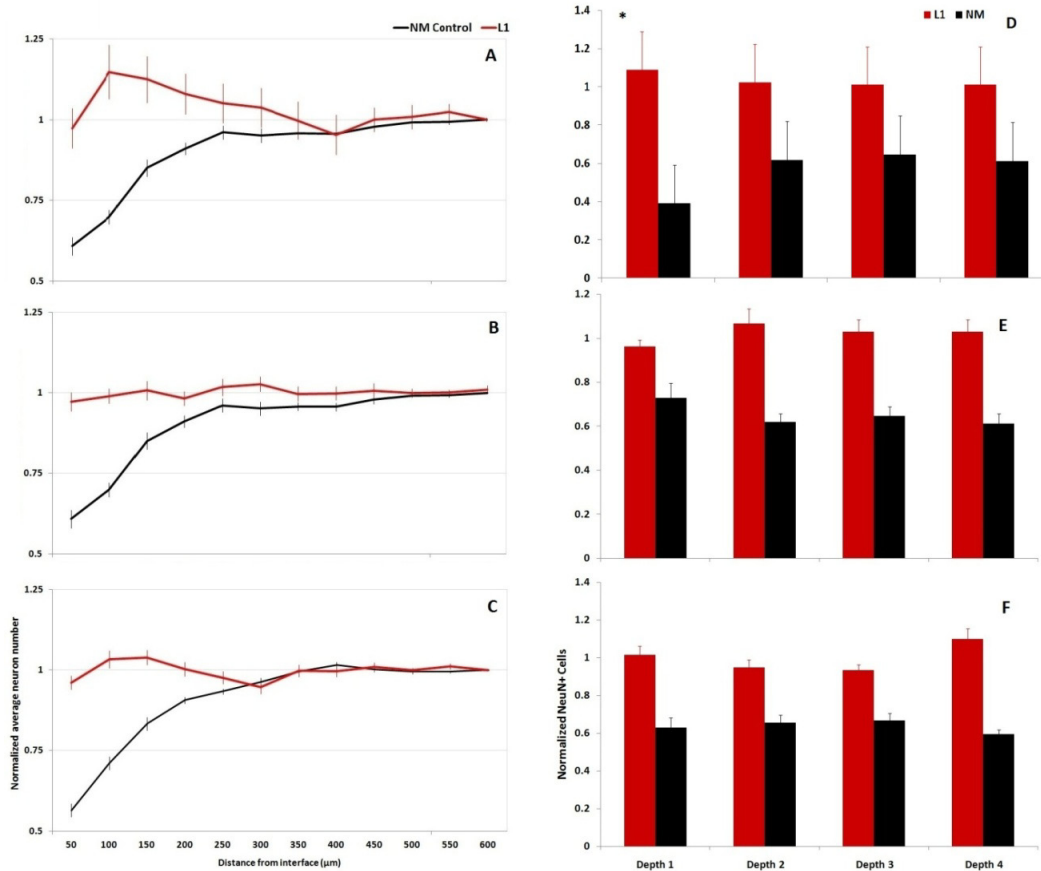


Figure 15. Neuronal number and density adjacent to L1 modified implants are associated with a higher NeuN+ cell count than NM control implants. (A-C) Comparison of average NeuN+ cell counts between L1 and NM control probe at each different time point shown as the normalized average neuron number ($n=14\pm 2$). (A – week 1, B – week 4, C – week 8). (D-F) Comparison of average NeuN+ cell counts at different depths in the cortex 0-100 μm away from the interface for different time points (D – week 1, E – week 4, F – week 8). t-test comparisons between each group (NM vs L1) showed a significance difference $*p < 0.05$. No significant difference was seen between time points and depth within each group (NM or L1).

NF-200 is a marker for mature axons. The average gray pixel intensity of NF stain was calculated and its normalized values to background intensity for each image are plotted as a function of distance (mean \pm s.e.m.) comparing the L1 modified and the NM control probes at three different time points (Figure 17A-C). The differences in NF intensity between two

conditions were compared at different distance zones around the electrode-tissue interface (Table 4). Mature axons showed a statistically significant lower density around the NM probe than L1 probes within the 100 μm zone around the electrode interface at all time points and within 100-200 μm for the first week (Table 4). In the NM control implants, we observed reductions in NF reactivity than background extending as far away as 200 μm in some cases, but on average through the time points the reduction was in a zone of 100 μm around the implant site as previously described (Figure 17A-C). However, on the L1 implants a mirrored significant increase in the axonal marker staining was seen (Figure 17A-C). At 0-100 μm away from the probe's interface there was significance in all comparisons of the two conditions besides the week 8 depth 1,3, and 4 (Figure 17F). Decrease of axonal density was prominent for the NM probe at all depths, and the axonal density was above the background density for the L1 modified probes for all depths and all time point conditions. An increase of NF reactivity was seen for depth 1 at week 1 and depth 1 and 2 at week 8, while no changes were seen between all depths for the NM probes.

Representative images for L1 and NM probes in the brain tissue stained for NF 200 are shown in Figure 18. The images were taken from the 8 week tissue samples, and NF is clearly more intense around the L1 probe tracts. NM probe had reduced NF density and showing a typical kill zone around the electrode.

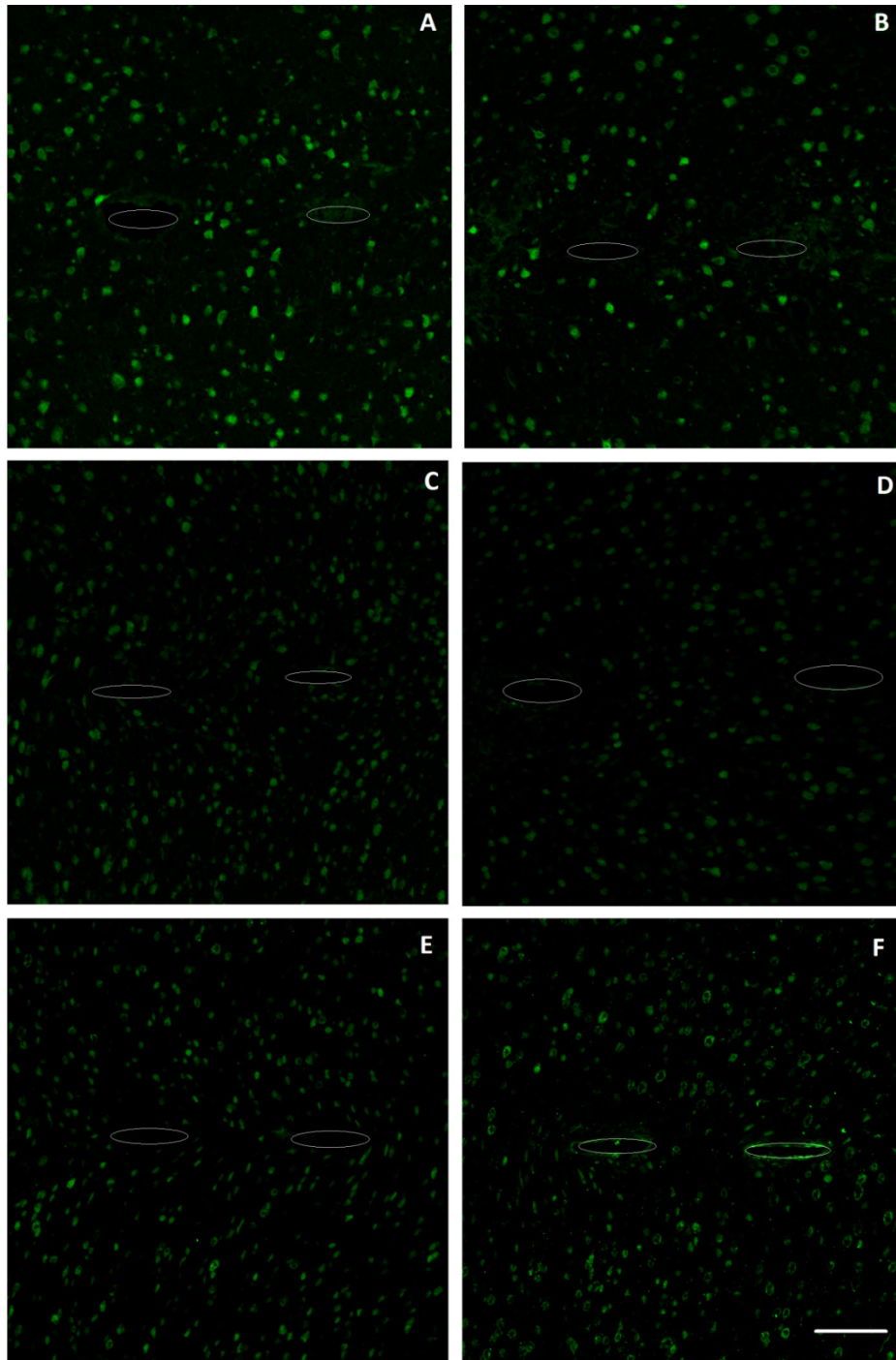


Figure 16. Representative images of NeuN+ cells (green). Probe tracts traced with an oval for better visualization. (A,C,E) Neuronal density around the L1 probe at week 1, 4, and 8 respectively. (B,D,F) Neuronal density around the NM probe at week 1, 4, and 8 respectively. Scale bar 100 μ m.

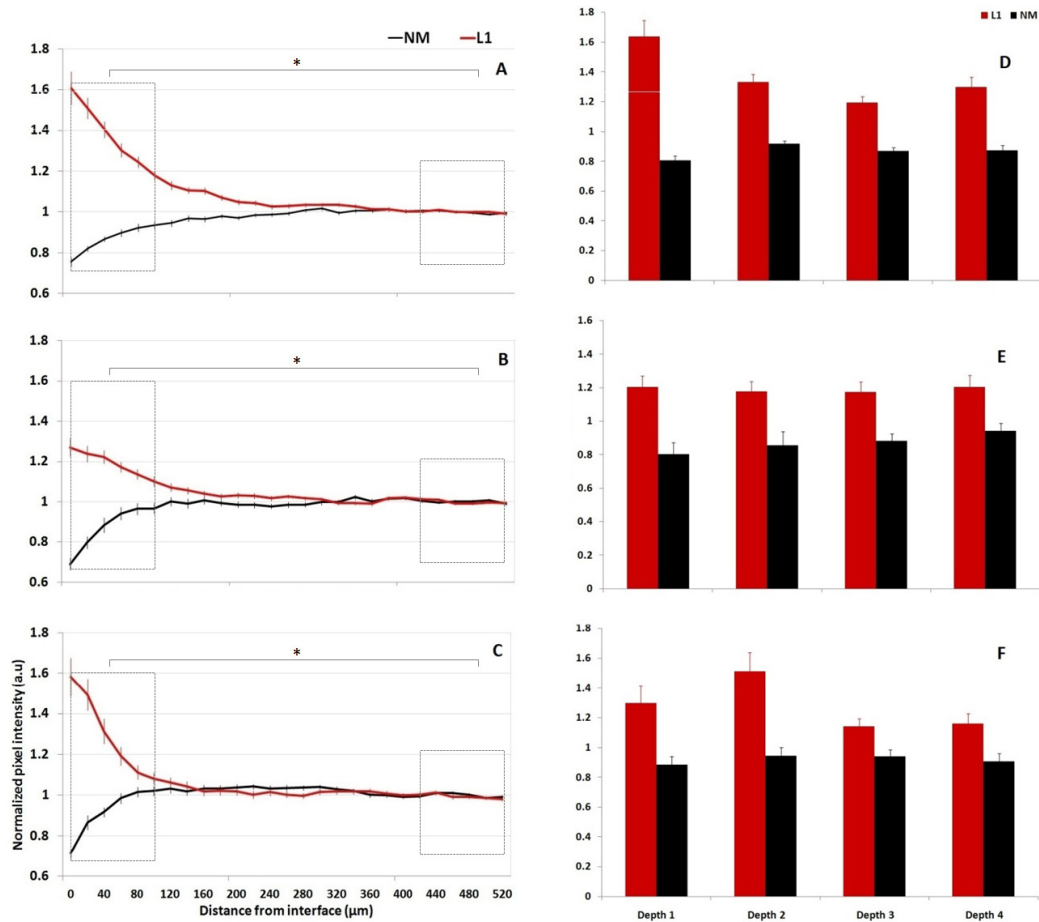


Figure 17. Mature axons adjacent to L1 modified implants are associated with a higher relative NF200 immunoreactivity than NM control implants. (A-C) Comparison of average NF intensity between L1 and NM control probe at each different time point shown as the normalized average intensity in arbitrary units (a.u.) ($n=14\pm 2$). (A – week 1, B – week 4, C – week 8). T-test comparison between the average intensity at 0-100 μm and the background intensity (420-520 μm) were made, significance was seen between these two measures ($*p<0.05$). (D-F) Comparison of average NF intensity at different depths in the cortex 0-100 μm away from the interface for different time points (D – week 1, E – week 4, F – week 8).

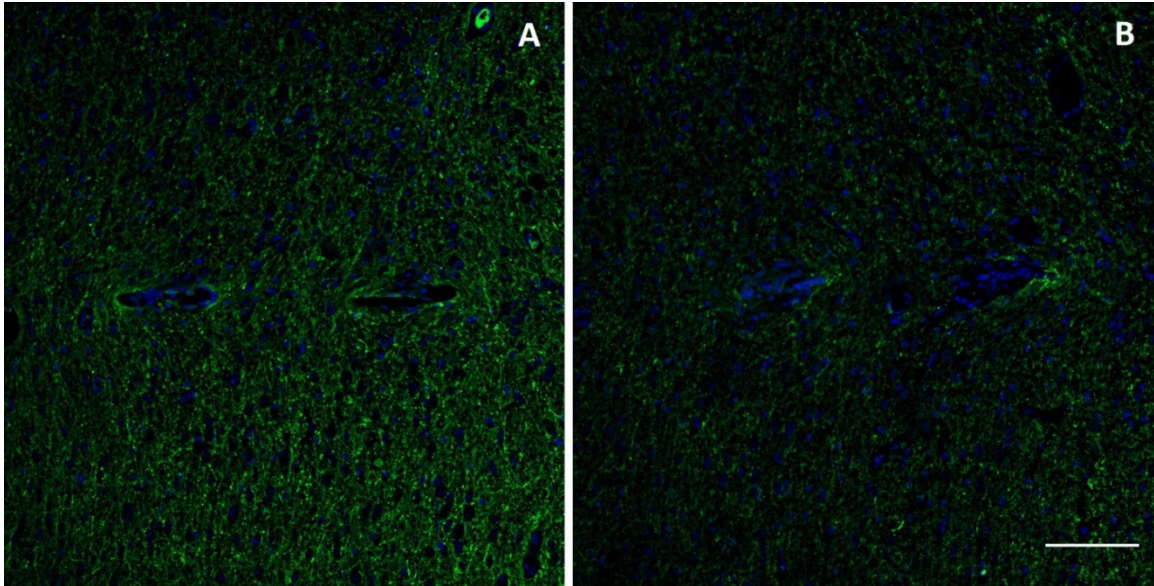


Figure 18. Representative images of NF 200 staining of 2 probe tracts shown per image. (A) L1 probe sites at week 4 time point. (B) NM control probe at week 4 time point. Both images, NF 200 (green) and Hoescht (blue). Scale bar 100 μm .

Table 4. P-values calculated from t-test analysis of the values from the NeuN and NF data at different interval distances from the probe interface. Yellow cells show significant p-values < 0.05 calculated from t-test analysis comparing NM and L1 data at 100 μm increments.

	0 -100 μm		100 -200 μm		200-300 μm		300-400 μm		400-500 μm	
week 1	0.018	0.013	0.047	0.032	0.084	0.278	0.125	0.302	0.151	0.432
week 4	0.028	0.042	0.048	0.095	0.086	0.177	0.122	0.353	0.115	0.359
week 8	0.030	0.034	0.046	0.099	0.214	0.145	0.134	0.412	0.177	0.546
	NeuN	NF	NeuN	NF	NeuN	NF	NeuN	NF	NeuN	NF

3.4.1.2 Astroglia reaction (GFAP and Vimentin)

GFAP is a commonly used marker to visualize astrogliosis, the known astrocytic reaction to induced brain injury. As expected from previous reported studies, GFAP expression was increased in the tissue surrounding the NM control probes. GFAP is expressed in mature astrocytes and vimentin is expressed in immature and reactive astrocytes, microglia, fibroblasts,

as well as endothelial cells. The intensity of GFAP and vimentin stained sections was quantified as a function of distance from insertion interface of the probes. Figures 20A-C show the distribution of GFAP positive cells surrounding the insertion site for both L1 and the NM control probes. Figures 21A-C show the distribution of vimentin positive cells surrounding the insertion sites. The normalized intensity curves are plotted as mean \pm s.e.m. from 0-520 μm away from the implant interface. Differences in intensity were observed as a function of time.

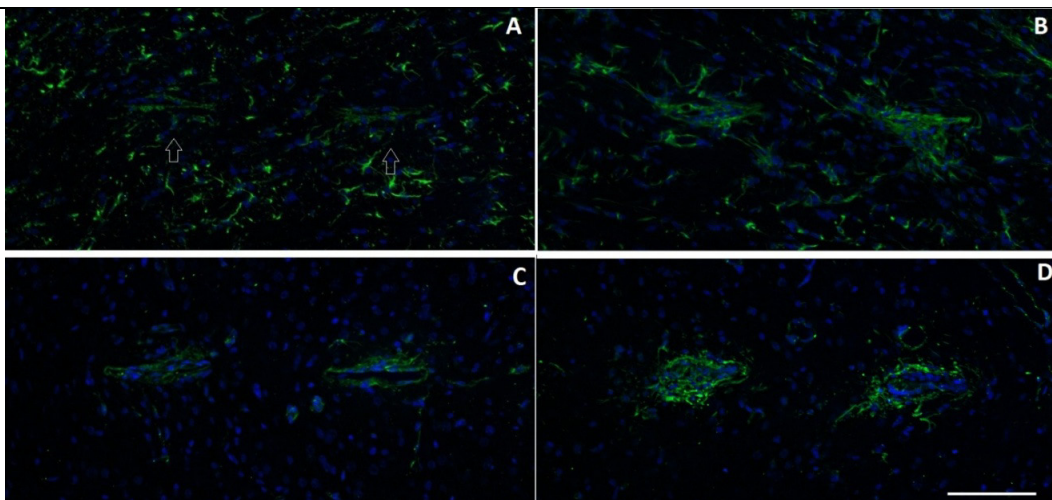


Figure 19. Representative images of GFAP (A, B) and Vimentin (C, D) staining at the 8 week time point for L1 (A, C) and NM probe (B, D). GFAP and Vimentin (green), Hoescht (blue). Arrows in figure A indicate the position of 2 probe tracks. Scale bar 100 μm .

The characteristics of the GFAP expression differed with distance from the electrode at three different end points (1, 4, 8 weeks) (Figure 20). After 1 week, the peak of the intensity curve was around 75 μm away from the interface. After 4 weeks, the peak in GFAP expression was closer to the interface (\sim 25 μm). After 8 weeks, the expression levels of GFAP were next to the electrode (Figure 19A,B). These observations were seen for both conditions (L1 and NM probes). However, there was a significant lower level of GFAP expression for the L1 probe at all time points in the 100 μm zone around the interface ($p < 0.05$) (Table 5). This trend is observed in

all depths along the electrode shaft at all time points (Figure 20D-F). The GFAP reaction for the first 100 μm away from the probe's interface was seen to be somewhat similar for all depths at week 1 for both L1 and NM. At week 4 a decrease of GFAP staining was seen as the depths increase for both probes. While at week 8 this trend was only seen for the L1 probe.

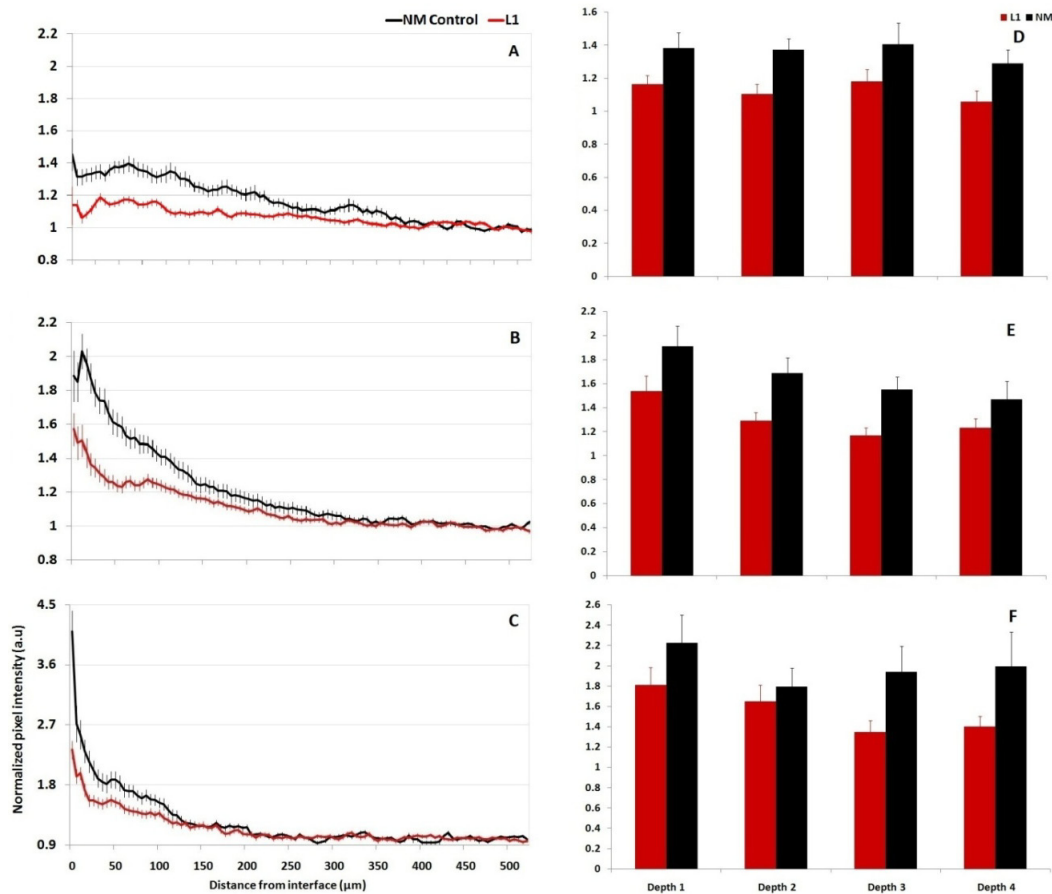


Figure 20. Tissue reaction adjacent to L1 modified implants is associated with a lower relative GFAP immunoreactivity than NM control implants. (A-C) Comparison of average GFAP intensity between L1 and NM control probe at each different time point shown as the normalized average intensity in arbitrary units (a.u.) ($n=14\pm 2$). (A – week 1, B – week 4, C – week 8). (D-F) Comparison of average GFAP intensity at different depths in the cortex 0-100 μm away from the interface for different time points (D – week 1, E – week 4, F – week 8).

Vimentin expression was similar to GFAP reaction for both L1 and NM control probes (Figure 19C,D). One week post implantation, vimentin expression for the NM control probe was

observed to be increased all around the interface and reaching normal intensity values at approximately 150 μm away from the probe's interface. At 4 and 8 weeks the normal intensity values for the NM control probes were reached around 100 μm from the interface. The intensity of the vimentin positive stain was significantly decreased around the L1 modified probes than the NM control for all time points within 100 μm interface distance (Figure 21A-C). Pairwise comparisons indicated significant differences between L1 and control in the pattern of vimentin immunoreactivity at week 1 and 4 at the 0-100 μm zone (Table 5). The average relative intensity of vimentin reactivity is lower for the L1 coated probes than the NM control all depth (Figure 21D-F). Depth differences seemed to vary at week 1 and 4 for both probes following the same trends but L1 probe showing significantly lower reactivity than the control probe. Week 8 results showed variability in depths for both probes.

Table 5. P values calculated from t-test analysis of the values from the GFAP and Vimentin intensity data analysis at different interval distances from the probe interface. Yellow cells show significant p-values < 0.05 calculated from t-test analysis comparing NM and L1 data at 100 μm increments.

	0 -100 μm		100 -200 μm		200-300 μm		300-400 μm		400-500 μm	
week 1	0.032	0.014	0.062	0.090	0.121	0.853	0.256	0.367	0.551	0.688
week 4	0.021	0.029	0.077	0.140	0.176	0.455	0.104	0.148	0.284	0.508
week 8	0.047	0.092	0.097	0.124	0.109	0.202	0.115	0.283	0.221	0.537
	GFAP	Vimentin	GFAP	Vimentin	GFAP	Vimentin	GFAP	Vimentin	GFAP	Vimentin

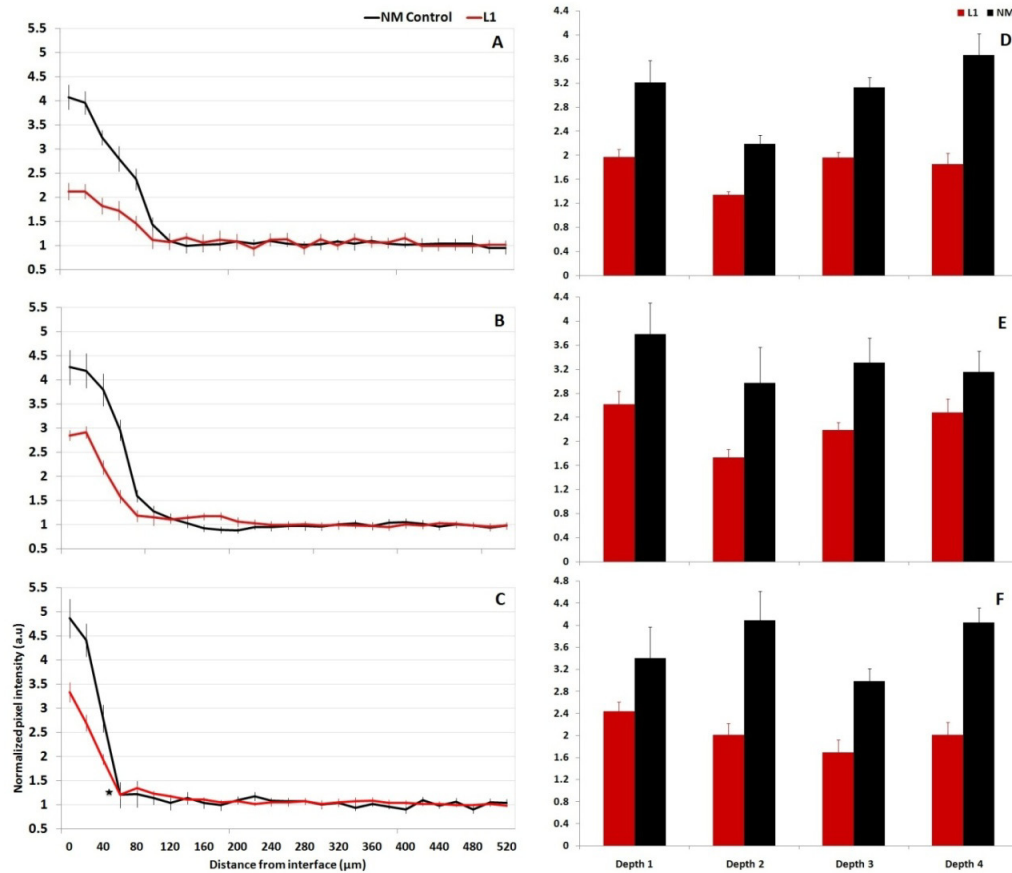


Figure 21. Tissue reaction adjacent to L1 modified implants is associated with a lower relative Vimentin immunoreactivity than NM control implants. (A-C) Comparison of average Vimentin intensity between L1 and NM control probe at each different time point shown as the normalized average intensity in arbitrary units (a.u.) ($n=14\pm 2$). (A – week 1, B – week 4, C – week 8). (D-F) Comparison of average Vimentin intensity at different depths in the cortex 0-100 μm away from the interface for different time points (D – week 1, E – week 4, F – week 8).

3.4.1.3 Microglia reaction (ED-1 and Iba1)

Microglia form a front line of defense during acute immune reaction and at the chronic time point, four weeks and after, these cells are known to be part of the persistent glial sheath. ED-1 is a marker specific for reactive microglia/macrophages. Comparison of ED-1 immunostaining revealed a significant elevation in immunoreactivity in animals with NM control

probes compared to L1 probes for all time points indicating a higher number of macrophages and activated microglia (Figure 23A-C). In both L1 and NM control implanted animals, most of ED-1⁺ cells were observed in close proximity to the electrode interface site (Figure 22A,C). One week following implantation, ED-1 intensity signal was present surrounding the insertion sites (Figure 23A-C). No significant change was seen between the intensity plots at each time point for the NM probes. The L1 modified probe showed a significant decrease of activated microglia when compared to the NM probe at all time points (Figure 23A-C). This significant decrease was also observed at each depth and time point for the distance of 0-100 μm away from the interface (Figure 23D-F). Pairwise comparisons in Table 6 reveal that L1 probe significantly reduced the microglia activation at 100 μm from the interface. Depth differences for the ED-1 marker were observed at week 4 for the NM probes and week 8 for the L1 probes.

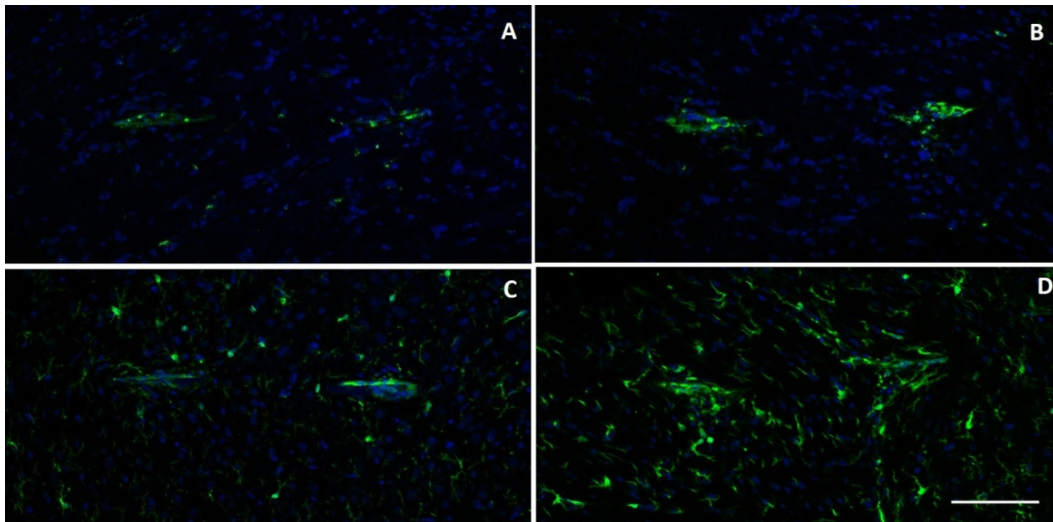


Figure 22. Representative images of ED-1 (A, B) and Iba1 (C, D) at the 8 week time point for L1 (A, C) and NM probe (B, D). ED-1 and Iba 1 (green), Hoescht (blue). Scale bar 100 μm .

Iba1 is expressed in normal microglia and upregulated in activated microglia. Iba1 intensity plots showed similar trends to ED-1 reactivity (Figure 24). Pairwise comparisons

revealed no significant change between L1 and NM probe at week 1. Depth differences were observed for the NM probe at all weeks, and for the L1 probe at week 4 and 8. In addition, a decreased Iba1 reactivity was seen at week 4 when compared to week 1 and 8 for both probe conditions. The NM probe showed an increase at depth 4 week 4.

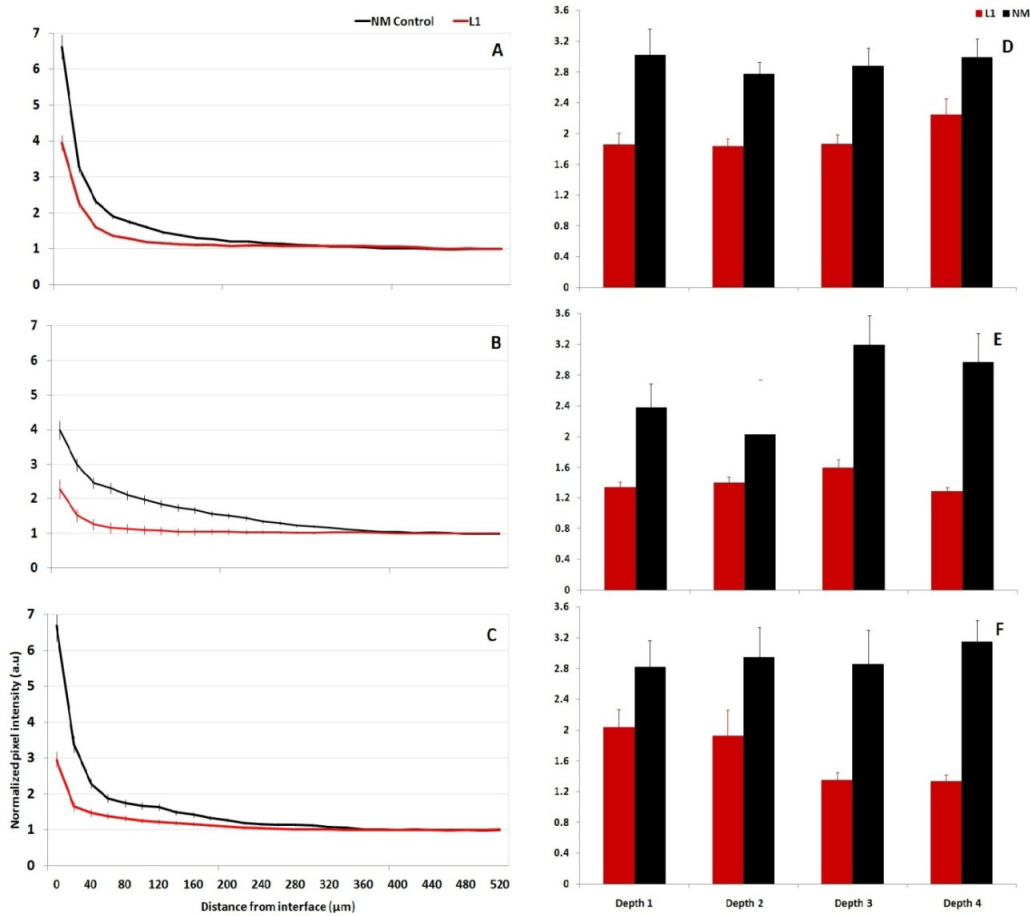


Figure 23. Tissue reaction adjacent to L1 modified implants is associated with a lower relative ED-1 immunoreactivity than NM control implants. (A-C) Comparison of average ED-1 intensity between L1 and NM control probe at each different time point shown as the normalized average intensity in arbitrary units (a.u.) ($n=14\pm 2$). (A – week 1, B – week 4, C – week 8). (D-F) Comparison of average ED-1 intensity at different depths in the cortex 0-100 μm away from the interface for different time points (D – week 1, E – week 4, F – week 8).

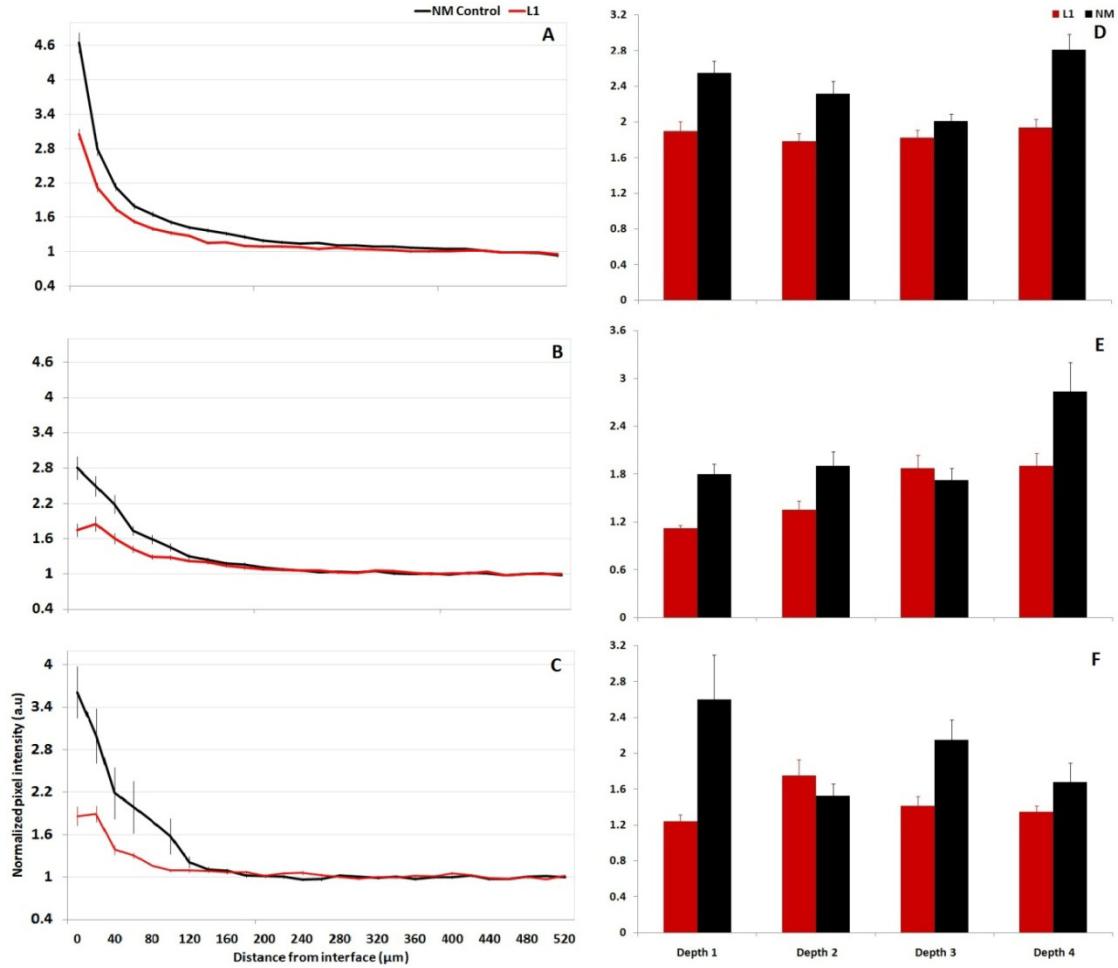


Figure 24. Tissue reaction adjacent to L1 modified implants is associated with a lower relative Iba1 immunoreactivity than NM control implants. (A-C) Comparison of average Iba1 intensity between L1 and NM control probe at each different time point shown as the normalized average intensity in arbitrary units (a.u.) ($n=14\pm 2$). (A – week 1, B – week 4, C – week 8). (D-F) Comparison of average Iba1 intensity at different depths in the cortex 0-100 μm away from the interface for different time points (D – week 1, E – week 4, F – week 8).

Table 6. P values calculated from t-test analysis of the values from the ED-1 and Iba1 intensity data analysis at different interval distances from the probe interface. Yellow cells show significant p-values < 0.05 calculated from t-test analysis comparing NM and L1 data at 100 μm increments.

	0 -100 μm		100 -200 μm		200-300 μm		300-400 μm		400-500 μm	
week 1	0.049	0.052	0.092	0.090	0.156	0.123	0.244	0.223	0.322	0.421
week 4	0.021	0.042	0.052	0.080	0.089	0.223	0.223	0.320	0.225	0.523
week 8	0.001	0.032	0.084	0.120	0.098	0.245	0.250	0.411	0.314	0.442
	ED-1	Iba 1	ED-1	Iba 1	ED-1	Iba 1	ED-1	Iba 1	ED-1	Iba 1

3.4.2 Qualitative observations

To observe the cell attachment on the probes after implantation we were able to stain them with specific antibodies for neuron and microglia. It has been shown that microglia attach and stay on the probes even after removal and we were able to observe this on the NM probe at 8 weeks (Figure 25C). On the other we observed attached neurons and their processes along the L1 modified probes after 1 and 4 weeks. Due to the probe's material prone to breakage, several NM and L1 probes were damaged during probe removal from brain tissue or during the staining procedure. In addition, double staining for β -tubulin III and Iba1 was attempted, but due to the autofluorescence properties of the probe's surface and failure of the double staining technique we were not able to visualize some of our results. In future experiments we plan to perfect these methods.

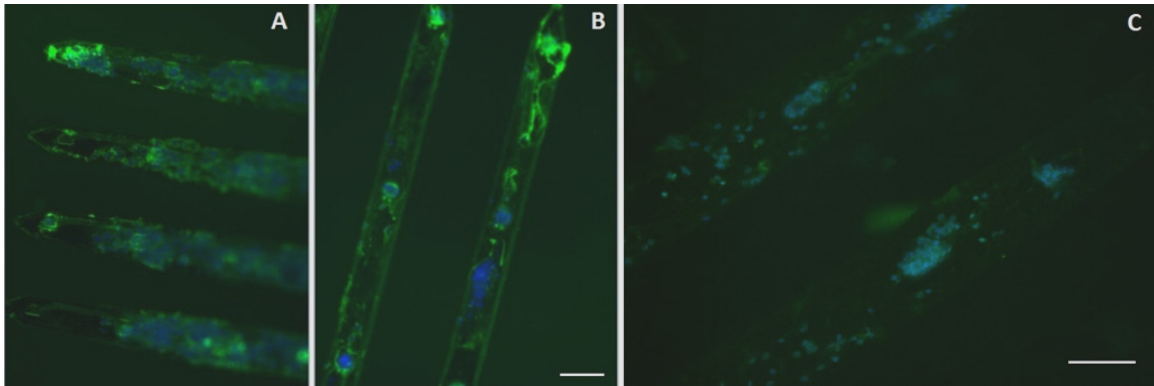


Figure 25. Representative images of neurons (A, B) and microglia (C) on the surface of probes after removal from fixed brain tissue. (A) L1 probe after 1 week, (B) L1 probe after 4 weeks (A and B same scale bar 100 μm), and (C) NM control probe after 8 weeks. β -tubulin III – green, Iba 1 – green, Hoescht – blue. Scale bar 100 μm .

H&E histology was performed to observe the probe tracts and to observe general tissue morphology around the probe tracks. From all H&E samples we were able to observe the aggregation of cell bodies at the NM probe (Figure 26B). However, the L1 probes did not show such strong cell recruitment at the 8 week time point (Figure 26A).

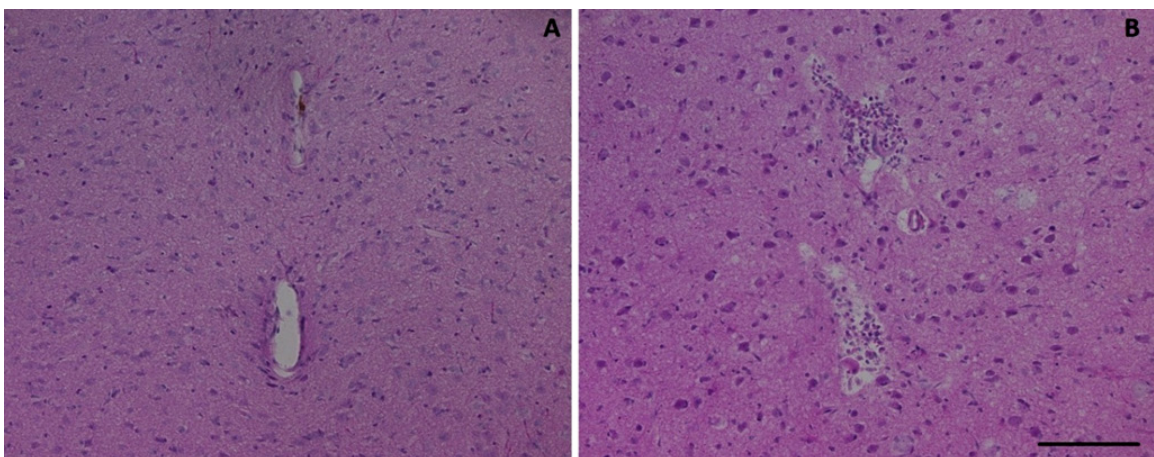


Figure 26. Representative images of H&E histology at the 8 week time point for L1 (A) and NM probe (B). Scale bar 100 μm .

CS56 has been reported to be specific for the glycosaminoglycan (GAG) portion of native chondroitin sulfate proteoglycan (CSPG), which is up-regulated by reactive astrocytes. As expected the CS56 staining was seen to be highly increased on the surroundings of the NM probe (Figure 27B) when compared with the L1 probe's surroundings at the 8 week time point (Figure 27A).

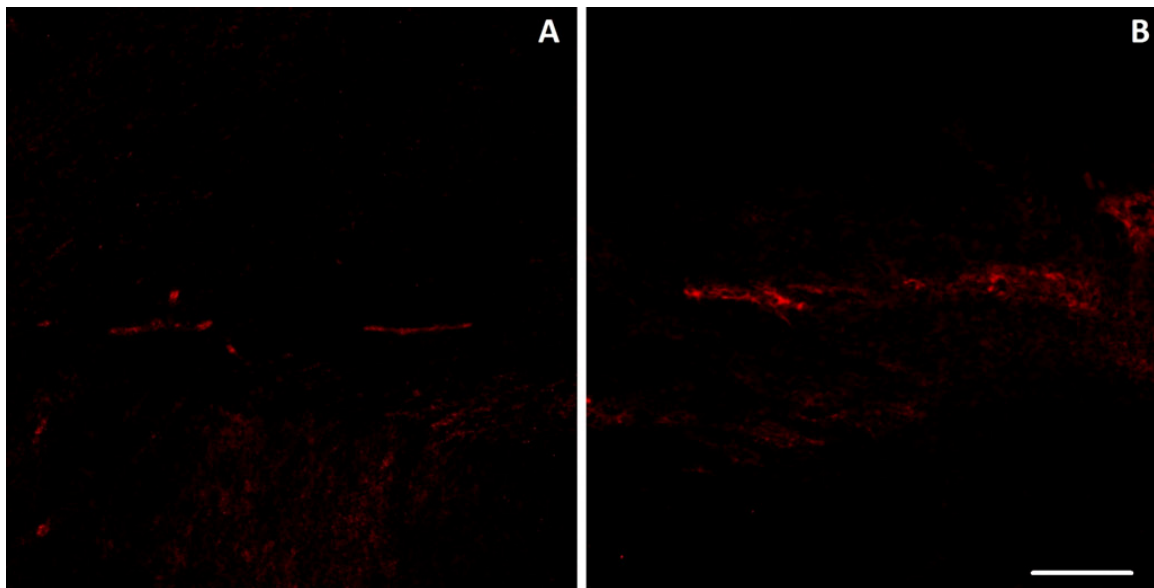


Figure 27. Representative images of CS56 staining (red) at the 8 week time point for L1 (A) and NM probe (B). Scale bar 100 μm .

3.5 DISCUSSION

Silicon- based neural prostheses are used as tools to study the nervous system and as therapeutic strategies to restore lost function in the nervous system because of trauma or diseases. Chronic implantation of these devices involves inevitable acute injury and chronic inflammation indicated by the loss of neurons and the persistent activation and encapsulation of microglia and

astrocytes [2, 29, 37, 55]. Current approaches to mitigate these responses include surface modification to promote neuronal attachment [117] and/or delivery of anti-inflammatory, neuroprotective, and neurotrophic factors directly at the implant-tissue interface [71, 75]. Although such strategies have been shown to successfully reduce the host response to various degrees, these strategies still remain to demonstrate a significant improvement of both neuronal density and gliosis at chronic time points.

In this study, we investigated the effect of the neural adhesion protein L1 on neuronal density and gliosis surrounding implanted probes. We found that the presence of L1 on the surface of the probe can decrease the cellular inflammatory responses to implanted neural probes and significantly increase neural loss and axonal growth around these modified neural probes.

We evaluated both acute and chronic inflammation at three different time points: 1 week, 4 weeks, and 8 weeks, to explore the evolution of the inflammatory tissue responses associated with the presence of the L1 modified and NM control probes. These conditions were chosen based on literature suggestion of the two critical time points in gliosis formation. 1 week is known as the acute response and 4 weeks is known to be the start of the chronic response where the process of gliosis is somewhat complete and this also indicating the reported time-line of electrode recording failures in several studies [37]. To mimic similar recording testing scenarios, the surgical techniques performed during this study followed the standard implantation procedures used for chronic recording electrodes [24]. In addition, anchoring/tethering these electrode arrays provides a more controlled condition than the use of an untethered electrode model, which would likely underestimate the tissue reaction when compared to functional electrodes tethered to the skull.

Neurons of the adult mammalian CNS usually fail to regenerate following an injury [51, 118]. This failure seems to involve the presence of inhibitory factors, as well as the absence of both neuronal survival and outgrowth factors. CNS neurons have some capacity to regenerate if they are provided with a permissive environment [61, 112-115, 118]. In particular, the glial environment following injury is likely responsible for many of the differences in neuron regenerative capacity. The adhesion molecule L1 is one of the few adhesion molecules known to be beneficial for repair processes in the adult CNS of vertebrates by promoting axonal growth and neuronal survival [98, 112-115, 119]. Previous studies and our *in vitro* study have shown that homophilic L1 interactions promote neural survival and neurite outgrowth on cultured neuronal cells [93, 96, 99, 109]. Therefore, we expected to find maintenance of neuronal count around the L1 probe and hopefully an increase of axonal density toward these implants. In this study, we demonstrate the spatial distribution of neuronal cell bodies as measured by NeuN immunoreactivity. A significant reduction in NeuN immunoreactivity was observed for the NM control probe at all time points. This reduction was restricted to a distance of 150-250 μm surrounding the NM control electrode, indicating that neuronal loss is a localized interfacial phenomenon. In this study we used 4 shank chronic Michigan electrodes, which are known to produce multiple penetrating injuries that would lead to pronounced neuronal loss around these types of electrodes [54, 57]. Winslow and Tresco also report loss in NF-160 within the first 100 μm from the electrode [56]. McConell et al. show a progressive loss in number of neurons at chronic end points (increased loss at 16 weeks compared to 8 weeks) [51]. Most of these authors speculate that neurotoxic factors released by microglia best explain the observed neuronal loss. In addition, we believe that neuronal loss around the reported implants may result from a number of variables including differing surgical procedures, differing tethering forces, cells that are

mechanically severed during implantation, and the provision of a pathway for meningeal cell migration. During this study, the number of NeuN+ cells surrounding the L1 modified probe did not decrease compared to the background, but remained stable from 1 to 8 weeks following microelectrode implantation. A reduction of immunoreactivity of neurofilament surrounding the electrode has also been described adjacent to similar planar silicon microelectrode arrays (not modified) [29, 51, 54, 56]. However, in this study we observed a reduction only on the NM control probes, while the L1 probe showed a remarkable increase in mature axons adjacent to the electrode at all time points. Although, the NF activity lowered in intensity during week 4, it seemed to be more compact and closer to the electrode site (80 μm) by week 8.

Nervous system cells during development adhere to themselves and their environment, extend axons, fasciculate and form synaptic networks via adhesion molecules such as L1. Thus, L1 and other neural adhesion molecules are critical for the proper function of the mature nervous system through their versatility or regulation/expression and other interactions in adhesion and neurogenesis [120]. Neurons are known to extend their axons on purified L1 via a homophilic interaction between L1 molecules. These L1 homophilic interactions may promote many critical events in neural development, such as cell recognition, adhesion, neurite elongation, and cell migration. L1 expression has been reported to be upregulated on sprouting axons, but not astrocytes, in the CNS following a lesion [121]. Therefore, L1 may play an important role in neural regeneration after the implantation induced injury, possibly by modifying the local environment, attracting the neuronal attachment, promoting the axonal regrowth and effectively inhibiting astrocyte activation at the site of injury.

In this study, we also provide evidence of the spatial distribution of reactive astrocytosis surrounding the silicon microelectrode as determined by GFAP. In the uninjured brain,

astrocytes are responsible for maintaining the local cellular microenvironment within the brain, as well as controlling synaptic stability [37]. GFAP immunoreactivity for both conditions did not increase as a function of time over the 8 week period in rat cortex. It therefore appears unlikely that reactive astrocytes progressively push neurons away from the recording zone as has been suggested as a failure mechanism for single unit recording with other electrode systems [122]. The spatial distribution of GFAP immunoreactivity did, however, change over time. The peak of relative intensity of GFAP immunoreactivity was located closer to the implant surface as a function of time, indicating contraction of the reactive astrocytes. At week 1 we observed the relative intensity of the NM control GFAP staining to reach background intensity approximately 450 μm away from the interface. At 4 weeks this distance decreased to ~ 300 μm and at 8 weeks ~ 150 μm . Others have reported similar findings for NM silicon electrodes. The L1 modified implant showed similar trends although with a significant 78%, 83%, and 57% (week 1, 4, and 8 respectively) decrease of the immediate (0-20 μm) intensity profile right at the probe's interface. Although the mechanism for the reduction of the astrocytes through L1 bound on the surface of the probe is not known, we hypothesize the following: 1) The immediate cues that L1 might release at the first presence in the brain might attract neurites to this neuron friendly surface. This attraction of neurites keeps neuronal bodies to the proximity of the probe thus not allowing astrocytes to get closer to the implant, 2) Astrocytes are recruited upon the presence of a trauma/foreign body. The L1 surface presents a more biological surface that might disguise astrocytes in behaving less responsive to the foreign implant, and 3) L1 might release other unknown cues to inhibit/lessen astrocyte activation.

Vimentin is expressed in reactive astrocytes but not mature astrocytes. Meningeal cells are fibroblast-like cells found in the meninges, including both the dura mater and pia mater.

Meningeal fibroblasts stain for vimentin but do not stain for GFAP, and are known to migrate down the electrode shaft from the brain surface and form the early basis for gliosis [66]. Vimentin in our study seemed to be confined closer to the implant interface unlike the spatial distribution of GFAP immunoreactivity, indicating the presence of fibroblast closer to the implant interface due to the initial vascular injury. L1 showed a decrease of this phenomenon indicating that the same hypothetical mechanisms mentioned above for the astrocytes might be relevant here too.

In our study, ED-1+ cells, a combination of hematogenous macrophages and activated microglia, were much more prevalent adjacent to all implants and this was observed at all time points. The presence of ED-1+ cells at the later time point indicates that local hemorrhaging occurs not only from the acute injury, but also at chronic time point. The initial implant vascular damage might increase the sustained activation of microglia next to the electrodes. It has also been suggested that ED-1 immune reaction is caused by or exacerbated by an increase in device motion due to electrode anchorage to the skull [55]. However, L1 modified implanted animals show a significant reduction of ED-1 immunoreactivity at the electrode-tissue interface. Iba1 immunoreactivity shows similar trends to both implants, with a broader spatial distribution since Iba1 stains for all microglia present in the brain tissue.

Chondroitin sulfate proteoglycans are important inhibitory molecules in the glial encapsulation/scarring [35]. Upregulated CSPGs have differential sulfation patterns which differentially inhibit neurite outgrowth [123, 124]. Increased levels of CS56 staining were observed around all NM probes and less was seen around the L1 probes at all time points. These observations reinforce the results of the glia cells staining.

In summary, we report the cellular responses associated with the presence of the biomolecule L1 on the silicon surface of microelectrode arrays. Around all L1 modified probes, at all tested time points, we observed a decreased stratified cellular response composed of a small activated zone of microglia attached to and residing most proximal to the probe's interface and a spatially distributed layer of GFAP reactive astrocytes surrounding the macrophages, and finally, in between these immune induced cells we saw a normal arrangement of neuronal bodies with a substantial spatial increase of mature axons around the L1 modified probe. We hypothesize that the covalent bound L1, performs similar mechanisms as it does during *in vitro* cellular environments. The presence of L1 on the surface of the probe makes the implant more biologically presentable to the brain cells and other molecules. In addition, we think that L1 once present on the surface of the probe, it might release cues to recruit other L1 through hemophilic binding. This phenomenon might continue for a long time thus keeping the properties of L1 we observe in this study intact. Detailed studies at cellular and molecular level are required to shed light on the precise mechanisms responsible for the effect of L1 coating. In addition, extensive studies involving longer time points and functional probes would further test the longevity of the effect and whether it leads to improvement in chronic recording.

3.6 CONCLUSIONS

The current study demonstrates that covalent attachment of the neural adhesion protein L1 on silicon based electrode arrays significantly influences the brain tissue reaction, by showing decreased astrogliosis, decreased macrophage/microglial activation, and most importantly

increased immunoreactivity against neurofilament and NeuN at the device brain tissue interface. Thus we can say that the L1 protein shows neuroprotective and neuroregenerative properties while inhibiting gliosis at acute and chronic time points. We can conclude that L1 coating can be a promising strategy to improve the biocompatibility of all types of neural probes and their chronic performance in the brain if a modification system is first established.

4.0 CHRONIC NEURAL RECORDING AND IMPEDANCE MEASUREMENT IN THE RAT BARREL CORTEX TO EVALUATE THE PERFORMANCE OF L1 COATED VS. UNMODIFIED NEURAL PROBES

4.1 INTRODUCTION

Neurons, once severely damaged, do not repair or regenerate themselves, leaving permanent and devastating deficits for millions of people worldwide [118]. Neural implants that interface with the brain tissue to replace or bypass motor functions continue to be one of the most attractive solutions for several neurological traumas and disorders. Significant growth of neural interface technologies is predicted as our society faces population growth and aging problems. To date, the clinically and commercially available neural implant systems still have a lot of room for improvement. For example, cochlear implants are still bulky, mechanically rigid, and functionally limited for the delicate and small organ it replaces. Many other implant systems are still at preclinical stages facing many bioengineering challenges. One of the most difficult challenges that should be overcome for such implants is the so called “foreign body response”, which occurs irrespective of the size or type of device or transplant [29, 35, 40, 44-46, 48, 51, 58, 59, 62, 125]. In the brain tissue, as described in other chapters, this foreign body response has the characteristic phenotype that includes inflammatory markers, reactive gliosis, and neuronal cell loss [35, 37, 54]. To date, significant effort has been focused on describing the events that

follow the implantation of neural devices. Particular emphases are directed at describing the chronological and spatial nature of the events that take place at the implant–tissue interface, and assessing the intensity of this response and how it affects device function [37, 47, 48, 126, 127]. It is clear that improvement of CNS implant technology requires a better understanding of the nature of the tissue that develops adjacent to implants, as well as a better understanding of how to modulate the properties of the tissue via surface modification measures or drug releasing procedures.

In the previous chapters we show the positive effect of the surface immobilized L1 protein *in vitro* on neuronal attachment and neurite outgrowth and *in vivo* on the neuronal density and axonal increase at the electrode tissue interface at several time points. We hypothesize that reported chronic recordings might fail due to a local neurodegenerative state developing at the vicinity of the chronically implanted probes. This phenomenon might also be triggered by gliosis formation which has been shown to be characterized by neuronal loss and axonal pathology in close proximity to the electrode surface [37, 51, 54]. The decrease of neurons around the electrodes (<200 μm), leads to recording signal degradation and eventually signal loss. Neuronal communication is known to be achieved through the propagation of action potentials via membrane depolarization. The distance between the electrode and the neuronal cell membrane necessary for these signals to be recorded is approximately 100 μm . We hypothesize that maintaining neuronal vicinity through the surface bounded L1 protein will form an initial connection between the neurons and the electrodes, which will subsequently stabilize recording signals at chronic time points.

The most common method to assess the implant induced tissue response is to insert model probes into the animal brains and sacrifice them at various time points. Brain tissue is

sectioned and stained to identify cell numbers, cell types, and other byproducts using H&E or immunohistochemical staining. The disadvantages of these methods are 1) the inability to follow the tissue reaction time course in a living animal model, 2) the large amount of time and labor required for histological work, and 3) the quantitative measures of tissue response which vary with different research groups.

Recently, impedance spectroscopy has been proposed to be an effective method of assessing the electrode-tissue interface non-invasively and in real time. Impedance measure is a method to study the biophysics of the passive electrical properties of biological tissues. The complex permittivity of biological tissue is known to vary as a function of frequency. The frequency range to predict changes in the structure of biological tissue is 10 kHz to 10 MHz [128]. A common measure of assessing the performance of chronic probes in the CNS is the magnitude of the impedance at the 1 kHz frequency [26, 50, 129-131]. Studies have been performed correlating changes in tissue impedance properties and tissue response [50, 131]. In the days and weeks after surgical implantation of an electrode in the CNS, electrode impedance typically increases [60, 129, 131]. These changes have been attributed to the attachment of proteins and glial cells directly to the electrode and the development of the glial encapsulation layer around the device. After several weeks, the glial sheath becomes more compact and the electrode-tissue impedance typically stabilizes [131]. Thus, impedance measurements offer a somewhat effective assessment of tissue response over time. However, significant research needs to be performed to determine this relationship.

Several researchers show extensive histology data, without correlation of recording data [30, 37, 54-56, 68, 71-73, 75]. Several other researches show impedance measurements, without correlation to recording data [50, 131]. In addition, every group has implemented their own

quantitative image analysis measures of histology information [30, 50-52, 54-56, 68, 75, 132]. To date a ‘gold standard’ model to quantify the tissue response and correlate this response with impedance properties and a controlled recording model remains to be established. Here, we report our initial approach in proposing a method to correlate recording and impedance measurements together with tissue reaction data analysis.

As a chronic recording model we propose the defined somatosensory cortex of the rat. The rat cortex shows a high degree of areal and laminar differentiation [133]. The primary somatosensory cortex of rodents layer IV contains periodic cell aggregates which are called barrels, because of their anatomical appearance [134, 135]. The arrangement of the respective barrels is so that each barrel is responsible for processing the tactile information that originates from the corresponding contralateral whisker (Figure 28) [136]. Furthermore, each barrel in layer IV represents the morphological connection to a functionally related group of neurons that is vertically arranged across the borders of layers, also called the cortical columns [137, 138]. The proposed barrel cortex recording model offers a controlled mechanism to study the stability of signal quality over time. Implantation of modified and control probes in the barrel cortex can record controlled stimulated whisker response at different time points. Over time the recorded signal quality can degrade or remain the same as observed from the controlled whisker stimulation.

We have developed our recording model with the goal of evaluating the quality, reliability, and longevity of neural electrodes. The model provides to evaluate several different parameters, allowing the researcher to measure the performance of different types of probes, or different modified probes, in a robust setting. In this study we report several impedance spectroscopy data and whisker stimulated neural recording data attained over 8 weeks. In

addition, we report the brain tissue histology data, acquired from two rats implanted with L1 immobilized probes and two implanted with a non modified (NM) control probes.

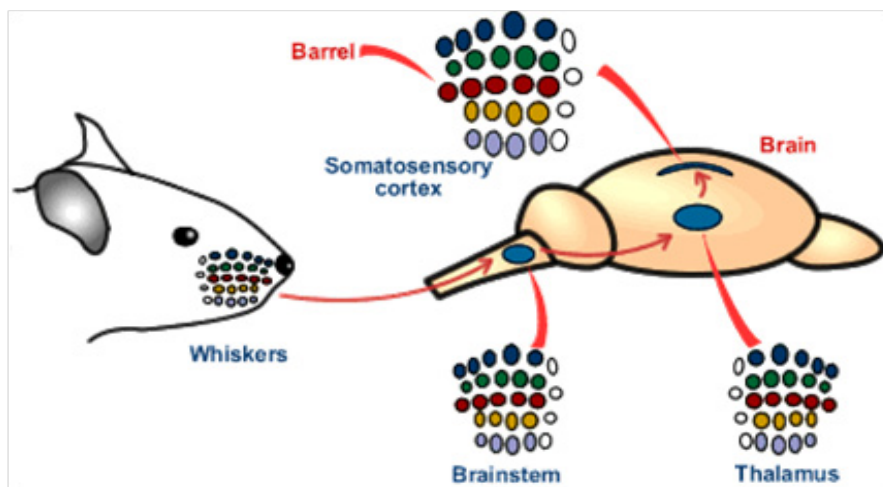


Figure 28. Schematic of the rat's whisker-to-barrel pathway. Rat whisker follicles are indicated by colored circles and at each level of the pathway an isomorphic arrangement of neuronal cell groups, reflecting the layout of the whiskers on the snout, can be found. These are called barrelettes in the primary trigeminal nucleus of the brainstem, barreloids in the ventrobasal thalamic nucleus and most prominent barrels in the primary somatosensory (barrel) cortex.

4.1.1 Probe modification and recording surgical procedure

Four adult male Sprague-Dawley rats (250-300 grams) were implanted with one shank chronic multielectrode arrays purchased from NeuroNexus Technologies (Ann Arbor, MI) (Figure 29). Two of these electrodes were modified with L1 and the other two served as non modified controls. The chronic silicon probes consisted of sixteen channels with $1250 \mu\text{m}^2$ iridium recording sites $100 \mu\text{m}$ away from each other, lying on a planar 2 mm long single shank. The reported impedance (at 1 kHz) of the electrodes from the manufacturer was between 300-500

k Ω . All implanted materials were sterilized using ethylene oxide at least 48 hrs prior to surgeries. The L1 probes were covalently modified with the L1 protein applying the same silane chemistry protocol provided in the previous chapters (see Section 2.3.1.2). Sterile techniques were practiced throughout all surgical procedures.

Rats were anesthetized for 5 minutes with a mixture of 5% isoflurane and 1 L/min oxygen prior to surgery. Animals were mounted on a stereotaxic frame using ear-bars positioned properly in the auditory meatus to firmly support their head during the surgery and anesthesia was maintained to effect (1-3% isoflurane and 1 L/min O₂). Surgical procedures followed as the ones reported in the previous chapter with little modifications (see Section 3.3.2). Briefly, each animal was positioned on the stereotaxic frame and its head was shaved followed by alcohol and betadine sterile rubs. A midline incision was made along the scalp and the skin was cut around the sides of the animal's head. The periosteum was cleared to expose bregma, lambda, and midline.

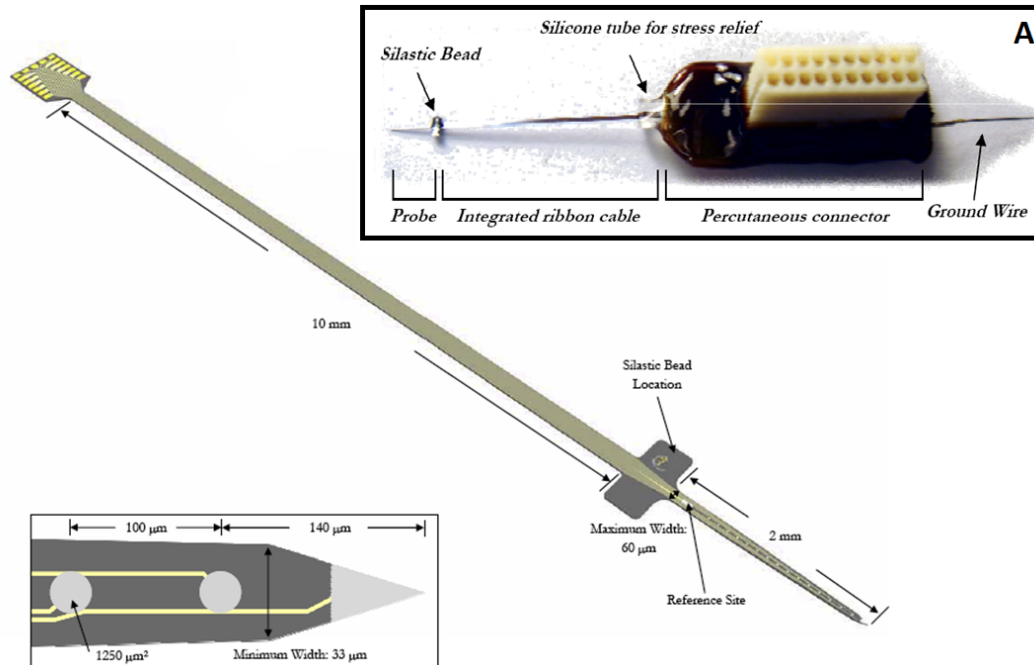


Figure 29. Dimensions of the silicon based electrodes used during recording *in vivo* studies. Inset (A): Components of the recording electrodes. Images were obtained from NeuroNexus Technologies (www.neuronexustech.com).

The coordinates for the somatosensory “barrel” cortex are 4-6 mm lateral to the midline and 1-3 mm posterior to bregma. A 3 x 3 mm craniotomy was centered over the barrel cortex using fine (0.5 mm, 45° angled tip) rongeurs (Fine Science Tools). In order to minimize iatrogenic damage, a hand drill was used to create skull screw holes and to initiate the craniotomy before using the fine rongeurs. The skull bone was very carefully removed with the aid of a surgical scope (Nikon). The dura was gently removed using a fine dura pick (Fine Science Tool). After the probe’s connector was secured to the animal’s skull, the probe was manually inserted into the barrel cortex using fine Teflon coated forceps (Figure 30). Stainless steel skull screws were inserted (dimensions = 0-80 x (1/16); Small Parts) throughout the skull. The electrode connector was grounded to a bone screw using its stainless steel ground wire

(Figure 30a). One skull screw (0 mm lateral and 2 mm posterior to the Lambda) was left exposed and served as the counter electrode during impedance measurements (Figure 29b). One electrode was implanted per rat. After probe implantation, the craniotomy was covered with gel foam (Henry Schein) in 0.9% saline. The craniotomies were further sealed and protected using a silicon elastomer (Kwik-cast, World Precision Instruments, Inc.) to allow for floating of the electrode with the brain. Dental acrylic (Dental Mfg. Co.) anchored to the skull by the rest of the bone screws and covered the rest of the exposed skull. The animal's skin was sutured around the dental acrylic and antibacterial ointment was used to protect from infection. Following impedance and recording measurements the animal was allowed to recover under careful observation in the surgical room. All implants were performed by the same surgeon to minimize variability in data analysis. All procedures were approved by the University of Pittsburgh's Institutional Animal Care and Use Committee.

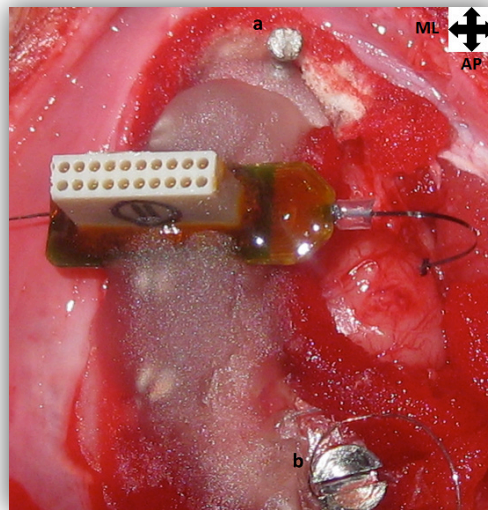


Figure 30. Image of implant in the barrel cortex of the rat brain (right). (a) skull screw used to ground the electrode (b) skull screw used as a counter during impedance measurements. Defined axis: ML (Mediolateral), AP (Anteroposterior – or Rostrocaudal [RC]).

4.1.2 Impedance spectroscopy and modeling

Electrochemical Impedance Spectroscopy (EIS) is an electrochemical technique measured by applying an AC potential to an electrochemical cell and measuring the current through the cell. *In vivo* impedance spectroscopy can be used for electrode characterization as well as tissue reaction detection [50, 131, 139].

Impedance spectroscopy for each animal was performed right after implantation and every 3-4 days thereafter for the remainder of the eight weeks. Throughout the data collection sessions, the animals were maintained under a controlled anesthetic state (1-3% isoflurane and 1 L/min O₂). Complex impedance spectra were carried out for all animals on the same days as the neural recordings using the Gamry FAS2 Femtostat (Gamry Instruments). A sinusoidal voltage (10 mV) signal was applied to the microelectrode, and impedance magnitude and phase were measured referenced to a distant low impedance stainless steel skull screw. Frequencies ranged logarithmically from 10 Hz to 100 kHz at a sweep of 10 points and were sampled at 100 Hz increments. Constant voltage, as opposed to constant current, was used such that changes in electrode properties due to the changing electrode potential are not misinterpreted [131].

Prior to implantation, complex impedance spectra were measured using a 3-electrode method using a platinum plate as the reference electrode and a camel electrode as the counter electrode. Measurements were made by immersing the electrode recording sites in 0.1 M phosphate buffer saline (PBS). This was performed in order to test the electrical properties of the electrodes with our system before implantation.

To model the impedance data, a window of 3 points above and below the 1 kHz frequency was taken to perform a local linear regression. It is expected that higher frequencies

have lower real impedance magnitudes, therefore a point was considered invalid if had a value deviated from the expected inverse relationship between frequency and impedance. If more than 3 points in this window were invalid the channel was removed from the experimental data and considered as an outlier. Otherwise, a linear relationship was fitted with a least squares regression, and the 1kHz/10Hz impedance magnitude point was computed from this line. The magnitude impedances were averaged across all channels and the data is presented as $\text{ave} \pm \text{s.e.m.}$ as a function of days.

4.1.3 Neural recording experiments and analyses

Neural electrophysiological recordings were collected from the four animals (two NM controls and 2 L1 modified probes) one week following surgery, and every 3-4 days thereafter over an 8 week time course. Animals were placed in a Faraday cage under a controlled anesthetic state (1-3% isoflurane and 1 L/min O₂), and segments of high speed data were acquired using a TDT multi-channel acquisition system (RX5; Tucker-Davis Technologies). The contralateral whiskers stimulations were performed using modified air jets connected to an air compressor tank that supplied 20 psi of constant air pressure through solenoid valves (Humphrey Mini-Mizer). These valves were attached to a precision regulator (Control Air Inc.) (Figure 31). The jets were controlled by the solenoid valve which was actuated through the computer using a relay circuit. This allowed precision timing of the air stimulus, as well as pre-programmed stimulation patterns. During trials air stimulations were programmed to release air pressure perpendicular to the whiskers every second for 10 trials. A spontaneous recording (no air) was also collected for comparison reasons. Stimulated and spontaneous neural electrophysiological data for all 16

recording channels were amplified and bandpass filtered; single- and multi-unit recordings were sampled at 25 kHz and bandpass filtered from 300 to 3000 Hz, while local field potentials (LFPs) were sampled at 1 kHz and bandpass filtered from 1 to 100 Hz. Neural recording segments were analyzed offline and followed by further analysis using MatLab (Mathworks Inc., MA) and/or Microsoft Office software.

The exact count (and therefore the exact firing rate) was somewhat arbitrary, but this provided a rough baseline firing rate that can then be used to determine the degree of a response to a stimulus. Snips were sorted using a template algorithm as a guide and then manually inspected for accuracy and irregular spikes. No irregular spikes were discarded, but an “unsorted” category was maintained to consider their effect. When multiple groups could be identified, these were manually isolated. Each category was then analyzed for consistency within the waveform as well as response to the stimulus. Data were reported as percent signal response.

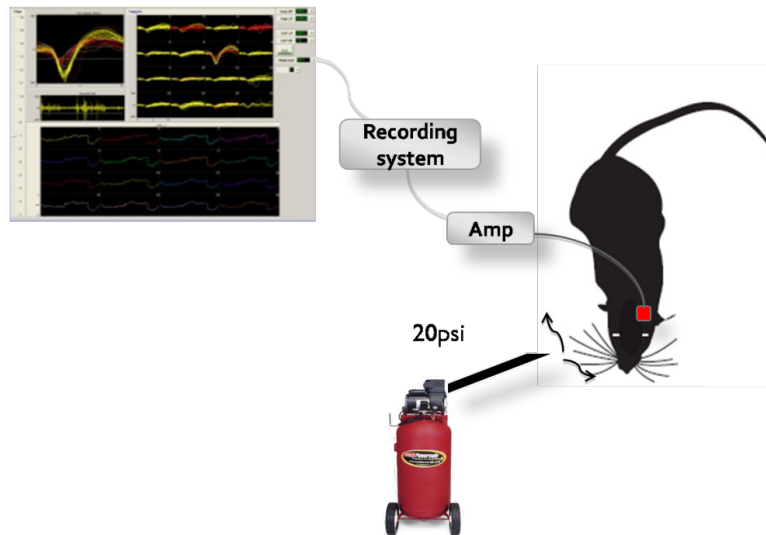


Figure 31. Schematic of the whisker stimulation setup and the recording setup. Air jets were positioned perpendicular to whiskers and contralateral to the recording implant. Raw data from all 16 channels were recorded from different whisker stimulation trials.

Peri-stimulus time histograms (PSTHs) were calculated for 10 presentations of air stimuli using a bin width of 1 s before and after the stimulation. These histograms were used to measure the neuronal response that is traditionally defined as a stimulus-locked change in the peak response magnitude, or firing rate, and which can be detected by summation of spike trains over repeated stimulus presentations. The base-line firing rate was computed by taking the mean across the histogram, and a channel was considered to be responding if the maximum firing rate on the histogram occurred following the stimulation and was at least twice as high as the mean firing rate. Candidate action potentials or multi unit recordings were discriminated from background noise based on the probability distribution of the samples given a time segment. We defined the noise as 2 times the root mean square (RMS) of the high pass filtered signal [32]. The signal reported was computed as the peak-to-peak amplitude of the sorted waveform. Candidate spikes were collected using a user-defined threshold, and then sorted with a combination of a template algorithm and manual inspection. The sorted waveforms were then averaged together to compute a mean waveform and the peak-to-peak amplitude of this waveform was defined as the reported signal. The waveforms used for the LFP calculations were collected during the single pressure stimulus trial in addition to spontaneous trials. LFP amplitude was calculated as the difference between the 95% quantile and the 5% quantile during the pressure stimulus trial. This provides a good estimate of the P-to-P amplitude of continuous data (Equation 1). All these parameters were plotted against time, which will demonstrate the quality, stability and longevity of the recording.

$$SNR = \frac{\text{signal amplitude}}{2 \times \text{calculated RMS noise voltage for a recording site}} \quad (1)$$

Standard techniques for identifying fundamental frequencies of LFP signals typically entail applying a fast Fourier transform (FFT) to the LFP time-series and then examining either the power spectrum or the spectrogram. To analyze the relation between LFP spectral power and spiking activity, we divided each recording session into 500 ms epochs before and after stimulus. This epoch length was chosen to provide a reasonable balance between temporal resolutions. To eliminate the effect of non-biological noise on our analysis, a threshold was defined as the mean plus 2 times the standard deviation of the recording activity. We calculated the mean power of selected data (10 stimuli per channel, over 16 channels), contained in the frequency band of 10 to 20 Hz using FFT. Furthermore, the LFP signal energy was calculated for the data 500 ms before the stimulus (B.S) and after stimulus (A.S.) and averaged across channels. The percent change of the signal energy was calculated using Equation 2.

$$\% \text{ change} = \frac{LFP \text{ A.S} - LFP \text{ B.S}}{LFP \text{ B.S}} \quad (2)$$

4.1.4 Tissue analysis: Brain tissue preparation for immunohistochemistry

After 8 weeks, each animal was anesthetized with 50 mg/ml ketamine, 5 mg/ml xylazine, and 1 mg/ml acepromazine administered via the intraperitoneal cavity with a dosage of 0.1 ml/100 g body weight. The animals were transcardially perfused with 4°C PBS prewash followed by 4% paraformaldehyde in PBS. The brains were removed and postfixed overnight (4°C). Following the retrieval of the electrodes, the rat brains were placed into 30% sucrose solution (4°C) until they sunk to the bottom. The brains were then cryoprotected with OCT compound. Horizontal to the barrel cortex, frozen tissue sections were cut to a final depth of ~2 mm from the surface.

Serial sections (20 μ m) were mounted directly to a SuperFrost Plus glass slides for better frozen tissue adhesion during immune staining. We utilized H&E staining to visualize general tissue morphology, while immunohistochemistry was used to visualize specific cellular markers.

4.1.5 Tissue analysis: Immunohistochemistry and quantitative analyses

To study the brain tissue response, three sections between approximately 500-600 μ m, 1100-1200 μ m, and 1700-1800 μ m below the brain surface were chosen to be stained. The tissue sections were stained simultaneously for each antibody of interest at to minimize variability during data analysis. Six consecutive serial sections were used to stain for six different cell markers at four different depths in the brain (see Section 3.3.4). One serial section at each depth was stained using H&E. The stains used were chosen to visualize the presence of neuronal nuclei (NeuN), astrocytes (GFAP), activated microglia/macrophages (ED-1), mature axons (NF-200), microglia (Iba1), and macrophages (Vimentin). Briefly, tissue sections were hydrated in buffer, and blocked with serum in PBS for 45 min followed with PBS containing 0.5% Triton X-100. The sections were then incubated overnight at 4°C, with the primary antibodies prepared in blocking solution with concentrations shown in table 3 of Chapter 3. The next day sections were rinsed with PBS and incubated for 1 hour in either goat anti-rabbit IgG (H + L) Alexa 488 or goat anti-mouse IgG1 Alexa 488 (Invitrogen) secondary antibodies diluted at a ratio of 1:200 in blocking solution. All sections were counterstained with Hoechst nuclear dye to observe all cell nuclei and cover-slipped with Fluoromount-G to preserve fluorescence over time. Buffer was used in place of primary antibodies for control tissue samples.

Confocal fluorescent and optical DIC images were acquired using a Nikon A1 confocal microscope with 10x or 20x objectives as described in the previous chapter (see Section 3.3.5). For analysis purposes a 10x objective was used, while the electrode site was centered in the camera field. For quantification purposes the images were analyzed for average pixel fluorescent intensity as a function of distance from the electrode-tissue interface was calculated using ImageJ as described in the previous chapter. NeuN stained images were quantified by estimating the number of neurons as a function of distance from the electrode interface, and reported as a function of distance from the electrode site.

4.2 RESULTS AND DISCUSSION

4.2.1 Impedance spectroscopy

We report the impedance magnitude of the electrode recording sites for the L1 and NM control probes at 1 kHz (the fundamental frequency of the neuronal action potential) and 10 Hz (in the frequency range of LFPs) in Figure 31. Impedance spectra were recorded prior to probe implantation (data not shown), the day of implantation (day 0), and every other 3-4 days for the remainder of the experiment. Data shown include 2 L1 modified probes and one NM control. The other control probe was omitted from the data analysis due to high impedance values that also correlated with low signal to noise ratio of neural recording, and an increased tissue reaction.

Although it is difficult to make any definitive conclusions based on the small sample size, one observation consistent with both L1 coated and NM probes is that there was an initial

increase of the 1kHz impedance magnitude in the first week or so post implantation (Figure 31A). This increase can be contributed to the acute tissue responses such as the increase of cells to the surface of the recording electrodes and the start of progressive glial encapsulation [31, 32]. During the remaining course of study, the impedance fluctuates between 200 and 700 kohms with no obvious trend observed.

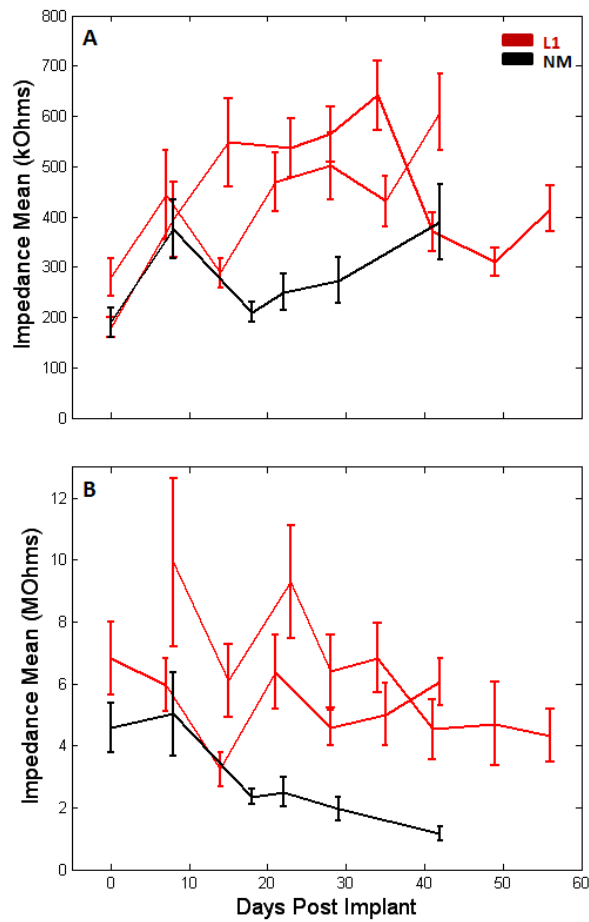


Figure 32. Impedance magnitude for L1 and NM probes at the (A) 1kHz frequency and (B) 10Hz frequency. For two of chronic probes, impedance recordings were terminated at day 42 because of apparatus (Gamry) failure. Data reported as mean \pm s.e.m.

4.2.2 Neural recording analysis

NeuroNexus electrodes work by taking the potential difference between the probe's recording sites and a reference site located on the probe. During recordings, it is preferred to use a reference with an impedance of an order of magnitude less than the recording sites. This allows the rejection of the majority of common mode noise. Electrodes also use a grounding wire, which typically has an impedance of two orders of magnitude below that of the recording sites. Due to inconsistencies in manufacturer documentation, the reference and ground sites were reversed during our recording experiments. This resulted in a higher noise, and difficulty in isolating quality waveforms or single unit. We have elected to use the data to demonstrate the analysis methods we developed. Future experiments will address this technical defect and true quantitative comparison between groups.

A pilot study was conducted comparing the signal quality of L1 modified probes with that acquired from NM control probes. Single shank chronic NeuroNexus silicon based electrodes were implanted in the barrel cortex of SD rats while recording whisker stimulated activity over an 8 week time span. An air jet was used to provide controlled stimulation to the rat's whiskers. Figure 33 shows representative PSTHs for the L1 and NM control at 2 different time points (on the left side of each figure) and LFP traces (on the right side). Stimulus - evoked LFPs and PSTHs were averaged across recording sites for each day.

Observations from these figures can suggest that the L1 probe performed better through time than the NM control probe. Spike counts after stimulus went from 15 to 10 at day 27 and the average LFP trace remained approximately the same (Figure 33B). For the NM control

probe, the spike counts decreased from 6 to 2 and the LFP magnitude seemed to decrease at day 27 (Figure 33D) showing almost no response to stimulus.

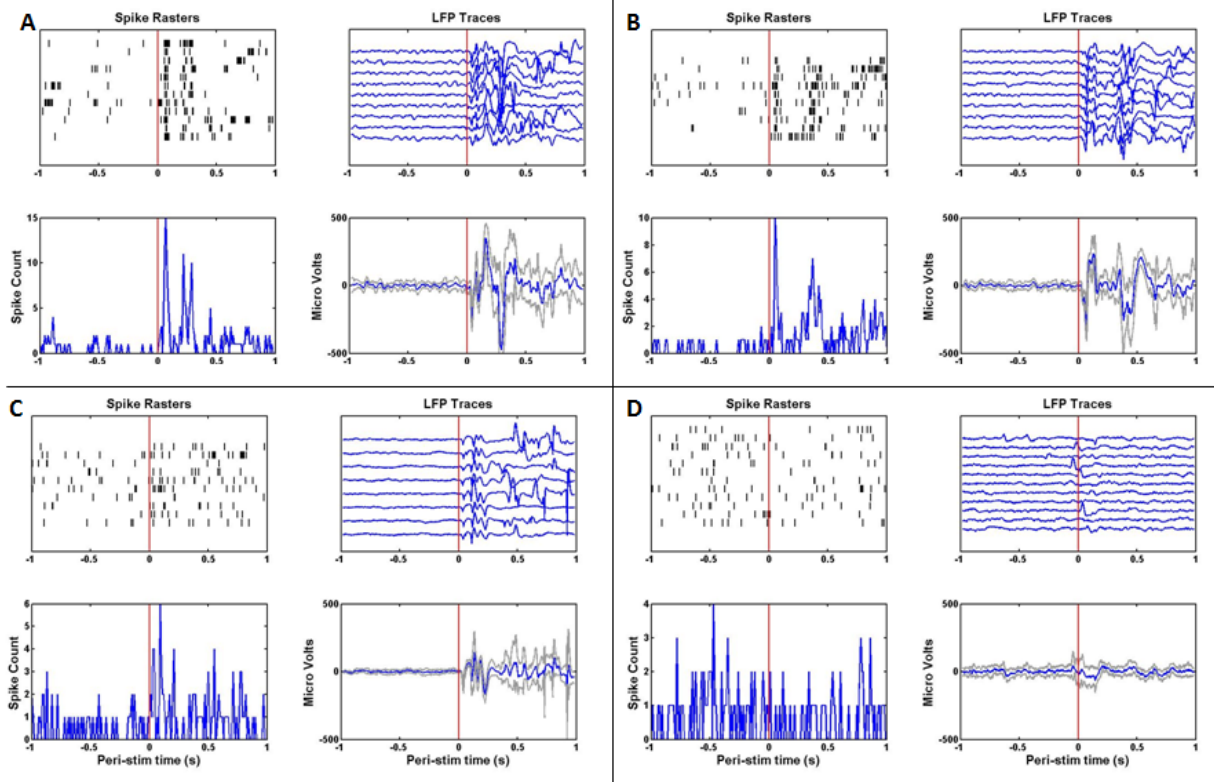


Figure 33. Stimulus-evoked PSTHs and LFP traces. L1 modified probe (A) 12 days post implantation and (B) 27 days post implantation. NM control probe (C) 12 days post implantation and (D) 27 days post implantation. Sixteen channels recorded neural activity 1s prior and 1s past stimulus presentation. The red line represents the start of stimulus application (air). Spike counts are averaged over the sixteen channels. LFP trace is averaged over the sixteen channels of the raw LFP data and the light gray line represents the standard error of mean.

The recording quality of the experimental probes may be evaluated by the parameters calculated in Figure 34. Percent response was calculated as fraction of the channels that recorded unit activity (above a set threshold) in response to a given air stimulus. This data can give insight on how well the implants are responding over time and a general idea on the degradation of

recordings. SNR and LFP amplitude can give further specific insight of the quality of the recorded signals at different time points. These data can be statistically compared to show differences between days or different experimental groups. These recording metrics can also be correlated with impedance measures at corresponding frequencies to reveal the cause of the signal change. Due to the small sample size, correlation studies were not performed during this study.

LFPs show neural signals that represent excitations from thousands of neurons that are near an electrode site. Another way of representing LFPs is through traditional spectrograms and power spectra. The data would give insights on neuronal firing rate concurrent with changes in the LFP power spectrum over time. Percent change in power energy over the frequency band of 10-20 Hz can provide comparisons between the experimental probes over time (Figure 35B).

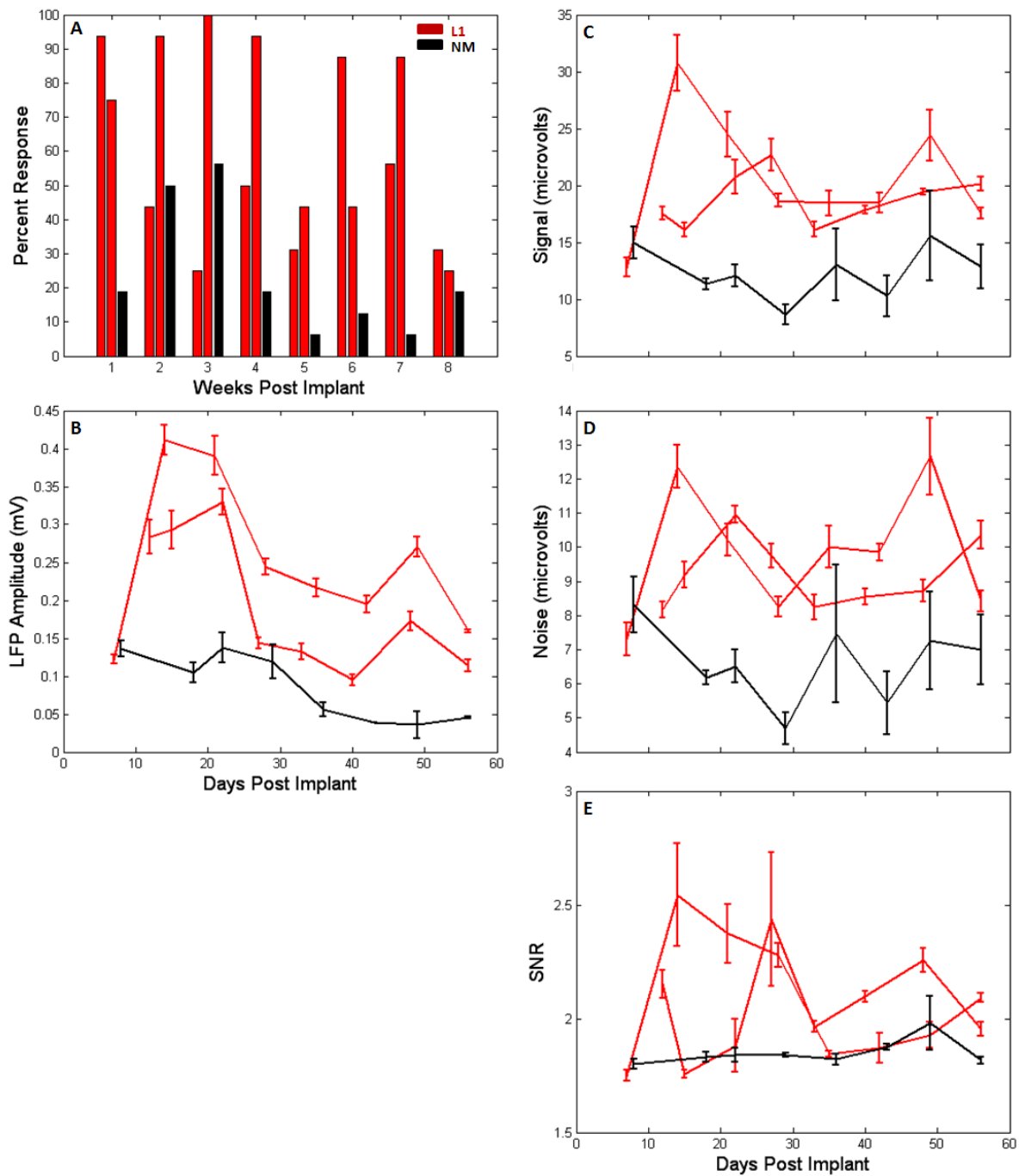


Figure 34. Data analysis representation of recording quality over the 8 week study period for L1 and NM control probes. (B-E) Data reported as mean \pm s.e.m.

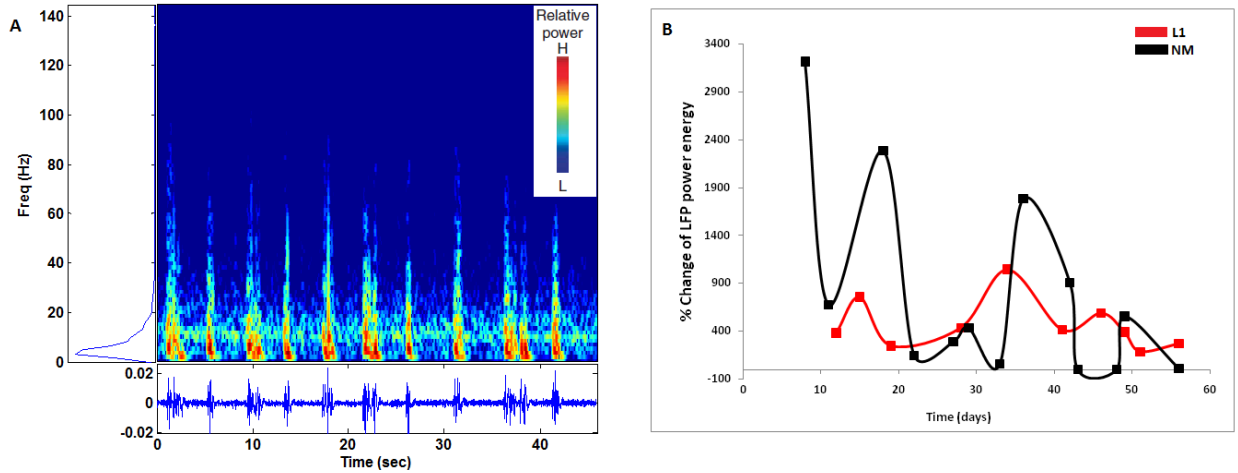


Figure 35. (A) Representative logarithmic power amplitude spectra showing the calculated fundamental frequency of the raw LFP signal for one channel. Bottom blue trace shows the raw LFP signal recorded over a 35 second period. 10 air stimulations were performed during this time, represented as an increase in amplitude (-0.02 – 0.02 mV y-axes). LFP data was passed through a Fourier analysis (Matlab software) to determine the logarithmic amplitude of the signal. The fundamental frequency was calculated from the peaks corresponding in the spectrum (y axis –Freq.) (B) Percent change of LFP power energy for L1 and NM control probes over time. The power energy level was calculated at the 10-20 Hz frequency band over 500 ms epoch before and after stimulus presentation.

4.2.3 Tissue analyses

Quantification of tissue analysis followed at the endpoint of the recording experiments for all rats (Figure 37). Around the L1 modified probes, we observed a decreased stratified cellular response composed of a small activated zone of microglia attached to and residing most proximal to the probe’s interface site and a spatially distributed layer of GFAP reactive astrocytes surrounding the macrophages, and finally, in between these immune induced cells we saw a normal arrangement of neuronal bodies with a substantial spatial increase of mature axons around the L1 modified probe. The results of the tissue response agree with our previous data reported in the

previous chapter for the L1 implants at the 8 week time point. In Figure 36 we show representative histology images from one of the NM probe. Increased gliosis response is shown by the reactivity of GFAP and ED-1 staining. This particular NM probe did also show an increase in impedance and a decrease of the signal to noise ratio. The results for this probe were not included in our reported analysis.

Extensive studies involving more time points and functional probes would provide statistical difference and correlation to the reported data.

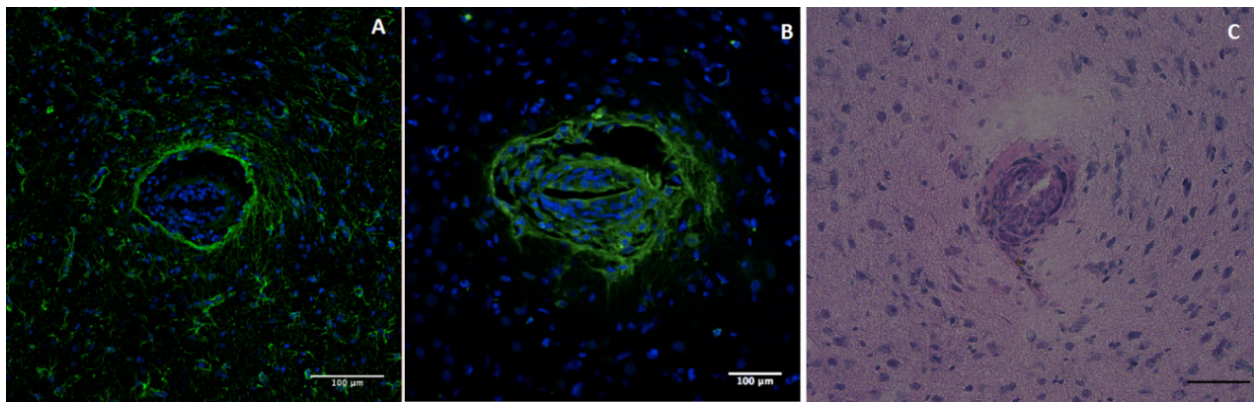


Figure 36. Representative histology from the NM probe (A) GFAP staining for astrocytes shown in green and nuclei in blue. (B) ED-1 staining for activated microglia shown in green and nuclei in blue. (C) H&E staining. Scale bar 100 μm .

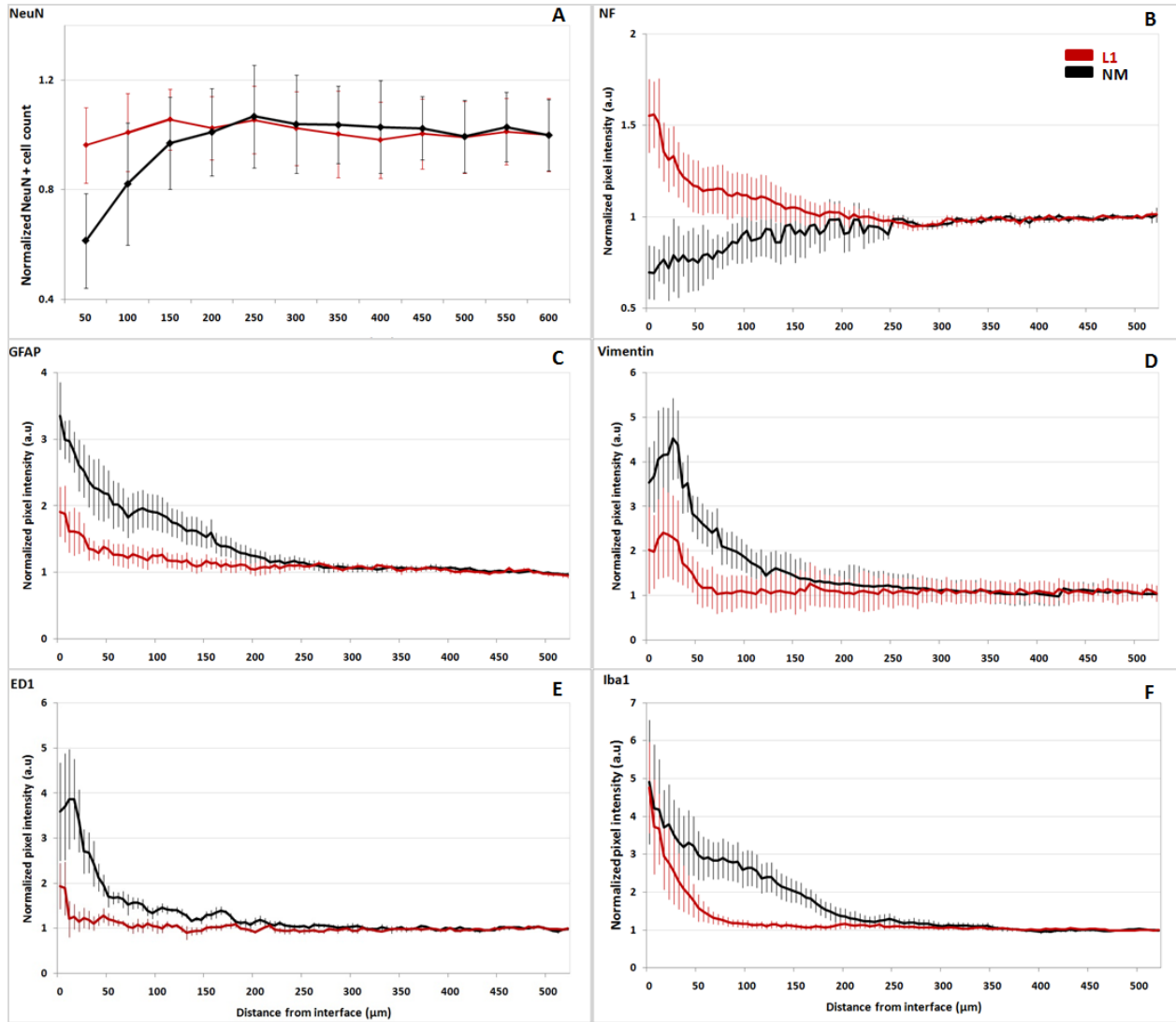


Figure 37. Tissue analysis at the 8 week time point for different markers as a function of distance from the electrode interface. Comparison between the L1 and NM control probes. Data is shown as mean±s.e.m.

4.2.4 Statistical analyses

To compare the above mentioned data we suggest using a linear mixed model ANOVA in order to assess the effect of time and condition on impedance and recording metrics. The random effect should be chosen to be the individual animal, and multiple electrode sites should be included as a repeated measure. Time and condition should be chosen as fixed factors. A linear mixed model

can also be used in tissue analysis to assess the effects of distance and condition on neuronal and non neuronal densities (although the data is averaged across multiple sections per animal and site-by-site analysis is not possible).

Correlation between impedance and recording metrics over the course of the study can be achieved using a linear mixed model in which the values are first standardized, and one variable is defined as a predictor (covariate). The individual animal is included as a random effect to control for correlated observations within the same rat. Significance should be defined at the 0.05 level for all tests.

4.3 EXPERIMENTAL OPTIMIZATION

To continue this study, several techniques should be optimized and followed during future proposed research. Surgical techniques require concentration and, due to anesthesia complications, need to be done to with minimum time but maximum precision. A microscope is required during these micro-surgeries. The head-cap is composed of dental acrylic and the percutaneous connector needs to be secured to the skull using bone screws. Previous research shows that the placement and the amount of bone screws are important during preliminary chronic surgical procedures [24, 137]. We observed that a large number of bone screws placed around the craniotomy held the head-cap tight for several months with no damage to the connector or to the implant. In addition, self-taping bone screws adhere to the bone without further damage. Precautions should be made during placement of the screws— just above the brain tissue—to avoid disturbance of blood vessels and the dura mater. During craniotomy, the

surgeon should use the ronger surgical tool. Rongers allow for accurate bone cutting and they minimize brain damage when compared to the hand-drill tool. Prior to probe implantation, the probe's connector should be secured to the skull using dental acrylic. The probe should be implanted after the dura layer has been carefully removed using a dura pick tool. Implanting the probe on top of major blood vessels should be avoided. Insertion tool devices or micro-manipulators should be used during probe implantation to prevent additional tissue damage. Preferably, recording should start as soon as the first electrode site is implanted in the brain tissue and the probe is advanced in its final position. Another way to improve implant location is to use subdural micro-EEG grids and their signals before probe implantation. EEG signals could provide a rough map of the barrel cortex area where the intracranial probe should be placed.

Recording procedures require the use of an anesthetic that will not interfere with brain activity. However, due to the high frequency of recordings performed (2~3 times a week), the anesthetic should also not interfere with the animal's health. During our studies we chose isoflurane as an appropriate anesthetic for the ease of procedure and quick animal recovery time. Choosing the appropriate amount of isoflurane during recording studies is important. However, more research should be performed to correlate recording activity with isoflurane induced anesthesia depth. Nembutal (Sodium pentobarbital) is a common used anesthetic that does not interfere with neural activity [140]. However, using this drug in chronic conditions requires for the animal to be carefully monitored during the recording procedure and the recovery period. Accidental overdose using this drug was observed during our preliminary studies.

Impedance recordings should be performed before and after probe implantation. Impedance measures are important in determining the tissue response around each electrode site

with time. Standard settings during impedance measurements should be kept throughout chronic procedures. During neural recordings several stimulation (air puffs) trials in 4 directions (up-down, back-forward) should be performed to observe whisker activity. When direction of stimulation is set, it should be used for all remaining recording procedures to observe signal quality of the same stimulation over time.

All recording procedures should be performed carefully and data analysis should follow after each procedure to observe any discrepancies in the data. Channel mapping should be checked before each experimental procedure to avoid any data contradiction. After each recording procedure histological methods should follow. Tissue reaction around the head-cap and other infections should be reported in order to further optimize surgical or other experimental techniques.

4.4 REMARKS AND FUTURE INSIGHTS

Studying the tissue response at acute/chronic time points of functional neural implants can offer critical information needed to advance the use of these implants in clinical setting. This work, represent our first steps towards this direction.

To our knowledge correlation between neural probe performance and tissue response still remains to be determined. This can be due to the lack of a good animal model for chronic recording evaluation. Also, discrepancies in recording quantification techniques and tissue analysis among groups exist. In this chapter we report the initial steps we have taken to determine a model that most researchers could use to study the chronic tissue response of

functional neural implants. Our model, although still needs further improvement, provides the necessary steps towards a more comprehensive study. We describe a controlled stimulation paradigm that offers the stable neural signals including both spike and LFP data, both of which are useful signals for neural prostheses. Several parameters have been established, such as SNR, unit amplitude, LFP amplitude, and can be used to evaluate the recording quality, stability and longevity over time. Our tissue processing and image analysis protocols offer comprehensive information of the cellular composition of the neural electrode/tissue interface. The image analysis technique we apply offers inclusive information about all pixel data provided in the stained image. These protocols may be used to study neural probes of different material, shape, or size. To perform a complete and conclusive study, additional number of animals at more time points would be necessary. Unfortunately, this was not possible for this thesis work due to time/funding constrains. However, the animal model and various protocols established will enable us to perform a more comprehensive study in the near future.

5.0 FUTURE EXPERIMENTS

As mentioned in the previous chapters, chronic failure of implantable microelectrodes is a major problem in preventing the recording of long-term stable neural signals. This problem has hindered research on these probes and also the availability and readiness for clinical use. One of the mechanisms of long-term failure is the host tissue response and more specifically its effect on decreased neuronal activity around the implant. Several investigators are studying the tissue response after implantation, but to our knowledge the recoding performance coupled with tissue response has not been evaluated to a great extent.

The objective of this research was to develop a biocompatible and neuroadhesive coating that can sustain long-term connectivity of the implant with the host neurons. The L1 molecule was specifically chosen with the goal to improve the implant-tissue interface and improve the long-term recording signal and recording stability of the electrodes. Our results show the promising effects of L1 when immobilized on the surface of silicon based neural probes. While we performed extensive histology measures, we believe that applying several other techniques will fortify the results of this study.

The continuation of this work would entail studying the role of L1 at other time points. Longer implant time-points will be needed to investigate whether or not L1 has the same effect on tissue response beyond 8 weeks. Earlier time points before 1 week will be necessary to further elucidate the initial effect of L1.

Future studies should also investigate the effect of inflammation and neurons surrounding chronic implants using several other markers. We are looking at investigating neurodegeneration by staining with Fluoro-Jade C, which is a marker for dead/dying neurons [51]. From the literature on chronic electrode implants, little is known about expression of pro-inflammatory cytokines, such as IL-1, IL-6, and TNF- α at the tissue electrode interface [30]. These biomolecules are thought to be released from activated microglia. Future work should investigate cytokine expression of tissue across several early (days) and late (months) time points at the electrode interface.

We are also working on analyzing combined impedance and recording changes for different time point animals. Future work will entail increasing animal sample size and the frequency of impedance measurements and recordings. In addition, correlations that reveal trends between impedance measurements, recordings, and tissue response will be made when animals are sacrificed at each time point of the impedance measurement/recording. We are working on perfecting our recording protocol to adjust for all these measures.

It will also be necessary to develop other joint methods for reducing the effects of inflammation, while mitigating the neurotoxic effects. Combining drug releasing electrodes with surface immobilization of L1 should reduce the gliosis response to a great extent. Work in our laboratory has been done involving coating and release of dexamethasone from polypyrrole doped electrodes [74].

At last, we are also investigating the effect of L1 when coated on other type of electrodes varying is size and material (Appendix). This is a necessary investigation to propose the use of L1 as a widespread application technique.

APPENDIX

L1 COATING STRATEGIES

We have developed an L1 surface immobilization method that can coat the surface of Parylene-C, the insulating layer of the Floating Microelectrode Array (FMA) electrodes [20].

Parylene-C wires that are used in the assembly of the FMA electrodes were cut to be approximately 0.5-1cm long during *in vitro* experiments. Parylene-C wires were coated with L1 and laminin (positive control) following an established protocol by our lab. Briefly, the Parylene-C wires were plasma treated for 10 seconds and immersed in either 100 µg/ml of L1 or 40 µg/ml of laminin protein solutions for 1 hour and followed by a PBS rinse. All conditions, (untreated wires, plasma treated wires, and protein (L1/laminin) coated wires) were mounted on round glass coverslips using Kwick Sil and placed in 24 well cell culture plates (Costar). To observe the effect of the L1 protein and its bioactivity while its present on the surface of the wire, three primary cell types (neurons, astrocytes, and microglia) were chosen for the *in vitro* experiments. Seven samples per treatment condition were tested for each cell type (n=7).

E18 Sprague Dawley rat cortices were purchased from BrainBits, LLC. Neuronal cell culture was performed following the methods by Brewer et al. The rat cortices were triturated with a 1 ml pipette and removed from Hibernate Media™ (Brain Bits, IL) by centrifugation at

800g for 1 minute. The cells were re-suspended in Neurobasal (Fisher)/B27 (Gibco)/0.5 mM glutamine/25 μ M glutamate (Sigma-Aldrich) culture medium. Neurons were plated on top of the Parylene-C wires (n=7 per condition) at a density of 1.5×10^5 cells/cm² and were cultured for three days at 37°C in 5% CO₂.

Primary astrocyte-enriched cultures were prepared by tryptic digestion of rat cortices from BrainBits, LLC. The resulting suspension was plated on uncoated tissue culture plates and grown in Dulbecco's modified Eagle's medium (DMEM) with 10% heat-inactivated fetal bovine serum (FBS (Hyclone). Astrocytes were passaged once a week, for up to 4 weeks. For experiments, glia were treated with 0.25% trypsin (Sigma–Aldrich), and plated on the samples at a density of 2×10^5 cells/cm² in 10% FCS/DMEM. Astrocytes were grown on the wire samples and maintained in culture for 2 days at 37°C in 5% CO₂.

Rat microglia-enriched cultures with a purity of >98%, were prepared from whole brains of 1-day-old Fischer 344 rat pups as described previously and with minor modification by Liu et al.[141]. In brief, the cells were seeded until they reached confluency into 175- cm² culture flasks and maintained in DMEM/nutrient mixture-F12 containing 10% heat-inactivated FBS, 2 mM L-glutamine, 1 mM sodium pyruvate, 100 mM non-essential amino acids, 50 U/ml penicillin, and 50 mg/ml streptomycin. The culture medium was replenished one and four days after plating and changed every three days thereafter. Upon reaching glial confluence (14–17 days), the microglia were separated from astrocytes by shaking the flasks at 180 rpm for 45 minutes. The collected microglia cells were spun for 5 min at 1100 rpm and were seeded on the Parylene-C samples at a density of 1.5×10^5 cells/cm² in DMEM/F12 medium for 3 days at 37°C in 5% CO₂.

Prior to immunocytochemistry all cultured cells grown on the Parylene-C wires were fixed in 4% paraformaldehyde for 10-15 min. The samples were then incubated for 1 hour at

room temperature in the appropriate antibodies against β -tubulin III (neurons), GFAP (astrocytes), or ED1 (activated microglia), at concentrations of 2 μ g/ml in 4% goat serum. All cells were counterstained using the nuclear dye Hoechst 33258 (Sigma-Aldrich) (2 μ g/ml) in PBS. Digital images of the stained cells were taken using a fluorescence microscope. Cell counts were performed on the top visible surface of each wire and cell number per surface area was calculated. The statistical analysis was performed using the standard Student's t-test ($\alpha = 0.05$) for comparison between two conditions.

RESULTS

Untreated Parylene-C samples do not support cell attachment and growth. Plasma treatment was found to be necessary and effective in promoting the attachment of the L1 protein onto the Parylene-C surface, demonstrated by the excellent neuron attachment and neurite outgrowth. In addition, significant reduction of astrocyte and microglia growth was observed when compared to untreated Parylene-C wire conditions.

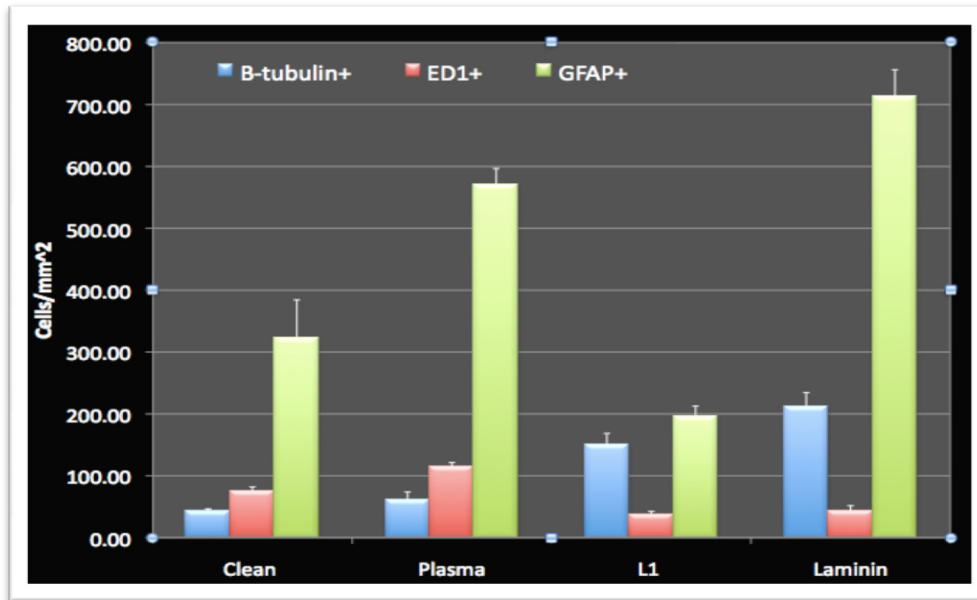


Figure 38. Data representing cell attachment and growth per surface area on untreated and modified Parylene-C wires. L1 treated wires showed a significant difference when compared to the untreated wires $*p<0.05$. β -tubulin III stains for neurons, ED1 stains for activated microglia, and GFAP stains for astrocytes.

The quantitative cell counts are summarized in Figure 38. Number of neurons increased on both types of wires with the L1 and laminin coating (Figure 39). However, there are significantly less astrocytes on the L1 coated wires than the laminin coated wires. This is expected based on the different bioactivities of the two proteins. L1 is a neuron specific adhesion molecule that promotes neuron growth and adhesion via homophilic binding, while laminin is an extracellular matrix protein that can bind to many types of cells via Integrin receptors. Therefore, the L1 treated surface, selectively promotes the neuron attachment and not the astrocytes and microglia.

These results suggest that plasma treatment and coating of L1 protein onto the surface of Parylene-C can provide a more biocompatible surface in the brain with the hope of improving

the chronic tissue-implant interface by reducing gliosis and maintaining neuronal density around the implant.

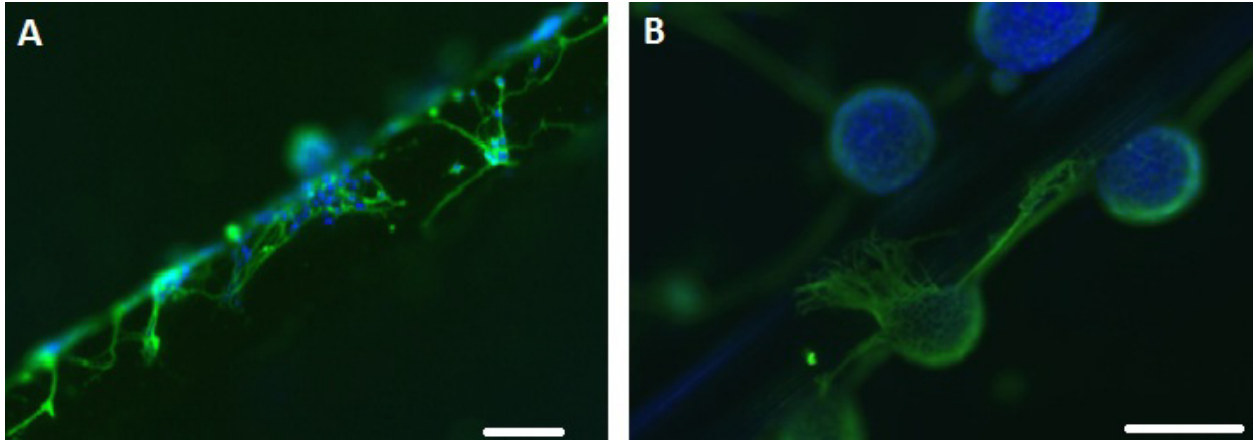


Figure 39. Representative images of β -tubulin III positive neurons grown on A) L1 modified Parylene C wire and B) laminin modified Parylene C wire. Scale bar 100 μ m.

BIBLIOGRAPHY

- [1] E. M. Schmidt, M. J. Bak, and J. S. McIntosh, Long-term chronic recording from cortical neurons. *Exp Neurol* 52(3) (1976) 496-506.
- [2] A. B. Schwartz, Cortical neural prosthetics. *Annu Rev Neurosci* 27 (2004) 487-507.
- [3] J. P. Donoghue, Bridging the brain to the world: a perspective on neural interface systems. *Neuron* 60(3) (2008) 511-521.
- [4] B. S. Wilson and M. F. Dorman, Cochlear implants: a remarkable past and a brilliant future. *Hear Res* 242(1-2) (2008) 3-21.
- [5] J. E. Arle and R. L. Alterman, Surgical options in Parkinson's disease. *Med Clin North Am* 83(2) (1999) 483-498, vii.
- [6] P. R. Kennedy and R. A. Bakay, Restoration of neural output from a paralyzed patient by a direct brain connection. *Neuroreport* 9(8) (1998) 1707-1711.
- [7] L. R. Hochberg, M. D. Serruya, G. M. Friehs, J. A. Mukand, M. Saleh, A. H. Caplan, A. Branner, D. Chen, R. D. Penn, and J. P. Donoghue, Neuronal ensemble control of prosthetic devices by a human with tetraplegia. *Nature* 442(7099) (2006) 164-171.
- [8] J. P. Donoghue, A. Nurmikko, M. Black, and L. R. Hochberg, Assistive technology and robotic control using motor cortex ensemble-based neural interface systems in humans with tetraplegia. *J Physiol* 579(Pt 3) (2007) 603-611.
- [9] J. P. Donoghue, A. Nurmikko, G. Friehs, and M. Black, Development of neuromotor prostheses for humans. *Suppl Clin Neurophysiol* 57 (2004) 592-606.

- [10] W. Truccolo, G. M. Friehs, J. P. Donoghue, and L. R. Hochberg, Primary motor cortex tuning to intended movement kinematics in humans with tetraplegia. *J Neurosci* 28(5) (2008) 1163-1178.
- [11] W. Truccolo, L. R. Hochberg, and J. P. Donoghue, Collective dynamics in human and monkey sensorimotor cortex: predicting single neuron spikes. *Nat Neurosci* 13(1) (2010) 105-111.
- [12] J. P. Donoghue, Connecting cortex to machines: recent advances in brain interfaces. *Nat Neurosci* 5 Suppl (2002) 1085-1088.
- [13] G. M. Friehs, V. A. Zerris, C. L. Ojakangas, M. R. Fellows, and J. P. Donoghue, Brain-machine and brain-computer interfaces. *Stroke* 35(11 Suppl 1) (2004) 2702-2705.
- [14] N. G. Hatsopoulos and J. P. Donoghue, The science of neural interface systems. *Annu Rev Neurosci* 32 (2009) 249-266.
- [15] A. Kubler, V. K. Mushahwar, L. R. Hochberg, and J. P. Donoghue, BCI Meeting 2005--workshop on clinical issues and applications. *IEEE Trans Neural Syst Rehabil Eng* 14(2) (2006) 131-134.
- [16] E. V. Evarts, Effects of sleep and waking on spontaneous and evoked discharge of single units in visual cortex. *Fed Proc* 19 (1960) 828-837.
- [17] A. C. Hoogerwerf and K. D. Wise, A three-dimensional microelectrode array for chronic neural recording. *IEEE Trans Biomed Eng* 41(12) (1994) 1136-1146.
- [18] K. E. Jones, P. K. Campbell, and R. A. Normann, A glass/silicon composite intracortical electrode array. *Ann Biomed Eng* 20(4) (1992) 423-437.
- [19] S. Metz, A. Bertsch, D. Bertrand, and P. Renaud, Flexible polyimide probes with microelectrodes and embedded microfluidic channels for simultaneous drug delivery and multi-channel monitoring of bioelectric activity. *Biosens Bioelectron* 19(10) (2004) 1309-1318.
- [20] S. Musallam, M. J. Bak, P. R. Troyk, and R. A. Andersen, A floating metal microelectrode array for chronic implantation. *J Neurosci Methods* 160(1) (2007) 122-127.

- [21] Y. Y. Chen, H. Y. Lai, S. H. Lin, C. W. Cho, W. H. Chao, C. H. Liao, S. Tsang, Y. F. Chen, and S. Y. Lin, Design and fabrication of a polyimide-based microelectrode array: application in neural recording and repeatable electrolytic lesion in rat brain. *J Neurosci Methods* 182(1) (2009) 6-16.
- [22] A. E. Ayoub, B. Gosselin, and M. Sawan, A microsystem integration platform dedicated to build multi-chip-neural interfaces. *Conf Proc IEEE Eng Med Biol Soc* 2007 (2007) 6605-6608.
- [23] D. R. Kipke, R. J. Vetter, J. C. Williams, and J. F. Hetke, Silicon-substrate intracortical microelectrode arrays for long-term recording of neuronal spike activity in cerebral cortex. *IEEE Trans Neural Syst Rehabil Eng* 11(2) (2003) 151-155.
- [24] R. J. Vetter, J. C. Williams, J. F. Hetke, E. A. Nunamaker, and D. R. Kipke, Chronic neural recording using silicon-substrate microelectrode arrays implanted in cerebral cortex. *IEEE Trans Biomed Eng* 51(6) (2004) 896-904.
- [25] M. A. Nicolelis, Brain-machine interfaces to restore motor function and probe neural circuits. *Nat Rev Neurosci* 4(5) (2003) 417-422.
- [26] P. J. Rousche and R. A. Normann, Chronic recording capability of the Utah Intracortical Electrode Array in cat sensory cortex. *J Neurosci Methods* 82(1) (1998) 1-15.
- [27] M. Velliste, S. Perel, M. C. Spalding, A. S. Whitford, and A. B. Schwartz, Cortical control of a prosthetic arm for self-feeding. *Nature* 453(7198) (2008) 1098-1101.
- [28] J. P. Seymour and D. R. Kipke, Neural probe design for reduced tissue encapsulation in CNS. *Biomaterials* 28(25) (2007) 3594-3607.
- [29] J. N. Turner, W. Shain, D. H. Szarowski, M. Andersen, S. Martins, M. Isaacson, and H. Craighead, Cerebral astrocyte response to micromachined silicon implants. *Exp Neurol* 156(1) (1999) 33-49.
- [30] R. Biran, M. D. Noble, and P. A. Tresco, Characterization of cortical astrocytes on materials of differing surface chemistry. *J Biomed Mater Res* 46(2) (1999) 150-159.

- [31] E. K. Purcell, D. E. Thompson, K. A. Ludwig, and D. R. Kipke, Flavopiridol reduces the impedance of neural prostheses in vivo without affecting recording quality. *J Neurosci Methods* 183(2) (2009) 149-157.
- [32] K. A. Ludwig, J. D. Uram, J. Yang, D. C. Martin, and D. R. Kipke, Chronic neural recordings using silicon microelectrode arrays electrochemically deposited with a poly(3,4-ethylenedioxythiophene) (PEDOT) film. *J Neural Eng* 3(1) (2006) 59-70.
- [33] K. A. Moxon, N. M. Kalkhoran, M. Markert, M. A. Sambito, J. L. McKenzie, and J. T. Webster, Nanostructured surface modification of ceramic-based microelectrodes to enhance biocompatibility for a direct brain-machine interface. *IEEE Trans Biomed Eng* 51(6) (2004) 881-889.
- [34] J. M. Anderson, A. Rodriguez, and D. T. Chang, Foreign body reaction to biomaterials. *Semin Immunol* 20(2) (2008) 86-100.
- [35] J. W. Fawcett and R. A. Asher, The glial scar and central nervous system repair. *Brain Res Bull* 49(6) (1999) 377-391.
- [36] D. T. Weldon, S. D. Rogers, J. R. Ghilardi, M. P. Finke, J. P. Cleary, E. O'Hare, W. P. Esler, J. E. Maggio, and P. W. Mantyh, Fibrillar beta-amyloid induces microglial phagocytosis, expression of inducible nitric oxide synthase, and loss of a select population of neurons in the rat CNS in vivo. *J Neurosci* 18(6) (1998) 2161-2173.
- [37] V. S. Polikov, P. A. Tresco, and W. M. Reichert, Response of brain tissue to chronically implanted neural electrodes. *J Neurosci Methods* 148(1) (2005) 1-18.
- [38] D. H. Szarowski, M. D. Andersen, S. Retterer, A. J. Spence, M. Isaacson, H. G. Craighead, J. N. Turner, and W. Shain, Brain responses to micro-machined silicon devices. *Brain Research* 983(1-2) (2003) 23-35.
- [39] Y. T. Kim, R. W. Hitchcock, M. J. Bridge, and P. A. Tresco, Chronic response of adult rat brain tissue to implants anchored to the skull. *Biomaterials* 25(12) (2004) 2229-2237.
- [40] T. G. H. Yuen and W. F. Agnew, Histological-Evaluation of Polyesterimide-Insulated Gold Wires in Brain. *Biomaterials* 16(12) (1995) 951-956.

- [41] J. Csicsvari, D. A. Henze, B. Jamieson, K. D. Harris, A. Sirota, P. Bartho, K. D. Wise, and G. Buzsaki, Massively parallel recording of unit and local field potentials with silicon-based electrodes. *Journal of Neurophysiology* 90(2) (2003) 1314-1323.
- [42] P. J. Rousche, D. S. Pellinen, D. P. Pivin, J. C. Williams, R. J. Vetter, and D. R. Kipke, Flexible polyimide-based intracortical electrode arrays with bioactive capability. *Ieee Transactions on Biomedical Engineering* 48(3) (2001) 361-371.
- [43] P. Menei, A. Croue, V. Daniel, A. Pouplardbarthelaix, and J. P. Benoit, Fate and Biocompatibility of 3 Types of Microspheres Implanted into the Brain. *Journal of Biomedical Materials Research* 28(9) (1994) 1079-1085.
- [44] M. M. Mofid, R. C. Thompson, C. A. Pardo, P. N. Manson, and C. A. VanderKolk, Biocompatibility of fixation materials in the brain. *Plastic and Reconstructive Surgery* 100(1) (1997) 14-20.
- [45] D. F. Emerich, M. A. Tracy, K. L. Ward, M. Figueiredo, R. L. Qian, C. Henschel, and R. T. Bartus, Biocompatibility of poly (DL-lactide-co-glycolide) microspheres implanted into the brain. *Cell Transplantation* 8(1) (1999) 47-58.
- [46] J. Mokry, J. Karbanova, J. Lukas, V. Paleckova, and B. Dvorankova, Biocompatibility of HEMA copolymers designed for treatment of CNS diseases with polymer-encapsulated cells. *Biotechnology Progress* 16(5) (2000) 897-904.
- [47] S. S. Stensaas and L. J. Stensaas, The reaction of the cerebral cortex to chronically implanted plastic needles. *Acta Neuropathol* 35 (1976) 187-203.
- [48] S. S. Stensaas and L. J. Stensaas, Histopathological evaluation of materials implanted in the cerebral cortex. *Acta Neuropathol (Berl)* 41 (1978) 145-155.
- [49] X. Liu, D. B. McCreery, L. A. Bullara, and W. F. Agnew, Evaluation of the stability of intracortical microelectrode arrays. *IEEE Trans Neural Syst Rehabil Eng* 14(1) (2006) 91-100.
- [50] G. C. McConnell, R. J. Butera, and R. V. Bellamkonda, Bioimpedance modeling to monitor astrocytic response to chronically implanted electrodes. *J Neural Eng* 6(5) (2009) 55005.

- [51] G. C. McConnell, H. D. Rees, A. I. Levey, C. A. Gutekunst, R. E. Gross, and R. V. Bellamkonda, Implanted neural electrodes cause chronic, local inflammation that is correlated with local neurodegeneration. *J Neural Eng* 6(5) (2009) 56003.
- [52] G. C. McConnell, T. M. Schneider, D. J. Owens, and R. V. Bellamkonda, Extraction force and cortical tissue reaction of silicon microelectrode arrays implanted in the rat brain. *IEEE Trans Biomed Eng* 54(6 Pt 1) (2007) 1097-1107.
- [53] J. N. Turner, W. Shain, D. H. Szarowski, M. Andersen, S. Martins, M. Isaacson, and H. Craighead, Cerebral astrocyte response to micromachined silicon implants. *Experimental Neurology* 156(1) (1999) 33-49.
- [54] R. Biran, D. C. Martin, and P. A. Tresco, Neuronal cell loss accompanies the brain tissue response to chronically implanted silicon microelectrode arrays. *Exp Neurol* 195(1) (2005) 115-126.
- [55] Y. T. Kim, R. W. Hitchcock, M. J. Bridge, and P. A. Tresco, Chronic response of adult rat brain tissue to implants anchored to the skull. *Biomaterials* 25(12) (2004) 2229-2237.
- [56] B. D. Winslow and P. A. Tresco, Quantitative analysis of the tissue response to chronically implanted microwire electrodes in rat cortex. *Biomaterials* 31(7) (2010) 1558-1567.
- [57] C. S. Bjornsson, S. J. Oh, Y. A. Al-Kofahi, Y. J. Lim, K. L. Smith, J. N. Turner, S. De, B. Roysam, W. Shain, and S. J. Kim, Effects of insertion conditions on tissue strain and vascular damage during neuroprosthetic device insertion. *J Neural Eng* 3(3) (2006) 196-207.
- [58] D. H. Szarowski, M. D. Andersen, S. Retterer, A. J. Spence, M. Isaacson, H. G. Craighead, J. N. Turner, and W. Shain, Brain responses to micro-machined silicon devices. *Brain Res* 983(1-2) (2003) 23-35.
- [59] D. J. Edell, V. V. Toi, V. M. McNeil, and L. D. Clark, Factors influencing the biocompatibility of insertable silicon microshafts in cerebral cortex. *IEEE Trans Biomed Eng* 39(6) (1992) 635-643.
- [60] A. B. Schwartz, X. T. Cui, D. J. Weber, and D. W. Moran, Brain-controlled interfaces: movement restoration with neural prosthetics. *Neuron* 52(1) (2006) 205-220.

- [61] J. Silver and J. H. Miller, Regeneration beyond the glial scar. *Nat Rev Neurosci* 5(2) (2004) 146-156.
- [62] W. J. Brown, T. L. Babb, H. V. Soper, J. P. Lieb, C. A. Ottino, and P. H. Crandall, Tissue reactions to long-term electrical stimulation of the cerebellum in monkeys. *J Neurosurg* 47(3) (1977) 366-379.
- [63] R. W. Griffith and D. R. Humphrey, Long-term gliosis around chronically implanted platinum electrodes in the Rhesus macaque motor cortex. *Neurosci Lett* 406(1-2) (2006) 81-86.
- [64] R. L. Rennaker, S. Street, A. M. Ruyle, and A. M. Sloan, A comparison of chronic multi-channel cortical implantation techniques: manual versus mechanical insertion. *J Neurosci Methods* 142(2) (2005) 169-176.
- [65] J. D. Kralik, D. F. Dimitrov, D. J. Krupa, D. B. Katz, D. Cohen, and M. A. Nicolelis, Techniques for long-term multisite neuronal ensemble recordings in behaving animals. *Methods* 25(2) (2001) 121-150.
- [66] X. Cui, J. Wiler, M. Dzaman, R. A. Altschuler, and D. C. Martin, In vivo studies of polypyrrole/peptide coated neural probes. *Biomaterials* 24(5) (2003) 777-787.
- [67] X. Y. Cui and D. C. Martin, Electrochemical deposition and characterization of poly(3,4-ethylenedioxythiophene) on neural microelectrode arrays. *Sensors and Actuators B-Chemical* 89(1-2) (2003) 92-102.
- [68] W. He, G. C. McConnell, and R. V. Bellamkonda, Nanoscale laminin coating modulates cortical scarring response around implanted silicon microelectrode arrays. *J Neural Eng* 3(4) (2006) 316-326.
- [69] M. R. Abidian, J. M. Corey, D. R. Kipke, and D. C. Martin, Conducting-polymer nanotubes improve electrical properties, mechanical adhesion, neural attachment, and neurite outgrowth of neural electrodes. *Small* 6(3) (2010) 421-429.
- [70] M. R. Abidian and D. C. Martin, Experimental and theoretical characterization of implantable neural microelectrodes modified with conducting polymer nanotubes. *Biomaterials* 29(9) (2008) 1273-1283.

- [71] D. H. Kim and D. C. Martin, Sustained release of dexamethasone from hydrophilic matrices using PLGA nanoparticles for neural drug delivery. *Biomaterials* 27(15) (2006) 3031-3037.
- [72] L. Spataro, J. Dilgen, S. Retterer, A. J. Spence, M. Isaacson, J. N. Turner, and W. Shain, Dexamethasone treatment reduces astroglia responses to inserted neuroprosthetic devices in rat neocortex. *Exp Neurol* 194(2) (2005) 289-300.
- [73] W. Shain, L. Spataro, J. Dilgen, K. Haverstick, S. Retterer, M. Isaacson, M. Saltzman, and J. N. Turner, Controlling cellular reactive responses around neural prosthetic devices using peripheral and local intervention strategies. *IEEE Trans Neural Syst Rehabil Eng* 11(2) (2003) 186-188.
- [74] R. Wadhwa, C. F. Lagenaur, and X. T. Cui, Electrochemically controlled release of dexamethasone from conducting polymer polypyrrole coated electrode. *J Control Release* 110(3) (2006) 531-541.
- [75] Y. Zhong and R. V. Bellamkonda, Dexamethasone-coated neural probes elicit attenuated inflammatory response and neuronal loss compared to uncoated neural probes. *Brain Res* 1148 (2007) 15-27.
- [76] E. K. Purcell, J. P. Seymour, S. Yandamuri, and D. R. Kipke, In vivo evaluation of a neural stem cell-seeded prosthesis. *J Neural Eng* 6(2) (2009) 026005.
- [77] E. K. Purcell, A. Singh, and D. R. Kipke, Alginate composition effects on a neural stem cell-seeded scaffold. *Tissue Eng Part C Methods* 15(4) (2009) 541-550.
- [78] E. Azemi, G. T. Gobbel, and X. T. Cui, Seeding neural progenitor cells on silicon-based neural probes. *J Neurosurg* (2010).
- [79] K. C. Cheung, Implantable microscale neural interfaces. *Biomed Microdevices* (2007).
- [80] E. M. Maynard, C. T. Nordhausen, and R. A. Normann, The Utah intracortical Electrode Array: a recording structure for potential brain-computer interfaces. *Electroencephalogr Clin Neurophysiol* 102(3) (1997) 228-239.

- [81] V. S. Polikov, M. L. Block, J. M. Fellous, J. S. Hong, and W. M. Reichert, In vitro model of glial scarring around neuroelectrodes chronically implanted in the CNS. *Biomaterials* 27(31) (2006) 5368-5376.
- [82] X. Cui, V. A. Lee, Y. Raphael, J. A. Wiler, J. F. Hetke, D. J. Anderson, and D. C. Martin, Surface modification of neural recording electrodes with conducting polymer/biomolecule blends. *J Biomed Mater Res* 56(2) (2001) 261-272.
- [83] W. R. Stauffer and X. T. Cui, Polypyrrole doped with 2 peptide sequences from laminin. *Biomaterials* 27(11) (2006) 2405-2413.
- [84] S. P. Massia, M. M. Holecko, and G. R. Ehteshami, In vitro assessment of bioactive coatings for neural implant applications. *J Biomed Mater Res A* 68(1) (2004) 177-186.
- [85] D. H. Davis, C. S. Giannoulis, R. W. Johnson, and T. A. Desai, Immobilization of RGD to < 1 1 1 > silicon surfaces for enhanced cell adhesion and proliferation. *Biomaterials* 23(19) (2002) 4019-4027.
- [86] W. He and R. V. Bellamkonda, Nanoscale neuro-integrative coatings for neural implants. *Biomaterials* 26(16) (2005) 2983-2990.
- [87] C. D. James, R. Davis, M. Meyer, A. Turner, S. Turner, G. Withers, L. Kam, G. Banker, H. Craighead, M. Isaacson, J. Turner, and W. Shain, Aligned microcontact printing of micrometer-scale poly-L-lysine structures for controlled growth of cultured neurons on planar microelectrode arrays. *IEEE Trans Biomed Eng* 47(1) (2000) 17-21.
- [88] Y. Wu, Q. Zheng, J. Du, Y. Song, B. Wu, and X. Guo, Self-assembled IKVAV peptide nanofibers promote adherence of PC12 cells. *J Huazhong Univ Sci Technolog Med Sci* 26(5) (2006) 594-596.
- [89] S. Golde, A. Coles, J. A. Lindquist, and A. Compston, Decreased iNOS synthesis mediates dexamethasone-induced protection of neurons from inflammatory injury in vitro. *Eur J Neurosci* 18(9) (2003) 2527-2537.
- [90] N. Nagano, M. Aoyagi, and K. Hirakawa, Extracellular matrix modulates the proliferation of rat astrocytes in serum-free culture. *Glia* 8(2) (1993) 71-76.

- [91] J. R. Couchman, M. Hook, D. A. Rees, and R. Timpl, Adhesion, growth, and matrix production by fibroblasts on laminin substrates. *J Cell Biol* 96(1) (1983) 177-183.
- [92] P. Liesi, Extracellular matrix and neuronal movement. *Experientia* 46(9) (1990) 900-907.
- [93] F. G. Rathjen and M. Schachner, Immunocytological and biochemical characterization of a new neuronal cell surface component (L1 antigen) which is involved in cell adhesion. *Embo J* 3(1) (1984) 1-10.
- [94] S. Kenwrick, A. Watkins, and E. De Angelis, Neural cell recognition molecule L1: relating biological complexity to human disease mutations. *Hum Mol Genet* 9(6) (2000) 879-886.
- [95] M. Hortsch, The L1 family of neural cell adhesion molecules: old proteins performing new tricks. *Neuron* 17(4) (1996) 587-593.
- [96] C. Lagenaur and V. Lemmon, An L1-like molecule, the 8D9 antigen, is a potent substrate for neurite extension. *Proc Natl Acad Sci U S A* 84(21) (1987) 7753-7757.
- [97] V. Lemmon, S. M. Burden, H. R. Payne, G. J. Elmslie, and M. L. Hlavin, Neurite growth on different substrates: permissive versus instructive influences and the role of adhesive strength. *J Neurosci* 12(3) (1992) 818-826.
- [98] M. Dihne, C. Bernreuther, M. Sibbe, W. Paulus, and M. Schachner, A new role for the cell adhesion molecule L1 in neural precursor cell proliferation, differentiation, and transmitter-specific subtype generation. *J Neurosci* 23(16) (2003) 6638-6650.
- [99] K. Webb, E. Budko, T. J. Neuberger, S. Chen, M. Schachner, and P. A. Tresco, Substrate-bound human recombinant L1 selectively promotes neuronal attachment and outgrowth in the presence of astrocytes and fibroblasts. *Biomaterials* 22(10) (2001) 1017-1028.
- [100] F. S. Walsh and P. Doherty, Neural cell adhesion molecules of the immunoglobulin superfamily: role in axon growth and guidance. *Annu Rev Cell Dev Biol* 13 (1997) 425-456.

- [101] J. R. Lu, M. J. Swann, L. L. Peel, and N. J. Freeman, Lysozyme adsorption studies at the silica/water interface using dual polarization interferometry. *Langmuir* 20(5) (2004) 1827-1832.
- [102] J. A. Mackintosh, D. A. Veal, and P. Karuso, Fluoroprofile, a fluorescence-based assay for rapid and sensitive quantitation of proteins in solution. *Proteomics* 5(18) (2005) 4673-4677.
- [103] S. K. Bhatia, L. C. Shriver-Lake, K. J. Prior, J. H. Georger, J. M. Calvert, R. Bredehorst, and F. S. Ligler, Use of thiol-terminal silanes and heterobifunctional crosslinkers for immobilization of antibodies on silica surfaces. *Anal Biochem* 178(2) (1989) 408-413.
- [104] G. J. Brewer, Serum-free B27/neurobasal medium supports differentiated growth of neurons from the striatum, substantia nigra, septum, cerebral cortex, cerebellum, and dentate gyrus. *J Neurosci Res* 42(5) (1995) 674-683.
- [105] T. Satomi, Y. Nagasaki, H. Kobayashi, H. Otsuka, and K. Kataoka, Density Control of Poly(ethylene glycol) Layer To Regulate Cellular Attachment. *Langmuir* 23(12) (2007) 6698-6703.
- [106] K. A. Kilian, T. Bocking, K. Gaus, M. Gal, and J. J. Gooding, Si-C linked oligo(ethylene glycol) layers in silicon-based photonic crystals: Optimization for implantable optical materials. *Biomaterials* 28(20) (2007) 3055-3062.
- [107] M. A. Nicolelis, D. Dimitrov, J. M. Carmena, R. Crist, G. Lehew, J. D. Kralik, and S. P. Wise, Chronic, multisite, multielectrode recordings in macaque monkeys. *Proc Natl Acad Sci U S A* 100(19) (2003) 11041-11046.
- [108] J. D. Stroncek, N. Bell, and W. M. Reichert, Instructional PowerPoint presentations for cutaneous wound healing and tissue response to sutures. *J Biomed Mater Res A* 90(4) (2009) 1230-1238.
- [109] E. Azemi, W. R. Stauffer, M. S. Gostock, C. F. Lagenaur, and X. T. Cui, Surface immobilization of neural adhesion molecule L1 for improving the biocompatibility of chronic neural probes: In vitro characterization. *Acta Biomater* 4(5) (2008) 1208-1217.
- [110] M. C. Dodla and R. V. Bellamkonda, Anisotropic scaffolds facilitate enhanced neurite extension in vitro. *J Biomed Mater Res A* 78(2) (2006) 213-221.

- [111] Y. Xiao, D. C. Martin, X. Cui, and M. Shenai, Surface modification of neural probes with conducting polymer poly(hydroxymethylated-3,4- ethylenedioxythiophene) and its biocompatibility. *Appl Biochem Biotechnol* 128(2) (2006) 117-130.
- [112] C. G. Becker, B. C. Lieberoth, F. Morellini, J. Feldner, T. Becker, and M. Schachner, L1.1 is involved in spinal cord regeneration in adult zebrafish. *J Neurosci* 24(36) (2004) 7837-7842.
- [113] J. Chen, J. Wu, I. Apostolova, M. Skup, A. Irintchev, S. Kugler, and M. Schachner, Adeno-associated virus-mediated L1 expression promotes functional recovery after spinal cord injury. *Brain* 130(Pt 4) (2007) 954-969.
- [114] J. Chen, C. Bernreuther, M. Dihne, and M. Schachner, Cell adhesion molecule 11-transfected embryonic stem cells with enhanced survival support regrowth of corticospinal tract axons in mice after spinal cord injury. *J Neurotrauma* 22(8) (2005) 896-906.
- [115] C. Roonprapunt, W. Huang, R. Grill, D. Friedlander, M. Grumet, S. Chen, M. Schachner, and W. Young, Soluble cell adhesion molecule L1-Fc promotes locomotor recovery in rats after spinal cord injury. *J Neurotrauma* 20(9) (2003) 871-882.
- [116] K. L. Drake, K. D. Wise, J. Farraye, D. J. Anderson, and S. L. BeMent, Performance of planar multisite microprobes in recording extracellular single-unit intracortical activity. *IEEE Trans Biomed Eng* 35(9) (1988) 719-732.
- [117] X. Cui and D. C. Martin, Electrochemical deposition and characterization of poly(3,4-ethylenedioxythiophene) on neural microelectrode arrays. *Sensors and Actuators B: Chemical* 89(1-2) (2003) 92-102.
- [118] I. Aubert, J. L. Ridet, and F. H. Gage, Regeneration in the Adult Mammalian Cns - Guided by Development. *Current Opinion in Neurobiology* 5(5) (1995) 625-635.
- [119] S. Chen, N. Mantei, L. Dong, and M. Schachner, Prevention of neuronal cell death by neural adhesion molecules L1 and CHL1. *J Neurobiol* 38(3) (1999) 428-439.
- [120] M. Katidou, M. Vidaki, M. Strigini, and D. Karagogeos, The immunoglobulin superfamily of neuronal cell adhesion molecules: lessons from animal models and correlation with human disease. *Biotechnol J* 3(12) (2008) 1564-1580.

- [121] S. D. Styren, P. D. Miller, C. F. Lagenaur, and S. T. DeKosky, Alternate strategies in lesion-induced reactive synaptogenesis: differential expression of L1 in two populations of sprouting axons. *Exp Neurol* 131(2) (1995) 165-173.
- [122] X. Liu, D. B. McCreery, R. R. Carter, L. A. Bullara, T. G. Yuen, and W. F. Agnew, Stability of the interface between neural tissue and chronically implanted intracortical microelectrodes. *IEEE Trans Rehabil Eng* 7(3) (1999) 315-326.
- [123] F. Properzi and J. W. Fawcett, Proteoglycans and brain repair. *News Physiol Sci* 19 (2004) 33-38.
- [124] F. Properzi, R. Lin, J. Kwok, M. Naidu, T. H. van Kuppevelt, G. B. Ten Dam, L. M. Camargo, R. Raha-Chowdhury, Y. Furukawa, T. Mikami, K. Sugahara, and J. W. Fawcett, Heparan sulphate proteoglycans in glia and in the normal and injured CNS: expression of sulphotransferases and changes in sulphation. *Eur J Neurosci* 27(3) (2008) 593-604.
- [125] J. C. Williams, "Performance of Chronic Neural Implants: Measurement, Modeling, and Intervention Strategies," Ph.D. dissertation, Arizona State University, 2001.
- [126] J. C. Collias and E. E. Manuelidis, Histopathological changes produced by implanted electrodes in cat brains; comparison with histopathological changes in human and experimental puncture wounds. *J Neurosurg* 14(3) (1957) 302-328.
- [127] N. H. Hosseini, R. Hoffmann, S. Kisban, T. Stieglitz, O. Paul, and P. Ruther, Comparative study on the insertion behavior of cerebral microprobes. *Conf Proc IEEE Eng Med Biol Soc* 2007 (2007) 4711-4714.
- [128] A. H. Kyle, C. T. Chan, and A. I. Minchinton, Characterization of three-dimensional tissue cultures using electrical impedance spectroscopy. *Biophys J* 76(5) (1999) 2640-2648.
- [129] W. M. Grill and J. T. Mortimer, Electrical properties of implant encapsulation tissue. *Ann Biomed Eng* 22(1) (1994) 23-33.
- [130] J. F. Hetke, J. L. Lund, K. Najafi, K. D. Wise, and D. J. Anderson, Silicon ribbon cables for chronically implantable microelectrode arrays. *IEEE Trans Biomed Eng* 41(4) (1994) 314-321.

- [131] J. C. Williams, J. A. Hippensteel, J. Dilgen, W. Shain, and D. R. Kipke, Complex impedance spectroscopy for monitoring tissue responses to inserted neural implants. *J Neural Eng* 4(4) (2007) 410-423.
- [132] G. Lin, C. S. Bjornsson, K. L. Smith, M.-A. Abdul-Karim, J. N. Turner, W. Shain, and B. Roysam, Automated image analysis methods for 3-D quantification of the neurovascular unit from multichannel confocal microscope images. *Cytometry : the journal of the International Society for Analytical Cytology* 66(1) (2005) 9-23.
- [133] K. Zilles, G. Schlaug, M. Matelli, G. Luppino, A. Schleicher, M. Qu, A. Dabringhaus, R. Seitz, and P. E. Roland, Mapping of human and macaque sensorimotor areas by integrating architectonic, transmitter receptor, MRI and PET data. *J Anat* 187 (Pt 3) (1995) 515-537.
- [134] K. F. Jensen and H. P. Killackey, Terminal arbors of axons projecting to the somatosensory cortex of the adult rat. I. The normal morphology of specific thalamocortical afferents. *J Neurosci* 7(11) (1987) 3529-3543.
- [135] J. F. Staiger, K. Zilles, and T. F. Freund, Innervation of VIP-immunoreactive neurons by the ventroposteromedial thalamic nucleus in the barrel cortex of the rat. *J Comp Neurol* 367(2) (1996) 194-204.
- [136] C. Welker, Microelectrode delineation of fine grain somatotopic organization of (SmI) cerebral neocortex in albino rat. *Brain Res* 26(2) (1971) 259-275.
- [137] D. J. Simons, Response properties of vibrissa units in rat SI somatosensory neocortex. *J Neurophysiol* 41(3) (1978) 798-820.
- [138] M. Armstrong-James and K. Fox, Spatiotemporal convergence and divergence in the rat S1 "barrel" cortex. *J Comp Neurol* 263(2) (1987) 265-281.
- [139] J. P. Frampton, M. R. Hynd, J. C. Williams, M. L. Shuler, and W. Shain, Three-dimensional hydrogel cultures for modeling changes in tissue impedance around microfabricated neural probes. *J Neural Eng* 4(4) (2007) 399-409.
- [140] P. W. Land and D. J. Simons, Metabolic activity in SmI cortical barrels of adult rats is dependent on patterned sensory stimulation of the mystacial vibrissae. *Brain Res* 341(1) (1985) 189-194.

- [141] B. Liu and J. S. Hong, Primary rat mesencephalic neuron-glia, neuron-enriched, microglia-enriched, and astroglia-enriched cultures. *Methods Mol Med* 79 (2003) 387-395.